

Sneutrino cold dark matter, a new analysis: relic abundance and detection rates

Chiara Arina, Nicolao Fornengo

Dipartimento di Fisica Teorica, Università di Torino and Istituto Nazionale di Fisica Nucleare, Sezione di Torino, via P. Giuria 1, I-10125 Torino, Italy
E-mail: arina@to.infn.it, fornengo@to.infn.it

ABSTRACT: We perform a new and updated analysis of sneutrinos as dark matter candidates, in different classes of supersymmetric models. We extend previous analyses by studying sneutrino phenomenology for full variations of the supersymmetric parameters which define the various models. We first revisit the standard Minimal Supersymmetric Standard Model, concluding that sneutrinos are marginally compatible with existing experimental bounds, including direct detection, provided they compose a subdominant component of dark matter. We then study supersymmetric models with the inclusion of right-handed fields and lepton-number violating terms. Simple versions of the lepton-number-violating models do not lead to phenomenology different from the standard case when the neutrino mass bounds are properly included. On the contrary, models with right-handed fields are perfectly viable: they predict sneutrinos which are compatible with the current direct detection sensitivities, both as subdominant and dominant dark matter components. We also study the indirect detection signals for such successful models: predictions for antiproton, antideuteron and gamma-ray fluxes are provided and compared with existing and future experimental sensitivities. The neutrino flux from the center of the Earth is also analyzed.

KEYWORDS: Dark Matter and Double Beta Decay, Cosmology of Theories beyond the SM, Gamma and Cosmic Rays, Supersymmetric Effective Theories, Supersymmetry Phenomenology, Supersymmetric Standard Model.

Contents

| | |
|--|-----------|
| 1. Introduction | 1 |
| 2. Standard minimal MSSM | 4 |
| 3. Models with a right-handed sneutrino field | 12 |
| 4. Models with a lepton-number violating term | 36 |
| 5. Models with right-handed sneutrinos and lepton-number violating interactions: the case for a see-saw neutrino mass | 45 |
| 5.1 Models with a TeV-scale Majorana mass-term | 46 |
| 5.2 Models with a large-scale Majorana mass-parameter | 53 |
| 6. Conclusions | 55 |
| 7. Appendix: The supersymmetric model | 61 |

1. Introduction

Sneutrino as a particle candidate to explain the Cold Dark Matter (CDM) present in the Universe has been investigated in the past in a number of interesting papers, where its relic abundance and its scattering cross-section off nucleons, relevant for the direct detection searches of dark matter, have been calculated and discussed. Sneutrinos in the Minimal Supersymmetric Standard Model (MSSM) have been studied in the past [1, 2, 3, 4, 5, 6], and from the direct detection searches they have been excluded as the major component of dark matter. The case of the inclusion of right-handed sneutrino fields [7, 8, 9, 10, 11] and of lepton-number violating terms [7, 8, 9, 10, 11, 12, 13, 14, 15] have also been studied, in connection also to the problem of neutrino masses. It has been shown that right-handed components may alter significantly neutrino phenomenology, due to a reduction of the coupling with the Z boson. Lepton-number violating terms, which can induce a mass splitting of the two mass eigenstates, also lead to a modified phenomenology since they alter the coupling to the Z boson, which is non-diagonal in the CP basis [12]. These models offer a nice realization of inelastic dark matter, which has been introduced in relation to direct detection searches [9, 10, 11, 12]. Sneutrinos in connection with the dark matter problem have also been discussed in different frameworks some of which may be found in Refs. [16, 17, 18, 19, 20, 21, 22].

Typically, the relic abundance and the direct detection rate (which offers a very stringent experimental bound to sneutrino dark matter) have been studied and some of the

models have been proposed in order to circumvent the character of exclusion of sneutrino dark matter in the minimal version of the MSSM. However, a thorough analysis as is typically done for neutralino dark matter, with a global study in the full parameter space of the supersymmetric models, has not been performed for sneutrinos. Indirect detection signals, especially those coming from dark matter annihilation in the Galaxy, have not been typically discussed in the literature.

In the present paper we wish to reconsider in a consistent way sneutrino as a cold relic from the early Universe and study its phenomenology relevant both for Cosmology and for relic-particle detection. First of all, we explicitly consider both cosmologically dominant and sub-dominant sneutrino configurations: in fact, we are interested not only in those configurations which are able to solve the CDM problem, but also those which provide a smaller amount of cosmological relic abundance but which could be potentially detectable by means of various astrophysical signals. We then study the sneutrino detection rates, both of direct and indirect type. Therefore, in addition to the quite relevant direct-detection signal, coded into the scattering cross-section off nuclei and which typically provides the most stringent limits to sneutrino CDM once the relic abundance bound is imposed, we calculate also the indirect detection signals which come from sneutrino pair-annihilation in the galactic environment: predictions for antiproton, antideuteron and gamma-rays signals are provided and discussed. This is a novel analysis for sneutrino CDM, and we will show that relic sneutrinos could have a chance of being detected by means of indirect searches. At the same time, for some particle physics models, indirect detection nicely complements direct searches in posing limits to the supersymmetric parameter space. Predictions for the neutrino flux from the center of the Earth, relevant for neutrino telescope searches, are also discussed.

The particle physics models we explicitly analyze in the paper are extensions of the Minimal Supersymmetric Standard Model (MSSM), where the sneutrino is the scalar super-partner of the left-handed neutrino. Since neutrinos have masses, as is now clearly understood by a host of independent and very robust experimental results and theoretical analyses [23, 24, 25, 26, 27], we will focus our attention on extensions of the MSSM which contain terms in the supersymmetric lagrangian which can drive neutrino masses. Connections between neutrino physics and the phenomenology of sneutrino CDM will therefore arise, and we will explicitly consider them whenever relevant. The models which we will be considering are therefore natural and direct extensions of the MSSM which incorporate at the same time the new physics required to explain two basic problems of astro-particle physics: the origin of neutrino masses and the nature of dark matter. We do not attempt to be totally exhaustive on the type of supersymmetric models (something which would require an exceedingly large analysis). Instead we concentrate on a number of the most direct extensions of the MSSM and derive the phenomenology of sneutrino CDM thoroughly.

We first review the case of the Minimal Supersymmetric extension of the Standard Model (MSSM), by enlarging the previous analyses to the case of sub-dominant sneutrino CDM. This is discussed in Sect. 2. This model, not very appealing for sneutrino CDM and actually already almost excluded by direct detection searches (we will explicitly show under what circumstances a sneutrino CDM may still be viable in these model) sets the

basis for the following extensions. For the sake of clarity, and due to the complexity of the overall analysis of this paper, we will name the different classes of models with specific labels. The standard MSSM will be called “STD model” in the discussion.

The first extension allows for the inclusion of a right handed field for the sneutrino [7, 8, 9, 10, 11] and is discussed in Sect. 3. We will label this class of models “LR models”. Since we are enlarging the parameter space of the supersymmetric models by adding terms (and therefore parameters) to the fundamental lagrangian, we will organize our discussion in two steps. We first discuss the sneutrino CDM phenomenology in terms of the new added parameters (by keeping a fixed configuration for the rest of the parameter space, whenever relevant). This will be useful to disentangle specific features of the relic abundance and direct detection rate for this specific class of models. We then extend our analysis to include a full scan of the supersymmetric parameter space. All the relevant experimental bounds on searches of Supersymmetry at accelerators and supersymmetric contributions to rare processes are properly taken into account. Indirect detection signals are discussed for the full-scan case only. We will show that “LR models” contain viable sneutrino CDM candidates for a large sector of its parameter space and possess a rich sneutrino CDM phenomenology with potentially detectable direct and indirect detection rates.

We then discuss a class of models with a lepton-number violating mass-term added to the lagrangian [12, 28, 14, 15]. In this case the two mass eigenstates are splitted and possess an off-diagonal coupling to the Z -boson which may sizeably alter both the relic abundance and the direct detection rate [12]. This class of models is named here “ \mathcal{L} models” and is discussed in Sect. 4. In this case, the new term in the lagrangian can lead to 1-loop contributions to the neutrino mass, which may be potentially large depending on the values of the parameters involved. We therefore bound our analysis to the neutrino mass limits, as an additional and relevant phenomenological constraint. In this class of models, once all the experimental bounds are taken into account, including neutrino mass limits, we do not find a very interesting phenomenology for CDM: we therefore discuss only the general analysis, but we skip the full parameter-space scan and the discussion of indirect detection signals.

The last class of models we consider contains right-handed sneutrino fields and lepton-flavour violating terms simultaneously [7, 8, 9, 10, 11, 12, 13, 14, 15] and is discussed in Sect. 5. These models, which we label as “MAJ models”, are very interesting from the theoretical point of view since they can successfully accommodate both Dirac and Majorana neutrino mass-terms with a renormalizable supersymmetric lagrangian. Neutrino masses are then obtained by means of the see-saw mechanism [29, 30, 31, 32, 33, 34]. A nice exhaustive analysis of this topic has been recently performed in Ref [35]. Also for this class of models we first perform a study of the parameter space relevant for the sneutrino sector (and by taking into account also neutrino-mass theoretical and phenomenological consequences). We then perform a full scan of the supersymmetric parameter space for two specific relevant sectors of the model, named “MAJ[A]” and “MAJ[B]”, for which we discuss explicitly also the indirect detection rates. We will show that the class of models “MAJ[A]” (characterized by a TeV-scale Majorana mass-parameter in the neutrino sector) have again a rich phenomenology from the point of view of sneutrino CDM.

2. Standard minimal MSSM

In the minimal MSSM, sneutrinos are the scalar partners of the left-handed neutrinos. Superfields \hat{L}^I contains the fermionic $SU(2)_L$ doublets $L^I \equiv (\nu_L^I, l_L^I)$ (where $I = e, \mu, \tau$ runs over the three families) and its corresponding scalar doublets $\tilde{L}^I \equiv (\tilde{\nu}_L^I, \tilde{l}_L^I)$. The supersymmetric lagrangian is constructed in the usual way (see, for instance, Refs. [36, 37]). We call this model “STD model”. We do not explicitly detail here all the terms of the supersymmetric lagrangian which involve the sneutrino fields. We instead quote only the terms which are relevant for our discussion. The complete set of interaction lagrangians can be found in Ref. [36, 37, 38].

The part of the superpotential relevant for the leptonic sector is (we use notations as in Refs. [36] and [35]):

$$W = \epsilon_{ij}(\mu \hat{H}_i^1 \hat{H}_j^2 - Y_l^{IJ} \hat{H}_i^1 \hat{L}_j^I \hat{R}^J) \quad (2.1)$$

where \hat{H}^1 and \hat{H}^2 are the two higgs-doublet superfields, \hat{R}^J denotes the right-handed charged lepton superfields (which contain the right-handed sleptons), μ is the usual higgs-mixing parameters and Y_l^{IJ} is a matrix which contains the Yukawa couplings. Repeated indices imply a sum-convention over them. In our analysis, which relies on a minimal version of the MSSM with a minimal set of relevant parameters, Y_l^{IJ} is real and diagonal in flavour space and the Yukawa couplings are linked to the charged-lepton masses by the usual relation $m_I = v_1 Y_l^{II}$, where v_1 is the vacuum expectation value of the neutral component of the H^1 Higgs field.

The soft-supersymmetry-breaking potential relevant for the sneutrino sector is:

$$V_{\text{soft}} = (M_L^2)^{IJ} \tilde{L}_i^{I*} \tilde{L}_j^J + [\epsilon_{ij}(\Lambda_l^{IJ} H_i^1 \tilde{L}_j^I \tilde{R}^J) + \text{h.c.}] \quad (2.2)$$

where Λ_l^{IJ} is a matrix, which we take real and diagonal in flavor space, as we do for the Yukawa matrix Y_l^{IJ} . Also the mass matrix M_L^2 , in the minimal version of MSSM, is taken to be diagonal and, in order to reduce the MSSM to a minimal set of parameters, all the three entries equal to a common value which we denote as m_L^2 . The scalar potential is determined as the sum $V = V_F + V_D + V_{\text{soft}}$, where the D-term V_D describes gauge-interactions [36, 37] and the F-term V_F is obtained by the superpotential by means of its derivatives over the scalar components ϕ_a as $V_F = \sum_a |\partial W / \partial \phi_a|^2$.

From all the above, the mass-term for the sneutrino field $\tilde{\nu}_L$ (for each family) is simply derived to be:

$$V_{\text{mass}} = \left[m_L^2 + \frac{1}{2} m_Z^2 \cos 2\beta \right] \tilde{\nu}_L^* \tilde{\nu}_L \quad (2.3)$$

where β is defined as usual from the relation $\tan \beta = v_2 / v_1$ where v_2 is the vacuum expectation value of the neutral component of the H^2 Higgs field and m_Z is the Z -boson mass. In this case, the three sneutrinos (one for each family) are also (degenerate) mass-eigenstates with squared-mass $m_1^2 = m_L^2 + 0.5 m_Z^2 \cos(2\beta)$. Here and thereafter we will denote by m_1 the mass of the lightest sneutrino mass-eigenstate, which in order to be a CDM candidate must also be the Lightest Supersymmetric Particle (LSP).

The experimental bounds on MSSM sneutrinos come from searches for supersymmetry at accelerators and, for sneutrinos lighter than $m_Z/2$, from their contribution to the

invisible Z -width:

$$\Delta\Gamma_Z = \frac{\Gamma_\nu}{2} \left[1 - \left(\frac{2m_1}{m_Z} \right)^2 \right]^{3/2} \theta(m_Z - 2m_1) \quad (2.4)$$

where $\Gamma_\nu = 167$ MeV is the Z -boson invisible width into one neutrino species. The bound we adopt is: $\Delta\Gamma_Z < 2$ MeV [39]. This bound constrains MSSM sneutrinos to be heavier than about 43.7 GeV for one sneutrino, and 44.7 for 3 degenerate sneutrino [39]. but will be evaded in non-minimal models, as we will discuss below.

The bound that comes from accelerator physics is induced by the non-observation of the corresponding charged sleptons. Contrary to MSSM sneutrinos, which are purely left-handed fields, charged sleptons possess both left- and right-handed components. The mass bound on the charged slepton depends on the assumptions made on the balance between left- and right-handed components (and on some more assumptions on the MSSM parameter space and mass splitting with neutralinos) and it is usually more conservative for the right-handed fields. For selectrons current limits are: 73 GeV for \tilde{e}_R and 107 GeV for \tilde{e}_L [39, 40]. For smuons: 94 GeV for $\tilde{\mu}_R$. For staus: 81.9 GeV for a generic mixing of $\tilde{\tau}_L$ and $\tilde{\tau}_R$.

These limits refer to the mass eigenstates of charged sleptons, which depend on two mass parameters: m_L , the soft-mass for the left-handed SU(2) doublet \tilde{L} and the soft-mass parameter for the right-handed sleptons m_R . These parameters are in general matrices in flavour space, but as we discussed above we assume them as diagonal and common over the three families. The mass matrix for sleptons is, in this case:

$$\mathcal{M}_l^2 = \begin{pmatrix} m_L^2 + m_Z^2 \cos 2\beta (\sin^2 \theta_W - \frac{1}{2}) + m_l^2 & m_l (A_l + \mu \tan \beta) \\ m_l (A_l + \mu \tan \beta) & m_R^2 - m_Z^2 \cos 2\beta \sin^2 \theta_W + m_l^2 \end{pmatrix} \quad (2.5)$$

where m_l is the mass of the partner lepton (which is negligible, except when $l = \tau$) and A_l is a trilinear coupling in the soft-breaking potential. The parameter m_L is common with sneutrinos, while m_R is an independent parameter. Therefore, in general, a bound to the mass of the lightest charged sleptons does not directly transfer to a mass limit to the corresponding sneutrino, but depends on the relative values of m_L and m_R (and, to a lesser extent, on A_l and μ for the τ case). For instance, in a minimal Supergravity scenario (mSUGRA), the values of the parameters at the electroweak-scale are induced by their renormalization-group equation evolution from the GUT scale and they read:

$$m_R^2 = m_0^2 + 0.15 m_{1/2}^2 \quad (2.6)$$

$$m_L^2 = m_0^2 + 0.52 m_{1/2}^2 \quad (2.7)$$

where m_0 and $m_{1/2}$ are defined at the GUT scale and are the common value for the soft susy-breaking mass parameters and the common gaugino mass parameter, respectively. In this framework the lower bound on the sneutrino mass is 84 GeV [39, 40]

The version of the MSSM we adopt in this paper is a low-energy supersymmetric extension of the Standard Model, which does not (necessarily) invoke mSUGRA relations.

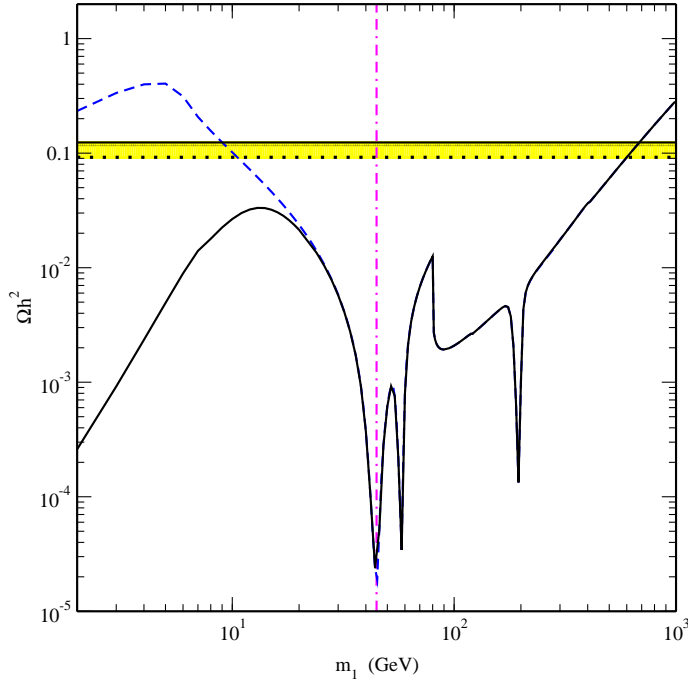


Figure 1: STD model – Sneutrino relic abundance Ωh^2 as a function of the sneutrino mass m_1 . The higgs masses for the lightest CP-even higgs is 120 GeV, for the heaviest CP-even H and the CP-odd A is 400 GeV. The solid (dashed) curves refer to models with (without) gaugino universality. The vertical line denotes the lower bound on the sneutrino mass coming from the invisible Z -width. The horizontal solid and dotted lines delimit the WMAP interval for cold dark matter.

This model has been widely used to study neutralino dark matter and we extend it here to develop the sector where sneutrino is the LSP and the dark matter candidate. The basic features of the model and the parameter space not directly related to the sneutrino sector, together with the experimental constraints which we adopt, are reported in Appendix 7. In this minimal version of the MSSM, we assume that all the soft-mass parameters of the charged sleptons are common at the electroweak-scale, and therefore we set $m_L = m_R$. In this case, the mass bound on the charged sleptons quoted above is transferred to a lower limit on the mass of the three degenerate sneutrinos which can be as low as the bound coming from the invisible Z width, depending on the value of $\tan \beta$. This is therefore the lower bound on the sneutrino mass in this class of models.

Let us turn now to the discussion of the sneutrino phenomenology relevant for dark matter. First of all, we have calculated the sneutrino relic abundance, by taking into account all the relevant annihilation channels and co-annihilation processes which may arise when the sleptons are close in mass to the sneutrinos. Table 1 lists all possible channels for annihilation and coannihilation, referred to the first family for definiteness. In this minimal MSSM models, the three neutrinos are degenerate in mass: they therefore must be considered jointly in the calculation of the relevant processes.

For general values of the model parameter space, sneutrinos may occasionally also co-

| Initial States | Annihilation Products | Available Channels |
|-------------------------------|---|--|
| $\tilde{\nu}_L \tilde{\nu}_L$ | $\nu \bar{\nu}$ $l \bar{l}$ $q \bar{q}$ $W^+ W^-$ ZZ hh, HH, hH AA Ah, AH $H^+ H^-$ $W^+ H^-$ Zh, ZH ZA | $Z(s), \tilde{\chi}_i^0(t, u) \quad i = 1, 4$ $Z(s), h(s), H(s), \tilde{\chi}_i^\pm(t, u) \quad i = 1, 2$ $Z(s), h(s), H(s)$ $Z(s), h(s), H(s), \tilde{e}_L(t), \text{ 4-point}$ $h(s), H(s), \tilde{\nu}_L(t, u), \text{ 4-point}$ $h(s), H(s), \tilde{\nu}_L(t), \text{ 4-point}$ $h(s), H(s), \text{ 4-point}$ $Z(s)$ $Z(s), h(s), H(s), \tilde{e}_L(t), \text{ 4-point}$ $h(s), H(s), \tilde{e}_L(t, u)$ $Z(s), \tilde{\nu}_L(t, u)$ $h(s), H(s)$ |
| $\tilde{\nu}_L \tilde{\nu}_L$ | $\nu \nu$ | $\tilde{\chi}_i^0(t, u) \quad i = 1, 4$ |
| $\tilde{e}_L \tilde{e}_L$ | $\nu \bar{\nu}$ $l \bar{l}$ $q \bar{q}$ $W^+ W^-$ ZZ $\gamma \gamma$ $Z \gamma$ hh, HH, hH AA Ah, AH $H^+ H^-$ $W^+ H^-$ Zh, ZH ZA | $Z(s), \tilde{\chi}_i^\pm(t, u) \quad i = 1, 2$ $\gamma(s), Z(s), h(s), H(s), \tilde{\chi}_i^0(t, u) \quad i = 1, 4$ $\gamma(s), Z(s), h(s), H(s)$ $\gamma(s), Z(s), h(s), H(s), \tilde{\nu}_L(t), \text{ 4-point}$ $h(s), H(s), \tilde{e}_L(t, u), \text{ 4-point}$ $\tilde{e}_L(t, u), \text{ 4-point}$ $\tilde{e}_L(t, u), \text{ 4-point}$ $h(s), H(s), \tilde{e}_L(t, u), \text{ 4-point}$ $h(s), H(s), \text{ 4-point}$ $Z(s)$ $\gamma(s), Z(s), h(s), H(s), \tilde{\nu}_L(t), \text{ 4-point}$ $h(s), H(s), \tilde{\nu}_L(t)$ $Z(s), \tilde{e}_L(t, u)$ $h(s), H(s)$ |
| $\tilde{e}_L \tilde{e}_L$ | ll | $\tilde{\chi}_i^0(t, u) \quad i = 1, 4$ |
| $\tilde{\nu}_L \tilde{e}_L$ | $\nu \bar{e}$ $W^+ Z$ $W^+ \gamma$ $W^+ h, W^+ H$ $W^+ A$ ZH^+ γH^+ AH^+ | $W^+(s), \tilde{\chi}_i^0(t, u) \quad i = 1, 4$ $W^+(s), \tilde{e}_L(t), \tilde{\nu}_L(t), \text{ 4-point}$ $W^+(s), \tilde{e}_L(t), \text{ 4-point}$ $W^+(s), H^+(s), \tilde{e}_L(t), \tilde{\nu}_L(t)$ $H^+(s)$ $H^+(s), \tilde{e}_L(t), \tilde{\nu}_L(t)$ $H^+(s), \tilde{e}_L(t)$ $W^+(s), \text{ 4-point}$ |
| $\tilde{\nu}_L \tilde{e}_L$ | $\nu_l l$ | $\tilde{\chi}_i^0(t, u) \quad i = 1, 4$ |

Table 1: Summary of the sneutrino annihilation and coannihilation channels. For definiteness, we report here the case of the first family.

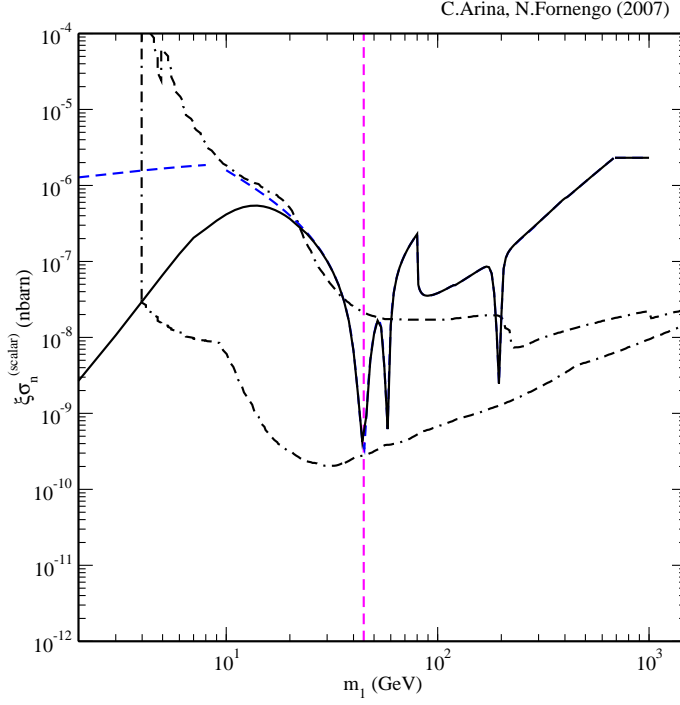


Figure 2: STD model – Sneutrino–nucleon scattering cross section $\xi\sigma_{\text{nucleon}}^{(\text{scalar})}$ as a function of the sneutrino mass m_1 , for the same set of parameters of Fig. 1. The solid (dashed) curves refer to models with (without) gaugino universality. The vertical line denotes the lower bound on the sneutrino mass coming from the invisible Z -width. The dashed–dotted curve shows the DAMA/NaI region, compatible with the annual modulation effect observed by the experiment [41, 42, 43, 44, 45].

annihilate with neutralinos and/or charginos. In the models we present in this paper we have explicitly neglected this case, by considering configurations which possess neutralinos at least 30% heavier than the lightest sneutrino. Co-annihilation with neutralinos and charginos is more accidental than the one with sleptons, whose masses depend on some parameters (mostly m_L) which are common with the sneutrino mass sector. The relic abundance is calculated by numerically solving the relevant Boltzmann equation, and the thermal-average of the (co)annihilation cross section is performed numerically as detailed in Ref. [49]. We have developed a detailed numerical code for this purpose [38].

An example of sneutrino relic abundance Ωh^2 for the minimal MSSM is plotted in Fig. 1 as a function of the sneutrino mass (we report also the result for values of the mass which are below the experimental bound discussed above for the sake of the discussion in the following Sections). In this plot we have fixed the value of the higgs masses at 120 GeV for the lightest CP-even state h and at 400 GeV for the heaviest CP-even H and for the CP-odd state A . The lightest neutralino mass is $m_\chi = \min(294 \text{ GeV}, 1.3 m_1)$ for the solid curve, and $m_\chi = 1.3 m_1$ for the dashed curve. This second case, which possesses light neutralinos, requires gaugino–non universality [50, 51, 52] in order to evade the neutralino mass lower bound of about 50 GeV which is instead derived for gaugino universal models. This is nevertheless a perfectly viable possibility.

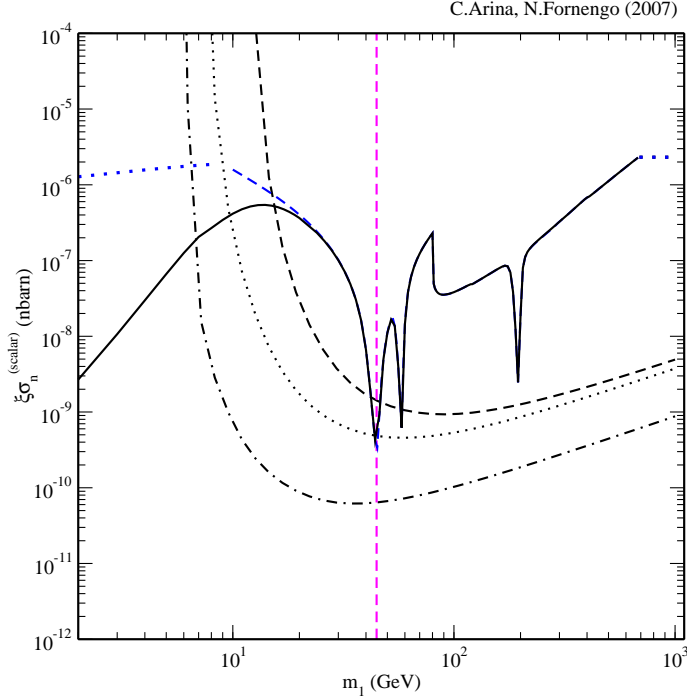


Figure 3: STD model – Sneutrino–nucleon scattering cross section $\xi\sigma_{\text{nucleon}}^{(\text{scalar})}$ as a function of the sneutrino mass m_1 . Notations are as in Fig. 2, except for the experimental curves which refer here to the upper limit from the CDMS experiment [46, 47, 48], as re-evaluated in Ref. [48] for three different galactic halo models which delimit the uncertainty band. The dotted line refers to the standard isothermal sphere with $v_0 = 220 \text{ km s}^{-1}$ and $\rho_0 = 0.3 \text{ GeV cm}^{-3}$. The upper dashed line refers to a cored-isothermal sphere with a core radius of 5 Kpc (model B1 in Ref. [48]) and with $v_0 = 170 \text{ km s}^{-1}$ and $\rho_0 = 0.2 \text{ GeV cm}^{-3}$. The lower dashed-dotted line refers to an axisymmetric density profile with a power-law potential (model C3 in Ref. [48]) with $v_0 = 270 \text{ km s}^{-1}$ and $\rho_0 = 1.66 \text{ GeV cm}^{-3}$.

The sneutrino relic abundance is typically very small [1, 3, 6], much lower than the cosmological range for cold dark matter derived by the WMAP analysis [53]:

$$0.092 \leq \Omega_{\text{CDM}} h^2 \leq 0.124 \quad (2.8)$$

This means that sneutrinos in the minimal version of MSSM are not good dark matter candidates, except for masses in a narrow range which we determine to be 600–700 GeV, consistent with previous analyses [6]. For all the mass range from the experimental lower bound of about $m_Z/2$ up to 600–700 GeV sneutrinos as the LSP are cosmologically acceptable (*i.e.* their relic abundance is below the WMAP bound) but they are typically underabundant. The three dips in the values of the relic abundance refer (from left to right) to the Z , h to the degenerate H and A poles in the (co)annihilation cross section, which occur when m_1 is close to half the mass of the exchanged particle. Since the mass of the Higgs particles are not fixed in the model, but they can span from their absolute lower bound of 90 GeV (which occurs for specific values of the Higgs mixing angle) to 114 GeV (for a SM-like light Higgs)[54, 55] up to several hundreds of GeV (depending on naturalness

assumptions), the dips shown in Fig. 1 may occur at different sneutrino masses. Since h is upper bounded in the MSSM at a value around 140–150 GeV, a dip below 75 GeV is always expected. The sharp drop in Ωh^2 at $m_1 \simeq 80$ GeV is instead due to the opening of the W^-W^+ annihilation channel.

Dark matter direct search, which relies on the possibility to detect the recoil energy of a nucleus due to the elastic scattering of the dark matter particle off the nucleus of a low-background detector, is known to be a strong experimental constraint for sneutrino dark matter [4]. The dependence of the direct detection rate on the DM particle rests into the particle mass and the scattering cross section. For sneutrinos, coherent scattering arises due to Z and Higgs exchange diagrams in the t -channel. The relevant cross section on nucleus is therefore:

$$\sigma_{\mathcal{N}} = \sigma_{\mathcal{N}}^Z + \sigma_{\mathcal{N}}^{h,H} \quad (2.9)$$

The Z -boson exchange cross section is:

$$\sigma_{\mathcal{N}}^Z = \frac{G_F^2}{2\pi} \frac{m_1^2 m_{\mathcal{N}}^2}{(m_1 + m_{\mathcal{N}})^2} [A_{\mathcal{N}} + 2(2\sin^2 \theta_W - 1)Z_{\mathcal{N}}]^2 \quad (2.10)$$

where $m_{\mathcal{N}}$ denotes the nucleus mass, $A_{\mathcal{N}}$ and $Z_{\mathcal{N}}$ are the mass number and proton number of the nucleus and G_F is the Fermi constant. The Higgs-bosons exchange cross section is:

$$\sigma_{\mathcal{N}}^{h,H} = \frac{m_{\mathcal{N}}^2}{4\pi(m_1 + m_{\mathcal{N}})^2} [f_p Z_{\mathcal{N}} + f_n (A_{\mathcal{N}} - Z_{\mathcal{N}})]^2 \quad (2.11)$$

where f_p and f_n denote the effective coupling of the sneutrino to the nucleus, whose determination (like in the case of neutralino-nucleus scattering) is rather involved and we do not reproduce it here. Details may be found for instance in Refs. [56, 57]. For the case of sneutrinos, the effective couplings may be written as:

$$f_i = m_N \left(\sum_q^{u,d,s} k_q + \sum_Q^{c,b,t} k_Q \right) \quad i = n, p$$

where k_q and k_Q are defined as:

$$\begin{aligned} k_q &= f_{T_q} \sum_{j=1,2} \frac{c_{\nu}^j c_q^j}{m_{h_j}^2} \\ k_Q &= \frac{2}{27} f_{T_G} \sum_{j=1,2} \frac{c_{\nu}^j c_Q^j}{m_{h_j}^2} \end{aligned} \quad (2.12)$$

with c_{ν}^j denotes the sneutrino-higgs couplings, c_q^i, c_Q^i are the quark-higgs couplings and f_{T_q} is the nucleon mass fraction due to light quark q and $f_{T_G} = 1 - \sum_q^{u,d,s} f_{T_q}$. From the analyses of Ref. [56, 57], we derive the following values: $f_{T_u} = 0.023$, $f_{T_d} = 0.034$ and $f_{T_s} = 0.14$ for the proton and $f_{T_u} = 0.019$, $f_{T_d} = 0.041$ and $f_{T_s} = 0.14$ for the neutron. We remind that these quantities are affected by a sizeable uncertainty which can increase the direct detection cross section up to a factor of a few [56].

Comparisons with experimental results are more easily and typically performed by using the cross section on a single nucleon $\xi\sigma_{\text{nucleon}}^{(\text{scalar})}$. Two classes of experiments are currently running. The DAMA Collaboration uses a large-mass highly-radiopure and stable 100-Kg NaI detector, which is specifically designed to search for the annual modulation effect which is expected for direct detection, as a result of the yearly relative motion of the Earth around the Sun [58, 59]. The DAMA/NaI Collaboration detects an annual modulation in its low-energy rate over a period of 7 years ($107731 \text{ kg} \times \text{day}$ of total exposure). The C.L. of this effect is 6.3σ [41, 42, 43, 44, 45]. When interpreted as due to a relic particle interaction, the allowed region shown in Fig. 2, whose contour is outlined by the dot-dashed curve, arises. The allowed region shown in Fig. 2 has been calculated by taking into account the astrophysical uncertainties arising from galactic halo modeling [60]. This is currently the only experiment which is designed to address the annual modulation effect. Further insight into the annual modulation effect are expected from the future results of the DAMA/LIBRA experiment, which is currently running with a mass of 250 Kg [61].

A second class of experiments do not attempt to exploit the annual modulation signature, but instead rely on the development of background-rejection techniques in order to reduce the background to the sum of neutrons plus dark matter recoils. These type of experiments provide upper bounds on the scattering cross section. In Fig. 3 the upper bound from the CDMS experiment ($72 \text{ kg} \times \text{day}$ with a 1.5 Kg Ge plus 0.6 Kg Si detector) [46, 47]. For three different galactic halo models, is shown as calculated in Ref. [48]. The upper experimental bound has to be regarded as a conservative limit, and the span of the three curves reflects the uncertainty on the galactic halo modeling. Recently results from the XENON10 Collaboration (15 Kg active liquid Xe) [62] have been presented (for the standard isothermal model only), with an exposure of $136 \text{ kg} \times \text{day}$: these limits appear to be more stringent than the CDMS ones by a factor which ranges from 2 to 10, depending on the mass. For a recent and detailed review on direct detection experiments, see Refs. [63, 64].

Due to the different nature of the experimental results (positive indication vs. upper limits) and in the absence of a solid criterion to consistently combine the various experimental results (which are derived from different techniques and whose treatment would require to correctly quantify uncertainties both of theoretical origin and of experimental nature, which are not under our control) we will present our direct detection analysis by comparing our results separately with the DAMA/NaI region with the CDMS upper bounds (for which we consider the upper curve of Fig. 3 as the conservative upper limit). In order not to exceed with the number of figures (already very large) we will show our results by alternating them with either the DAMA/NaI region or the CDMS curves. The minimal MSSM is the only case where we present both for the same theoretical predictions.

When compared with the DAMA/NaI annual modulation region in Fig. 2 we see that direct detection is indeed a strong constraint on sneutrino dark matter in the minimal MSSM [6], but some very specific configurations are still viable and could explain the annual modulation effect. We have to consider that, whenever the dark matter particle is subdominant in the Universe, also its local density ρ_0 in the Galaxy is very likely reduced with respect to the total dark matter density. This means that the dominant component of

dark matter is not the sneutrino, but still sneutrinos form a small amount of dark matter and may be eventually detectable. In this case we rescale the local sneutrino abundance by means of the usual factor:

$$\xi = \min(1, \Omega h^2 / 0.092) \quad (2.13)$$

where the value 0.092 is the lower bound for CDM abundance from WMAP, given by Eq. (2.8). This situation is the same we encounter for neutralino dark matter, which also may be subdominant but nevertheless interesting to study as a relic from the early Universe. Since the direct detection rate is linearly dependent on the local dark matter density, and the experimental bounds are derived for a dominant dark matter candidate, the theoretical scattering cross section has to be rescaled by the factor ξ . In the following, when we will discuss indirect detection signals, ξ will enter quadratically in the determination of the theoretical fluxes, since in that case the signals depend on the square of the local density.

Comparison of Fig. 1 and 2 shows that the MSSM sneutrino is only viable when strongly subdominant. The mass range 600-700 GeV where the sneutrino possesses a relic abundance in the cosmologically relevant range is clearly excluded by direct detection. On the other hand, MSSM sneutrinos are still viable, but they require the special condition to stay on the pole of the annihilation cross section through Higgs exchange. This may appear a fine-tuned condition, but it is no different from the case of relic neutralinos in mSUGRA models, where the relic abundance is acceptable mostly in very specific regions of parameter space, where strong coannihilation occurs or the pole of the A -boson exchange is met [50, 51, 52]. We also notice that, since the masses of the Higgs bosons can vary, the dips in $\xi \sigma_{\text{nucleon}}^{(\text{scalar})}$ (due to the rescaling factor) may occur at any value of the sneutrino mass. This means that all the mass range from the lower bound on m_1 up to about 200 GeV may be compatible with the DAMA/NaI results.

Fig. 3 compares our calculations with the CDMS upper limit [46, 47]. For a standard isothermal halo the bound completely excludes the possibility of sneutrino dark matter. Some very marginal room may still be present for the conservative upper limit, when the sneutrino mass matches the pole condition for annihilation through a light Higgs. Nevertheless, this option appears to be very marginal (we remind that only the mass range above 70 GeV is allowed by accelerator searches).

The results of this analysis are in agreement with the previous analyses which excluded the MSSM sneutrino as a dominant component of dark matter [6, 65]. Differently from that studies, we explicitly consider subdominant sneutrinos as viable relic particles to be explored and we show that there is still an open possibility for MSSM sneutrinos, although very marginal.

3. Models with a right-handed sneutrino field

In this class of models, the neutrino/sneutrino sector is enlarged by the inclusion of right-handed superfields \hat{N}^I , whose scalar component are right-handed sneutrino fields \tilde{N}^I [7, 8, 9, 10, 11]. We call this class of models as “LR models”. The right-handed fermionic components lead to Dirac-type masses $(m_D)^I$ for the massive neutrinos. The relevant

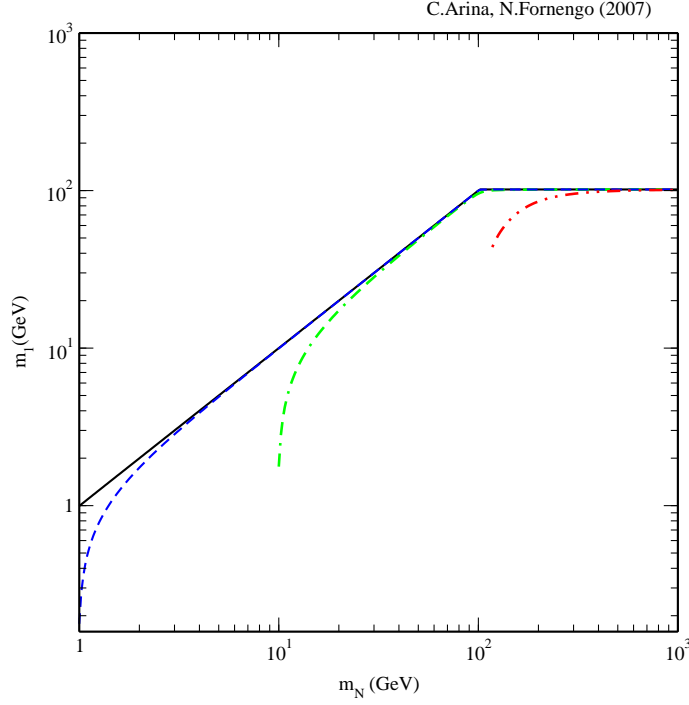


Figure 4: LR models – Sneutrino mass m_1 as a function of the right-handed soft-mass m_N , for different values of the off-diagonal parameter F^2 : the [black] solid, [blue] dashed, [green] dot-dashed and [red] dot-dot-dashed refer to $F^2 = 10, 10^2, 10^3, 10^4$ GeV², respectively. The left-handed soft-mass m_L is fixed here at the value of 120 GeV.

terms in the superpotential are now:

$$W = \epsilon_{ij}(\mu \hat{H}_i^1 \hat{H}_j^2 - Y_l^{IJ} \hat{H}_i^1 \hat{L}_j^I \hat{R}^J + Y_\nu^{IJ} \hat{H}_i^2 \hat{L}_j^I \hat{N}^J) \quad (3.1)$$

where Y_ν^{IJ} is a matrix, which we again choose real and diagonal, from which the Dirac mass of neutrinos are obtained $m_D^I = v_2 Y_\nu^{II}$. Also the soft-breaking potential gets modified:

$$V_{\text{soft}} = (M_L^2)^{IJ} \tilde{L}_i^{I*} \tilde{L}_j^J + (M_N^2)^{IJ} \tilde{N}^{I*} \tilde{N}^J - [\epsilon_{ij}(\Lambda_l^{IJ} H_i^1 \tilde{L}_j^I \tilde{R}^J + \Lambda_\nu^{IJ} H_i^2 \tilde{L}_j^I \tilde{N}^J) + \text{h.c.}] \quad (3.2)$$

where we take both the matrices M_N^2 and Λ_ν^{IJ} real and diagonal, as we do for M_L^2 and Λ_l^{IJ} . The diagonal common entries for M_N^2 are denoted as m_N^2 .

The sneutrino mass-term potential is now (we omit the family index for simplicity):

$$V_{\text{mass}} = \left[m_L^2 + \frac{1}{2} m_Z^2 \cos(2\beta) + m_D^2 \right] \tilde{\nu}_L^* \tilde{\nu}_L + [m_N^2 + m_D^2] \tilde{N}^* \tilde{N} + F^2 (\tilde{\nu}_L^* \tilde{N} + \tilde{N}^* \tilde{\nu}_L) \quad (3.3)$$

The parameter F^2 , which mixes the left- and right-handed sneutrino fields is:

$$F^2 = v \Lambda_\nu \sin \beta - \mu m_D \cot \beta \quad (3.4)$$

In the basis defined by the vector $\Phi^\dagger = (\tilde{\nu}_L^*, \tilde{N}^*)$, we can define the sneutrino mass potential as:

$$V_{\text{mass}} = \frac{1}{2} \Phi_{LR}^\dagger \mathcal{M}_{LR}^2 \Phi_{LR} \quad (3.5)$$

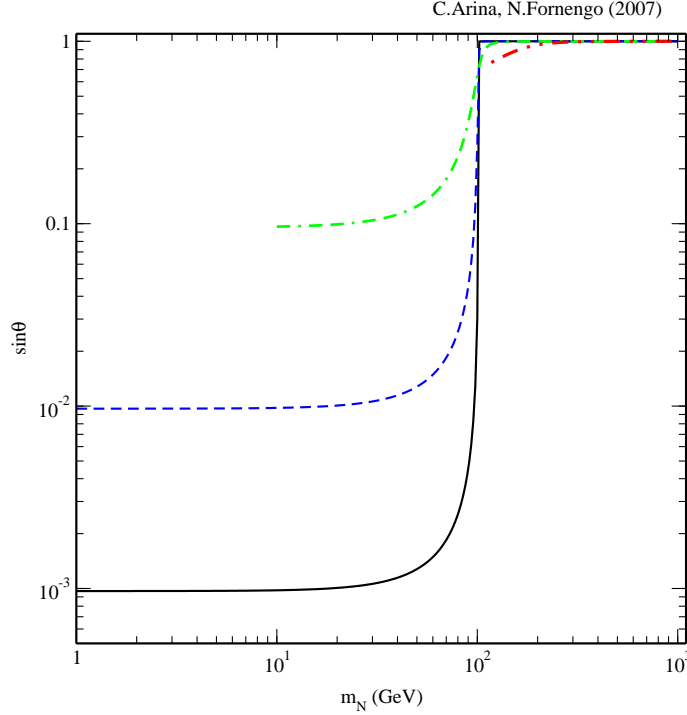


Figure 5: LR models – Sneutrino left–right mixing angle θ as a function of the right–handed soft–mass m_N , for different values of the off–diagonal parameter F^2 : the [black] solid, [blue] dashed, [green] dot–dashed and [red] dot–dot–dashed refer to $F^2 = 10, 10^2, 10^3, 10^4$ GeV², respectively. The left–handed soft–mass m_L is fixed here at the value of 120 GeV.

where the squared–mass matrix \mathcal{M}_{LR}^2 is:

$$\mathcal{M}_{LR}^2 = \begin{pmatrix} m_L^2 + \frac{1}{2}m_Z^2 \cos(2\beta) + m_D^2 & F^2 \\ F^2 & m_N^2 + m_D^2 \end{pmatrix} \quad (3.6)$$

The Dirac neutrino mass is small, and can be safely neglected. The parameter m_N in general is independent of the other mass parameters, especially m_L , which instead is related to the charged leptons masses, as discussed in the previous Section. We are therefore allowed to vary freely m_N , and whenever m_N is small enough, sneutrinos lighter than those encountered in the previous Section are in principle viable. As long as the left–handed mass m_L is compatible with the mass lower bounds on the charged leptons (which occurs for $m_L \gtrsim 80 - 90$ GeV) m_1 can be small, provided that $m_N \ll m_L$, without entering in conflict with accelerator bounds. In this case, light sneutrinos may arise, and the only relevant limit which remains is the one provided by the invisible Z –width, which we discuss in a moment.

The off–diagonal term F^2 is relevant for the mixing among the mass eigenstates, obtained by diagonalizing \mathcal{M}_{LR}^2 . For Λ_ν aligned along the Yukawa matrix Y_ν , *i.e.* for $\Lambda_\nu = \eta Y_\nu$, F^2 is necessarily very small as compared to the diagonal entries (especially the element $(\mathcal{M}_{LR}^2)_{11}$ of the matrix), because in that case F^2 is proportional to the neutrino mass m_D , and is therefore negligible since both v and μ are electroweak–scale parameters.

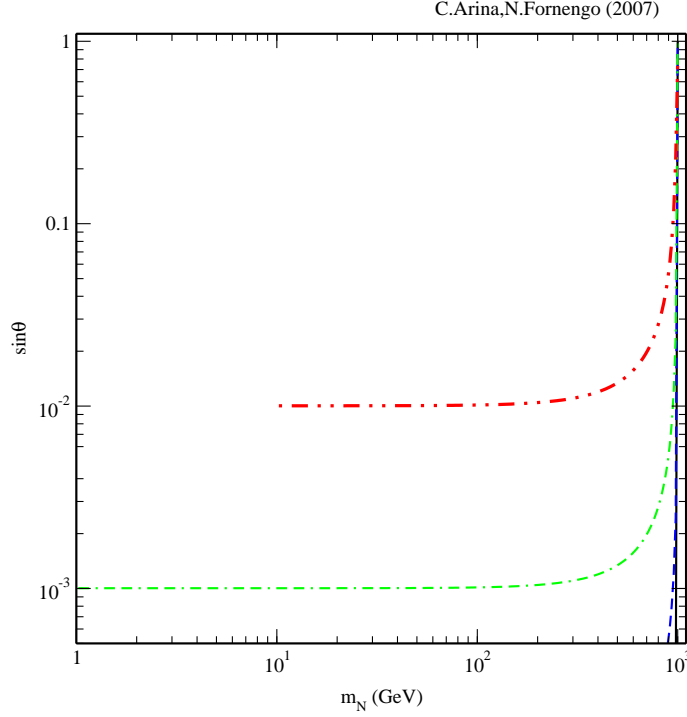


Figure 6: LR models – Sneutrino left–right mixing angle θ as a function of the right–handed soft–mass m_N . Notations are as in Fig. 5. The left–handed soft–mass m_L is fixed here at the value of 1 TeV.

However, Λ_ν is in general a free parameter. In this case $F^2 \simeq v\Lambda_\nu \sin \beta$ may naturally be of the order of the other entries of the matrix, and induce a sizeable mixing of the lightest sneutrino in terms of left–handed and right–handed fields. We define the mixing as follows:

$$\begin{cases} \tilde{\nu}_1 = -\sin \theta \tilde{\nu}_L + \cos \theta \tilde{N} \\ \tilde{\nu}_2 = +\cos \theta \tilde{\nu}_L + \sin \theta \tilde{N} \end{cases} \quad (3.7)$$

where θ is the LR mixing angle. Sizeable mixings reduce the coupling to the Z –boson, which couples only to left–handed fields, and therefore have relevant impact on all the sneutrino phenomenology, as recognized in Refs. [7, 8, 9, 10, 11].

The first important consequence is that the lightest sneutrino may be lighter than $m_Z/2$ and, due to the mixing angle, still pass the invisible Z –width constraint, which now is modified as:

$$\Delta\Gamma_Z = \sin^4 \theta \frac{\Gamma_\nu}{2} \left[1 - \left(\frac{2m_1}{m_Z} \right)^2 \right]^{3/2} \theta(m_Z - 2m_1) \quad (3.8)$$

Also $\tilde{\nu}_1$ annihilation and scattering cross sections which involve Z exchange are reduced because of the mixing. Also diagrams with higgs exchange are modified, but in a different way. For details.

The free parameters in the sneutrino sector for the LR models are therefore: m_L , m_N F^2 . We will study the model by varying m_N and F^2 freely, while for m_L we will assume a

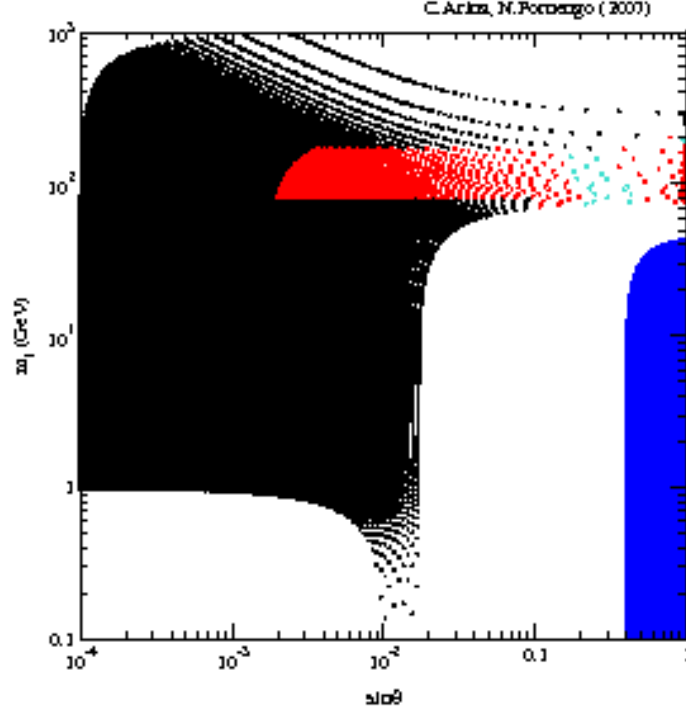


Figure 7: LR models – Sneutrino mass m_1 vs. the sneutrino left–right mixing angle θ for $F^2 = 10^2$ GeV^2 and for a scan of the soft–mass parameters m_L and m_N in the ranges: $120 \text{ GeV} \leq m_L \leq 1 \text{ TeV}$ and $1 \text{ GeV} \leq m_N \leq 1 \text{ TeV}$. The rightmost full [blue] area denotes the region which is excluded by the invisible Z –width. The black darker area denotes the region where the sneutrino relic abundance is in excess of the WMAP bound; the other areas cover the region where the relic abundance is acceptable; in addition, in the lighter [light blue] area, the direct–detection scattering cross–section is inside the DAMA/NaI annual modulation region. The white areas are not covered by models for the values of the parameters adopted here.

lower bound of 100 GeV, in order to assure that the mass limits on the charged sleptons is satisfied.

In Figs. 4, 5 and 6 we show some features of the model relevant for our analysis. In Fig. 4 the mass m_1 of the lightest sneutrino is plotted versus the right–handed mass m_N for various values of F^2 and for $m_N = 120 \text{ GeV}$. Whenever $m_N \lesssim m_L$, sneutrinos are light, and largely mixed with the right–handed component \tilde{N} , as is clear from Fig. 5 where the $\sin \theta$ is plotted against m_N , for the same set of configurations of Fig. 4. Each line starts from the value of m_N below which a negative mass–squared eigenvalue m_1^2 occurs. If we increase the value of m_L , the tachionic bound is met for lower values of m_N for any fixed F^2 , and the mixing angle diminishes (*i.e.* the mixing to the right–handed component increases). This is clear from Fig. 6, where $\sin \theta$ vs. m_N is plotted for a larger value of the left–handed mass parameter: $m_L = 1 \text{ TeV}$. Figs. 5 and 6 also show that, especially for large values of m_L and F^2 , small mixings may be obtained also for heavy sneutrinos.

Light sneutrinos and (very) small mixings may occur: the invisible Z –width may therefore be a relevant constraint. Figs. 7, 8 and 9 show, in the plane $\sin \theta$ – m_1 and for different values of F^2 , the region which is excluded by this constraints, as the rightmost

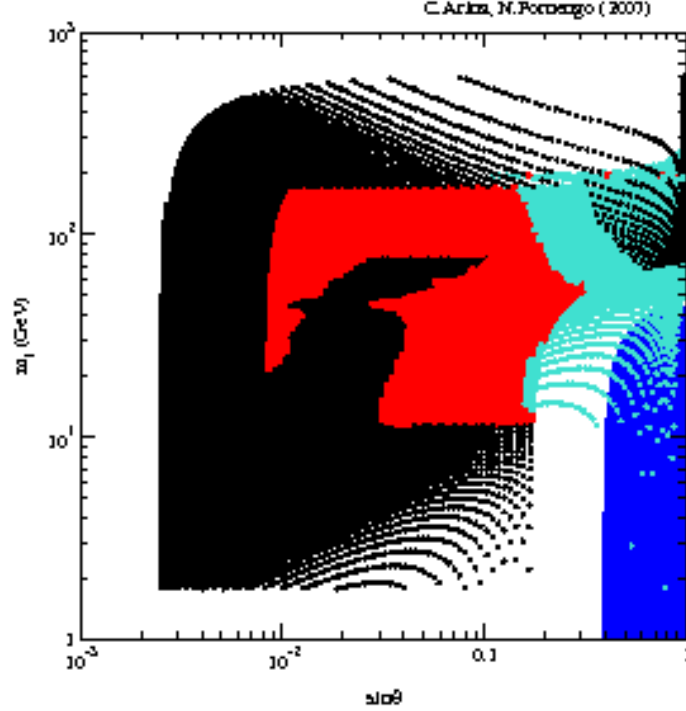


Figure 8: LR models – Sneutrino mass m_1 vs. the sneutrino left–right mixing angle θ for $F^2 = 10^3$ GeV^2 and for a scan of the soft–mass parameters m_L and m_N in the ranges: $120 \text{ GeV} \leq m_L \leq 1 \text{ TeV}$ and $1 \text{ GeV} \leq m_N \leq 1 \text{ TeV}$. Notations are as in Fig. 7, except for the lighter [light blue] area where now the direct–detection scattering cross–section is below the CDSM conservative upper bound.

full [blue] area. Clearly this bound applies only for $m_1 < m_Z/2$, and for light sneutrinos it is evaded for $|\sin \theta| \lesssim 0.4$, as is clear from Eq. 3.8. The scatter plot shows the distribution of points obtained by scanning the soft–mass parameters m_L and m_N in the ranges: $120 \text{ GeV} \leq m_L \leq 1 \text{ TeV}$ and $1 \text{ GeV} \leq m_N \leq 1 \text{ TeV}$. The off-diagonal parameter F^2 is fixed at different values in each Figure. We notice that a large fraction of points passes the Z –width bound and therefore represents viable models. We also see, in Fig. 7, that for small values of F^2 the mixing angles are typically very small for light sneutrinos. Light eigenstates are possible only for small values of m_N , since m_L is lower bounded at 120 GeV in our scan, and therefore the lightest sneutrino is already mostly right–handed, which implies almost vanishing mixing angle. When $m_N > m_L$ the lightest sneutrino is mostly left–handed, but when $m_N \simeq m_L$, even a small F^2 can allow for rotation with small mixing angles. When F^2 increases, larger mixing angles are possible also for light sneutrinos, and in this case the Z –width bound becomes important. This is clearly seen in Figs. 8 and 9. These features are quite relevant for the sneutrino relic abundance and detection rates, since a small mixing into $\tilde{\nu}_L$ implies reduced interactions, and therefore larger relic abundance and smaller direct detection rate.

The relic abundance for the LR models is shown in Fig. 10, for a full variation of the sneutrino parameter space, and for a fixed configuration of the other supersymmetric parameters. The sneutrino parameters are varied in the ranges: $120 \text{ GeV} \leq m_L \leq 1 \text{ TeV}$,

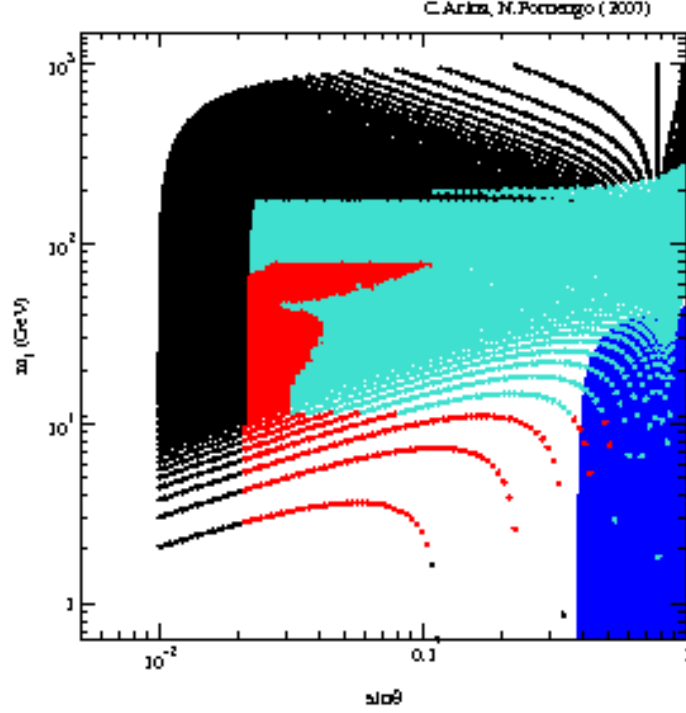


Figure 9: LR models – Sneutrino mass m_1 vs. the sneutrino left–right mixing angle θ for $F^2 = 10^4$ GeV^2 and for a scan of the soft–mass parameters m_L and m_N in the ranges: $120 \text{ GeV} \leq m_L \leq 1 \text{ TeV}$ and $1 \text{ GeV} \leq m_N \leq 1 \text{ TeV}$. Notations are as in Fig. 7, except for the lighter [light blue] area where now the direct–detection scattering cross–section is below the CDSM conservative upper bound.

$1 \text{ GeV} \leq m_N \leq 1 \text{ TeV}$ and $10 \text{ GeV}^2 \leq F^2 \leq 10^4 \text{ GeV}^2$. The other parameters are fixed at the same values used in the previous Section for Figs. 1, 2 and 3: the lightest neutralino is 30% heavier than the sneutrino (which implies gaugino non–universality when the neutralino mass is light) and higgs masses of 120 GeV for the lightest CP–even higgs h and 400 GeV for the heaviest CP–even H and the CP–odd A . All the models shown in the plot are acceptable from the point of view of all experimental constraints, including the invisible Z –width. The horizontal solid and dotted lines delimit the WMAP interval for cold dark matter.

Contrary to the previous case of the minimal MSSM model, in LR models sneutrinos may represent the dominant dark matter component for a wide mass range, which extends (for the specific supersymmetric configurations discussed here) from a few GeV to about 300 GeV. This is in fact due to the reduced Z coupling which occurs as a consequence of the mixing to the right–handed field \tilde{N} . The dips in the scatter plot are again due to the Z , h and (H,A) poles in the annihilation cross section (from left to right). We remind that the location of the higgs poles is a consequence of the choice of the higgs masses we are using for this specific case. The sharp drop at $m_1 = m_W$ is due to the opening of the annihilation channel into the W^+W^- pair. The points with an acceptable relic abundance at masses below 10 GeV are obtained for light neutralinos, since in this case the annihilation cross section into neutrinos through the exchange of neutralinos gets enhanced,

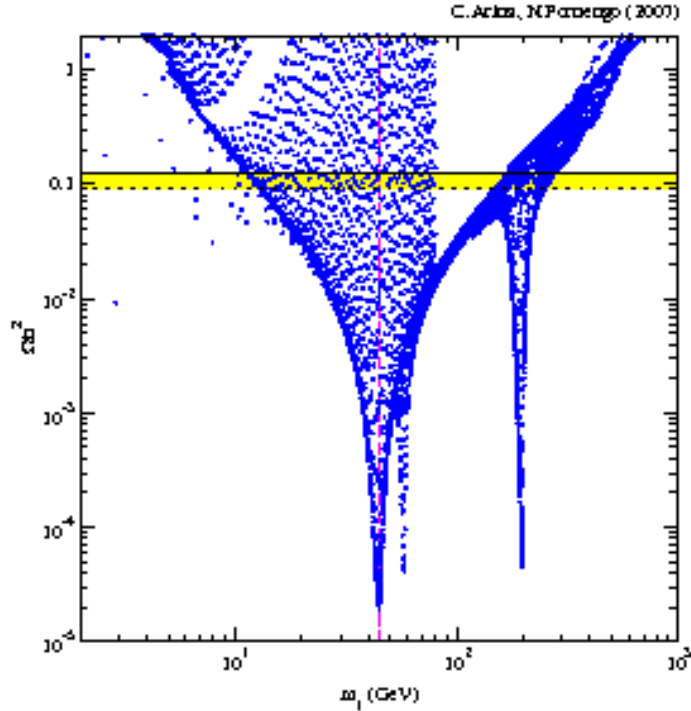


Figure 10: LR models – Scatter plot of the sneutrino relic abundance Ωh^2 as a function of the sneutrino mass m_1 , for supersymmetric models with the lightest neutralino 30% heavier than the sneutrino (which implies gaugino non-universality when the neutralino mass is light) and higgs masses of 120 GeV for the lightest CP-even higgs h and 400 GeV for the heaviest CP-even H and the CP-odd A . The sneutrino parameters are varied as follows: $120 \text{ GeV} \leq m_L \leq 1 \text{ TeV}$, $1 \text{ GeV} \leq m_N \leq 1 \text{ TeV}$ and $10 \text{ GeV}^2 \leq F^2 \leq 10^4 \text{ GeV}^2$. All the models shown in the plot are acceptable from the point of view of all experimental constraints. The horizontal solid and dotted lines delimit the WMAP interval for cold dark matter.

and therefore reduces the relic abundance to acceptable levels. This possibility occurs if the gaugino sectors possesses non-universality [66] (otherwise the lightest neutralino mass is lower bounded at the value of 50 GeV by LEP2 analyses [67, 68, 54, 69]): gaugino non-universality therefore appears instrumental in allowing light sneutrinos to be cosmologically viable [66, 70, 71, 72].

Figs. 7, 8 and 9 show how the configurations with acceptable relic abundance are distributed in the $\sin\theta$ – m_1 plane. When F^2 is small, it typically induces very small mixings for light sneutrinos. This is clearly shown in Fig. 7, which refers to $F^2 = 10^2 \text{ GeV}^2$. Light sneutrinos are possible in these models, and due to the small mixing with the Z boson they easily evade the invisible Z –width bound. However, the small-mixing angle, typically much smaller than $2 \cdot 10^{-2}$, leads to values of the relic abundance in excess of the cosmological bound. The strong suppression of the Z coupling for sneutrinos lighter than m_W in these models with small F^2 , require the opening of the W^+W^- channel in order to reduce the relic abundance to acceptable levels. Only for sneutrinos in the mass range 80–200 GeV cosmologically acceptable configurations are found. When F^2 increases, the cosmologically allowed parameter space opens up. For $F^2 = 10^3 \text{ GeV}^2$, shown in Fig. 8, mixing angles are

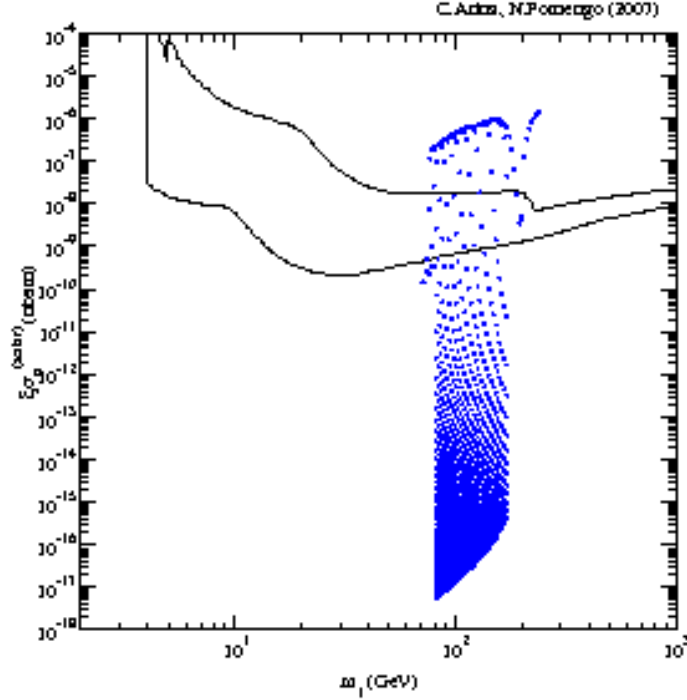


Figure 11: LR models – Sneutrino–nucleon scattering cross section $\xi\sigma_{\text{nucleon}}^{(\text{scalar})}$ as a function of the sneutrino mass m_1 , for $F^2 = 10^2 \text{ GeV}^2$ and for a scan of the soft-mass parameters m_L and m_N in the ranges: $120 \text{ GeV} \leq m_L \leq 1 \text{ TeV}$ and $1 \text{ GeV} \leq m_N \leq 1 \text{ TeV}$. The other model parameters are as in Fig. 10. The solid curve shows the DAMA/NaI region, compatible with the annual modulation effect observed by the experiment [41, 42, 43, 44, 45]. All the configurations shown possess relic abundance compatible with the WMAP bound.

typically larger than in the previous case also for light sneutrinos, and they may reach values of 0.2. Cosmologically acceptable configurations are obtained for masses which range from 10 GeV up to 200–300 GeV. Larger values of F^2 may allow for a further enlargement of the allowed mass range: for $F^2 = 10^4 \text{ GeV}^2$, shown in Fig. 9, sneutrinos are cosmologically allowed starting from a few GeV mass up to 200–300 GeV.

The sneutrino–nucleon cross section $\xi\sigma_{\text{nucleon}}^{(\text{scalar})}$, for the same supersymmetric configurations used in Fig. 10, is shown in Figs. 11, 12 and 13 for progressively larger values of F^2 . The direct detection bound, although relevant for many configurations, now is easily evaded. Most of the configurations are allowed, and a large fraction of these would be a candidate to explain the DAMA/NaI annual modulation effect. The compatibility with sneutrino dark matter and the annual modulation effect increase when F^2 is increased, especially for light sneutrinos. Fig. 11, which refers to $F^2 = 10^2 \text{ GeV}^2$ shows the lower bound of 80 GeV in the sneutrino mass which is due to the relic abundance bound, and that was discussed in relation to Fig. 7. For cosmologically acceptable sneutrinos, most of the configurations are compatible with direct detection searches. Larger values of F^2 open up the possibility of lighter sneutrinos, as is shown in Fig. 12, where $F^2 = 10^3 \text{ GeV}^2$ has been adopted. All configurations for sneutrinos lighter than 60 GeV are currently compatible with direct detection searches. Fig. 13, which refers to $F^2 = 10^4 \text{ GeV}^2$, *i.e.* to a value of

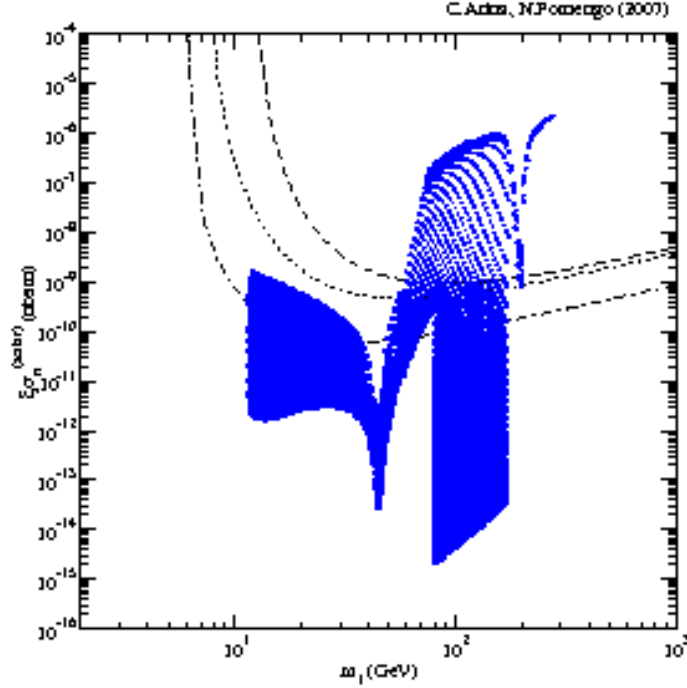


Figure 12: LR models – Sneutrino–nucleon scattering cross section $\xi\sigma_{\text{nucleon}}^{(\text{scalar})}$ as a function of the sneutrino mass m_1 , for $F^2 = 10^3 \text{ GeV}^2$, $120 \text{ GeV} \leq m_L \leq 1 \text{ TeV}$ and $1 \text{ GeV} \leq m_N \leq 1 \text{ TeV}$. The other model parameters are as in Fig. 10. The dashed, dotted and dot–dashed curves denote the CDMS upper bounds [46, 47], as in Fig. 3.

the same order of magnitude of the diagonal mass terms in \mathcal{M}_{LR}^2 of Eq. (3.6), show that in the whole mass range from few GeV up to 200 GeV sneutrinos are compatible with the annual modulation effect, without invoking any fine–tuned condition on the parameters. This is a quite remarkable feature of LR models.

The analysis presented so far, useful to discuss the features of the sneutrino relic abundance and direct detection rate, was specific to fixed values of the higgs masses and peculiar values of the neutralino and chargino masses. We now extend our analysis to a full scan of the supersymmetric parameter space, analogous to the studies for neutralino dark matter. The parameter space is defined in Appendix 7, where also the experimental constraints on the supersymmetric model are discussed. Parameters specific to the sneutrino sector are varied in the following intervals: $100 \text{ GeV} \leq m_L \leq 3 \text{ TeV}$, $1 \text{ GeV} \leq m_N \leq 1 \text{ TeV}$ and $1 \text{ GeV}^2 \leq F^2 \leq 10^6 \text{ GeV}^2$.

The sneutrino relic abundance is shown in Fig. 14. The most relevant new feature is that for the full supersymmetric scan, the mass range allowed by the cosmological constraints is enlarged up to 800 GeV, and all the mass interval above the Z –pole may lead to strongly subdominant sneutrinos. This is due to either to the occurrence of the higgs poles in the annihilation cross section discussed above or to the mixing with the right–handed field. The occurrence of sizeable mixings with the \tilde{N} field is specially important for allowing lighter sneutrinos and for enhancing the relic abundance around the Z pole. From Fig. 14 we can conclude that, for a full scan of the supersymmetric parameter space

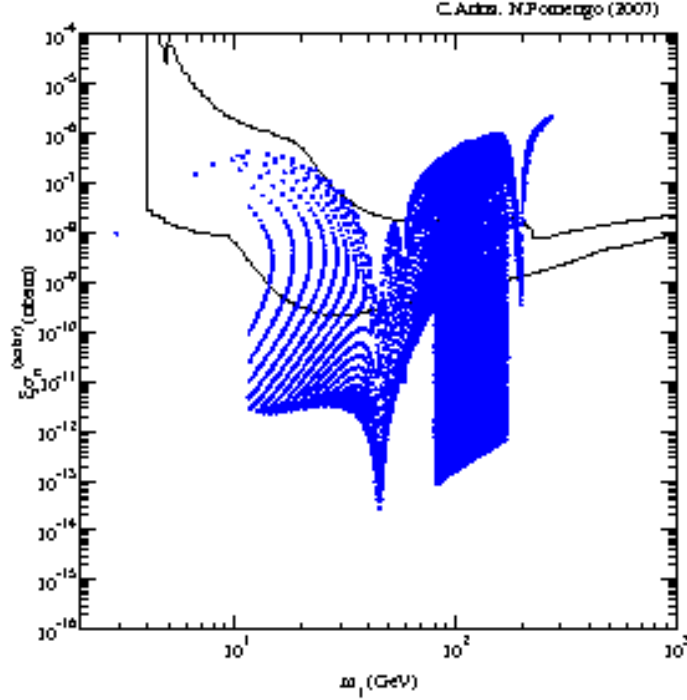


Figure 13: LR models – Sneutrino–nucleon scattering cross section $\xi\sigma_{\text{nucleon}}^{(\text{scalar})}$ as a function of the sneutrino mass m_1 , for $F^2 = 10^4 \text{ GeV}^2$, $120 \text{ GeV} \leq m_L \leq 1 \text{ TeV}$ and $1 \text{ GeV} \leq m_N \leq 1 \text{ TeV}$. The other model parameters are as in Fig. 10. The solid curve shows the DAMA/NaI region, compatible with the annual modulation effect observed by the experiment [41, 42, 43, 44, 45].

in LR models, after all experimental (and theoretical) constraints are imposed, sneutrino dark matter is perfectly viable, both as a dominant and as a subdominant component, for the whole mass range $15 \text{ GeV} \lesssim m_1 \lesssim 800 \text{ GeV}$. The lower limit of 15 GeV represents therefore a cosmological bound on the sneutrino mass in LR models, under the assumption of R -parity conservation. This result may be confronted with the one obtained for relic neutralinos in gaugino non-universal models [66, 70, 71, 72], which is about 6 GeV.

The sneutrino–nucleon cross section is shown in Fig. 15. Only points which are accepted by the cosmological constraint are shown. We see that the presence of the mixing with the right-handed \tilde{N} fields opens up the possibility to have viable sneutrino cold dark matter. A fraction of the configurations are excluded by direct detection, but now, contrary to the minimal MSSM case, a large portion of the supersymmetric parameter space is compatible with the direct detection bound, both for cosmologically dominant (denoted by [red] crosses) and subdominant ([blue] points) sneutrinos. The occurrence of sneutrinos which are not in conflict with direct detection limits and, at the same time, are the dominant dark matter component, is a very interesting feature of this class of models. Fig. 15 compares our theoretical calculations with the DAMA/NaI region (comparison with the CDMS upper bounds in straightforward): it is clearly seen that sneutrino dark matter could explain the annual modulation effect (as well as neutralinos do in many realizations of supersymmetric theories [73, 74, 75]).

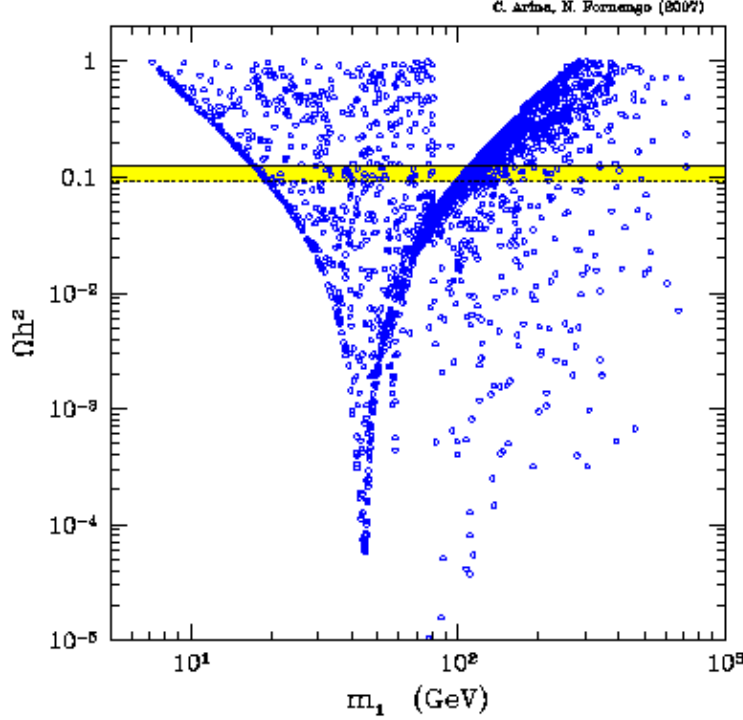


Figure 14: LR models – Scatter plot of the sneutrino relic abundance Ωh^2 as a function of the sneutrino mass m_1 , for a full scan of the supersymmetric parameter space, as explained in the text. The sneutrino parameters are varied as follows: $100 \text{ GeV} \leq m_L \leq 3 \text{ TeV}$, $1 \text{ GeV} \leq m_N \leq 1 \text{ TeV}$ and $1 \text{ GeV}^2 \leq F^2 \leq 10^6 \text{ GeV}^2$. The horizontal solid and dotted lines delimit the WMAP interval for cold dark matter.

The correlation between the direct-detection relevant cross section $\xi \sigma_{\text{nucleon}}^{(\text{scalar})}$ and the relic abundance is shown in Fig. 16. Cosmologically dominant (or slightly subdominant) sneutrinos are compatible with the current level of sensitivity of direct-detection experiments, as discussed above. Nevertheless, a fraction of these configurations refer to direct-detection cross-sections which are up to 4 orders of magnitude below current sensitivities. At the same time, a fraction of the configurations which are at the level of direct detection sensitivity refer to quite small values of the sneutrino relic abundance: these subdominant sneutrinos correspond to a case where the dark matter is mostly composed of a different candidate, but nevertheless represent a relic from the early Universe potentially detectable in the laboratory (a very interesting situation by itself!). Fig. 16 shows that, provided a suitable model like the LR one discussed here, sneutrino dark matter may exhibit a phenomenology which is not very different from the neutralino in a low-energy effective MSSM.

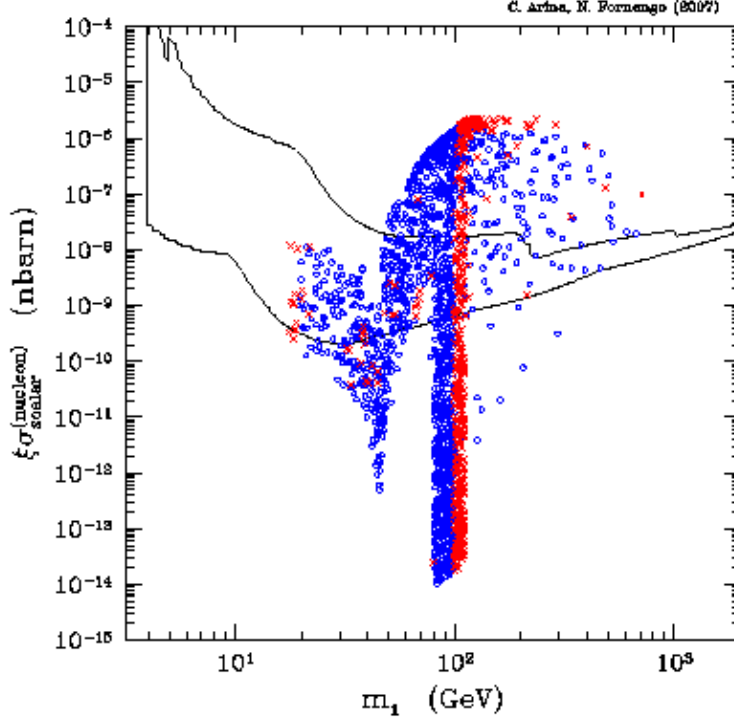


Figure 15: LR models – Sneutrino–nucleon scattering cross section $\xi\sigma_{\text{nucleon}}^{(\text{scalar})}$ as a function of the sneutrino mass m_1 , for a full scan of the supersymmetric parameter space. Parameters are varied as in Fig. 14. [Red] crosses refer to models with sneutrino relic abundance in the cosmologically relevant range; [blue] open circles refer to cosmologically subdominant sneutrinos. The solid curve shows the DAMA/NaI region, compatible with the annual modulation effect observed by the experiment [41, 42, 43, 44, 45].

Figs. 17, 18 and 19 show the distribution of the allowed configurations in three different sections of the sneutrino parameter space. In all three figures, [red] crosses refer to models with sneutrino relic abundance in the cosmologically relevant range; [blue] dots refer to cosmologically subdominant sneutrinos; open dots mark the configurations which have a direct–detection cross section in the current sensitivity range. Fig. 17 shows that, when m_N is below 100 GeV, cosmologically allowed configurations require m_L to be close to its lower limit: this is necessary in order to have a large enough mixing angle θ , which otherwise would produce an exceedingly large relic abundance. The off-diagonal parameter F^2 needs also to be tuned accordingly, in a range from 10^2 GeV^2 to 10^4 GeV^4 , as displayed in Fig. 18. When m_N crosses the lower bound on m_L , more wide possibilities open up. Light sneutrinos, with masses below 40–50 GeV, need values of the mixing angle such that $\sin \theta$ is around 0.05–0.5, with the specific correlation shown in Fig. 19. The correlation with

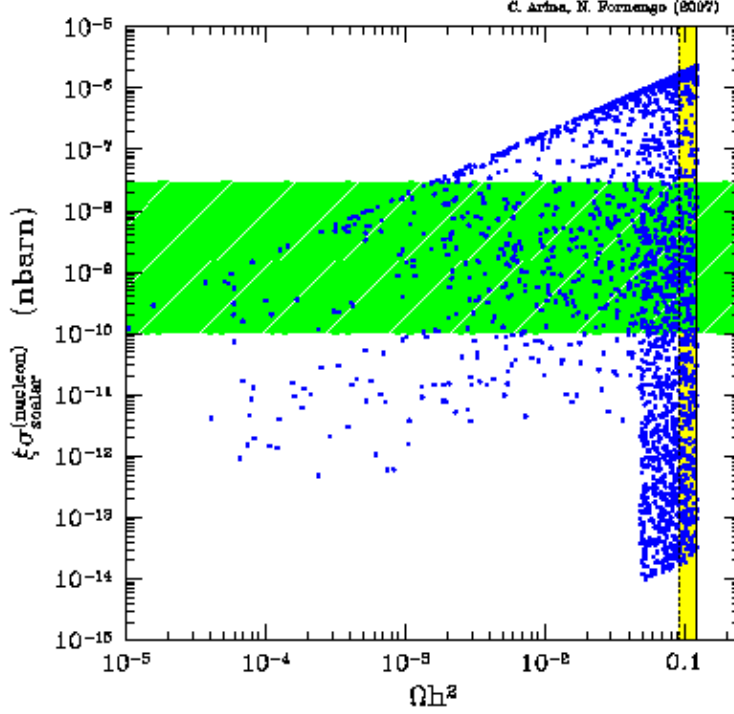


Figure 16: LR models – Sneutrino–nucleon scattering cross section $\xi\sigma_{\text{nucleon}}^{(\text{scalar})}$ vs. the sneutrino relic abundance Ωh^2 , for a full scan of the supersymmetric parameter space. Parameters are varied as in Fig. 14. The horizontal [green] band denotes the current sensitivity of direct detection experiments; the vertical [yellow] band delimits the WMAP interval for cold dark matter.

values of $\xi\sigma_{\text{nucleon}}^{(\text{scalar})}$ in the current direct–detection sensitivity range are also displayed: the most relevant feature is that they require F^2 to be large when m_N is large, in order to procure enough mixing to reduce the direct detection cross–section to acceptable levels at large sneutrino masses.

Now that we have assessed the possibility to have viable sneutrino dark matter candidates, let us now move to the study of their indirect detection signals. Dark matter particles distributes in the galactic halo may annihilate in pairs and produce a bunch of possible signals. Among these signals antimatter, namely antiprotons and antideuterons [76], and gamma–rays may be produced. Exhaustive and detailed studies have been performed for the case of neutralino dark matter, but not yet for sneutrino relics.

We start by studying the antiproton signal. The antiproton source term $q_{\bar{p}}^{\text{DM}}(r, z; T_{\bar{p}})$ at a given position in the Galaxy, defined by the radial component along the galactic plane

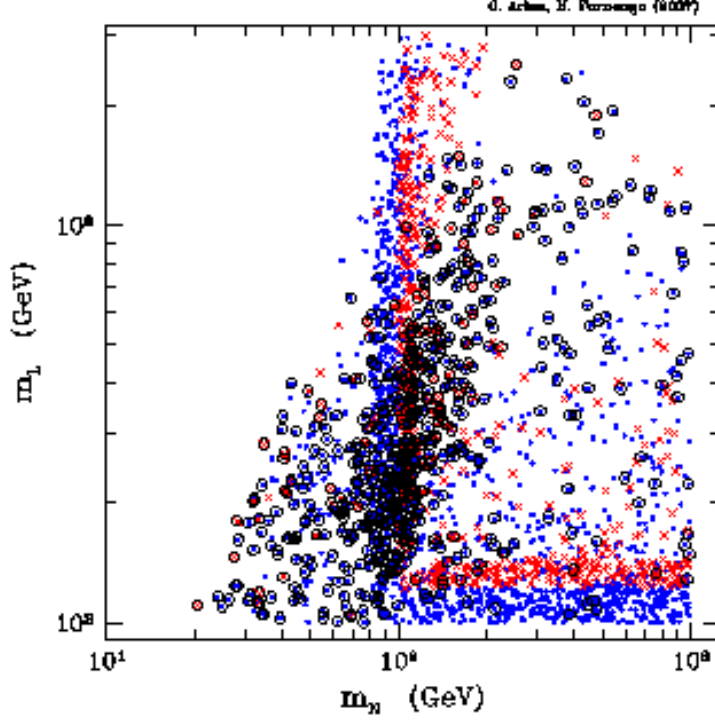


Figure 17: LR models – Distribution of cosmologically acceptable models in the $m_N - m_L$ plane, when a full scan of the supersymmetric parameter space is performed. Parameters are varied as in Fig. 14. [Red] crosses refer to models with sneutrino relic abundance in the cosmologically relevant range; [blue] dots refer to cosmologically subdominant sneutrinos; open dots mark the configurations which have a direct-detection cross section in the current sensitivity range.

r and the vertical component z , is defined as:

$$q_{\bar{p}}^{\text{DM}}(r, z; T_{\bar{p}}) = \frac{1}{2} \langle \sigma_{\text{ann}} v \rangle_0 g_{\bar{p}}(T_{\bar{p}}) \left[\frac{\rho_{\tilde{\nu}_1}}{m_1} \right]^2 \quad (3.9)$$

where $T_{\bar{p}}$ is the antiproton kinetic energy, $\langle \sigma_{\text{ann}} v \rangle_0$ denotes the sneutrino annihilation cross section averaged over the velocity distribution of sneutrinos in the Galaxy (which are strongly non-relativistic since their average velocity is of the order of $\beta \sim 10^{-3}$), $g_{\bar{p}}(T_{\bar{p}})$ is the antiproton energy-spectrum per annihilation event and $\rho_{\tilde{\nu}_1}(r, z)$ denotes the sneutrino density distribution, which is assumed to be proportional to the total dark matter density distribution as $\rho_{\tilde{\nu}_1}(r, z) = \xi \rho_{\text{DM}}(r, z)$, in order to take into account both dominant and subdominant sneutrino relics. The energy-spectrum $g_{\bar{p}}(T_{\bar{p}})$ is a sum over the different

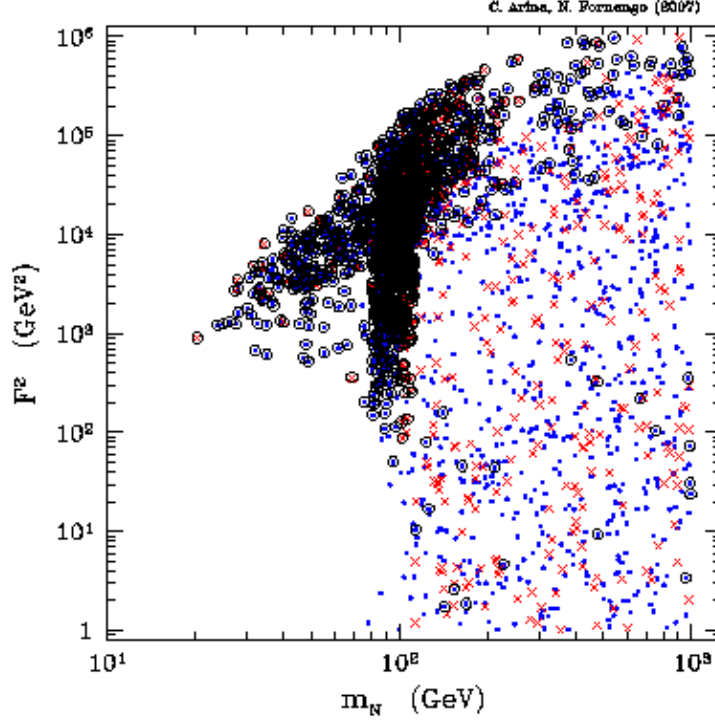


Figure 18: LR models – Distribution of cosmologically acceptable models in the $m_N - F^2$ plane, when a full scan of the supersymmetric parameter space is performed. Parameters are varied as in Fig. 14. [Red] crosses refer to models with sneutrino relic abundance in the cosmologically relevant range; [blue] dots refer to cosmologically subdominant sneutrinos; open dots mark the configurations which have a direct-detection cross section in the current sensitivity range.

energy spectra produced by the various final states of the annihilation process:

$$g_{\bar{p}}(T_{\bar{p}}) = \sum_F \text{BR}(\tilde{\nu}_1 \tilde{\nu}_1 \rightarrow F) \left(\frac{dN_{\bar{p}}^F}{dT_{\bar{p}}} \right) \quad (3.10)$$

where F labels the final states. We have modelled the spectra $dN_{\bar{p}}^F/dT_{\bar{p}}$ as discussed in Refs. [77], by means of a semi-analytic calculation which follows the production and decay chain of each final state until a quark is produced. We use detailed fits and interpolations over the results of PYTHIA [78] simulations for the treatment of the processes involved in the quark hadronization the subsequent hadron decays [77]. The antiproton source spectra are then propagated in the galactic environment to determine the antiproton flux at the local position in the Galaxy $\Phi(R_0, 0, T_{\bar{p}})$:

$$q_{\bar{p}}^{\text{DM}}(r, z; T_{\bar{p}}) \longrightarrow \Phi(R_0, 0, T_{\bar{p}}) \quad (3.11)$$

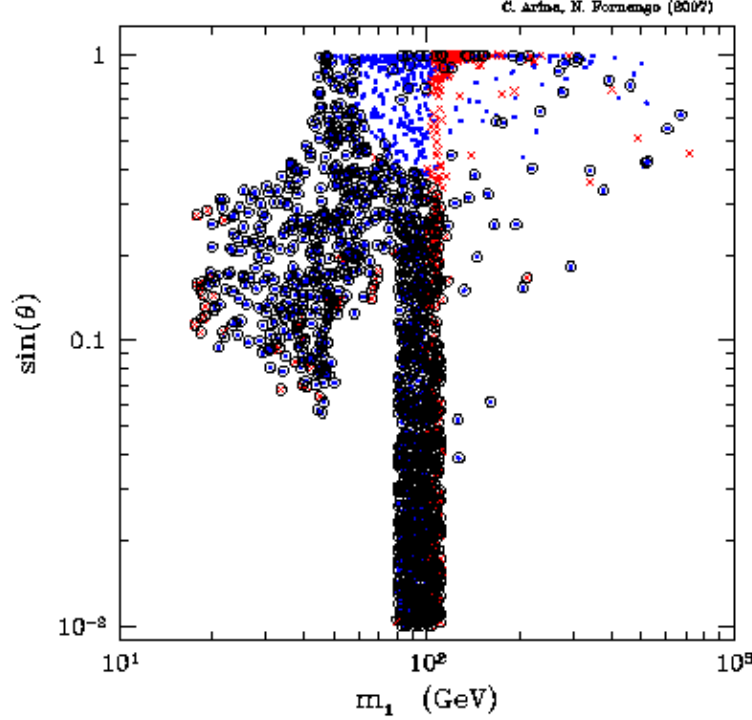


Figure 19: LR models – Distribution of cosmologically acceptable models in the $m_1 - \sin \theta$ plane, when a full scan of the supersymmetric parameter space is performed. Parameters are varied as in Fig. 14. [Red] crosses refer to models with sneutrino relic abundance in the cosmologically relevant range; [blue] dots refer to cosmologically subdominant sneutrinos; open dots mark the configurations which have a direct-detection cross section in the current sensitivity range.

We model the galactic environment as a two-zone diffusion model and for the solution of the propagation equation, which takes into account antiproton diffusion, scattering, annihilation, energy losses, propagation against the galactic wind and reacceleration, we use the results of Ref. [77], where a detailed analysis which takes into account astrophysical uncertainties (relevant for the antiproton signal) are discussed. Theoretical uncertainties are large and we will comment on this point: in all our figures we will show the result for the median estimate of the antiproton signal, as defined in Ref. [77]. The antiproton flux has then to be propagated against the solar wind in order to provide fluxes at the Earth position, *i.e.* "top-of-atmosphere" (TOA) fluxes. We will show our results for a period of solar minimum activity.

Antiproton fluxes from sneutrino annihilation in the galactic halo are provided in Fig. 20 and 21 which show scatter plots of fluxes calculated at fixed antiproton kinetic energies: $T_{\bar{p}} = 0.23$ GeV in Fig. 20 and $T_{\bar{p}} = 37.5$ GeV in Fig. 21. The scatter plots refer to

cosmologically acceptable configurations: the [red] crosses denote cosmologically dominant sneutrinos, the [blue] points refer to the case of subdominant sneutrinos. The small grey points show those configurations which are excluded by direct detection. In Fig. 20, which refers to the flux in a low-energy bin where the antiproton signal may have better possibility to be disentangled by the background which is due to cosmic-rays spallation over the galactic medium. The [yellow] shaded area denotes the amount of exotic antiprotons which can be accommodated in the BESS data [79, 80] in that energy bin. This has been established on the basis of the theoretical calculation of the antiproton background [81] and of the BESS measurements [79, 80], by determining the maximal amount of exotic antiproton flux which can be accommodated on the top of the background, without entering in conflict with the BESS data and its experimental error, at 90% C.L. We see that the theoretical predictions are not currently excluded by BESS: the maximal predictions, which occur for sneutrino masses in the range 50–200 GeV, are at least one order of magnitude below the current BESS bound. However, we have to remind that the theoretical estimates of the antiproton signal are largely affected by astrophysical uncertainties related to the knowledge of the parameters which enter the diffusion equation. It has been shown in Ref. [77] that this uncertainty can lead to an increase of about a factor of 8 or a decrease of up to a factor of 10. Therefore, our prediction in Fig. 20 may be altered by this factor for different choices of the propagation parameters in their allowed ranges [82]. In the case of the choice of astrophysical parameters which produce the maximal antiproton signal, the scatter plot in Fig. 20 would be enhanced by a factor of 8: in this case, still BESS data would not exclude any sneutrino configuration, but all the mass range from 50 to 200 GeV would have configurations potentially detectable with just a small increase in the experimental sensitivity.

Prospects for the future are shown by the dashed and dotted horizontal lines, which denote our estimated sensitivity of the PAMELA [83] (dashed line) and AMS [84] (dotted line) detectors to exotic antiprotons after a run of 3 years: the sensitivities are determined as admissible excess within the statistical experimental uncertainty if the measured antiproton flux consists only in the background (secondary) component. The estimate has been performed by using the background calculation of Ref. [81], and refers to a $1\text{-}\sigma$ statistical uncertainty. All the supersymmetric configurations in Fig. 20 above the dashed or dotted lines can be potentially identified by PAMELA or AMS as a signal over the secondaries, while those which are below the dashed or dotted lines will not contribute enough to the total flux in order to be disentangled from the background. We therefore see that, in the case of the median antiproton flux shown in the Figure, only AMS will have the possibility to detect a signal from sneutrino dark matter, for masses around 60 GeV or for masses in the range 100–200 GeV. We notice that most of these configurations refer to subdominant sneutrinos: this justifies the approach to consider relic particle candidates also when they are not dominant dark matter components, since a signal from relic particles in the galaxy may well be discovered.

Fig. 20 also shows that, in the case of astrophysical propagation parameters close to the values which provide the maximal antiproton signal, both PAMELA and AMS will have good chances of detection, for sneutrinos in the mass range 50–200 GeV. We also

notice that in this case a large fraction of configurations with masses in the range 65–130 GeV, and which could be potentially detectable by AMS, are actually already excluded by direct detection (grey points). This shows a very nice interplay between different dark matter searches techniques. This is further elucidated in Fig. 22, where the antiproton signal is plotted against the direct detection cross section $\xi\sigma_{\text{nucleon}}^{(\text{scalar})}$. The current bound from both BESS data and from direct detection experiments is shown, as well as the foreseen capabilities of PAMELA and AMS, together with the current direct-detection sensitivity region. From this figure we see that a fraction of the configurations which are currently excluded by direct detection would have been in reach of PAMELA and AMS. More interestingly, Fig. 22 shows that direct detection and antiproton searches offer a good deal of complementarity. Direct detection is sensitive to configurations which will be hardly probed by antiproton searches (those points inside the vertical [green] band and which refer to low antiproton fluxes). On the contrary, some configurations which refer to a large antiproton signal but are below current direct detection sensitivity are also present. Nevertheless, from this figure direct detection appears to be a stronger probe to sneutrino dark matter (in the sense that it can explore a wider region of the parameter space) but good chances of antiproton detection are also present.

We come back now to Fig. 21, where the antiproton signal is calculated for a higher antiproton kinetic energy: $T_{\bar{p}} = 37.5$ GeV. At this energy, the CAPRICE experiments reports the detection of a flux which is potentially in excess of the theoretical background [85]. Although this excess has a small statistical significance, nevertheless is an intriguing possibility to be studied. In Fig. 21 we show the band which refers to a signal which would fill the CAPRICE excess. The scatter plot of the theoretical prediction for sneutrino dark matter is not able to reach the level of the CAPRICE excess, for the median choice of astrophysical parameters. We nevertheless comment that for the maximal choice, a marginal compatibility would arise, for sneutrino masses in the range 200–500 GeV. In Fig. 21 we also show our estimated sensitivities for PAMELA and AMS, determined as we discussed above for the lower energy bin. For the median choice of astrophysical parameters, AMS will have a marginal detection potential, while for the maximal case, both AMS and PAMELA will probe configurations in the mass range 200–500 GeV. Light sneutrinos are not probed at this antiproton energies: they cannot produce antiprotons at energies above their mass, since annihilation occurs almost at rest.

Another indirect detection signal which is very promising is the production of antideuterons [76]. In this paper especially it has been shown that the low energy tail of the antideuteron signal offers a good possibility to disentangle the signal from the background, since kinematical conditions allow low-energy antideuterons to be produced in the dark matter pair annihilation easily, while the spallation process is suppressed below a kinetic energy per-nucleon of $T_{\bar{D}} = 1\text{--}3$ GeV/n. The predictions for sneutrino dark matter are shown in Fig. 23 for $T_{\bar{D}} = 0.23$ GeV/n. No experimental limit is currently available, but detectors, which will be able to reach good sensitivities, are under development: Fig. 23 shows the expected sensitivity of the GAPS [86, 87] and AMS [84] detectors. We see that antideuteron searches will offer a sensitivity to sneutrino dark matter similar to antiproton searches. A signal detectable in one channel by two different detectors, will be

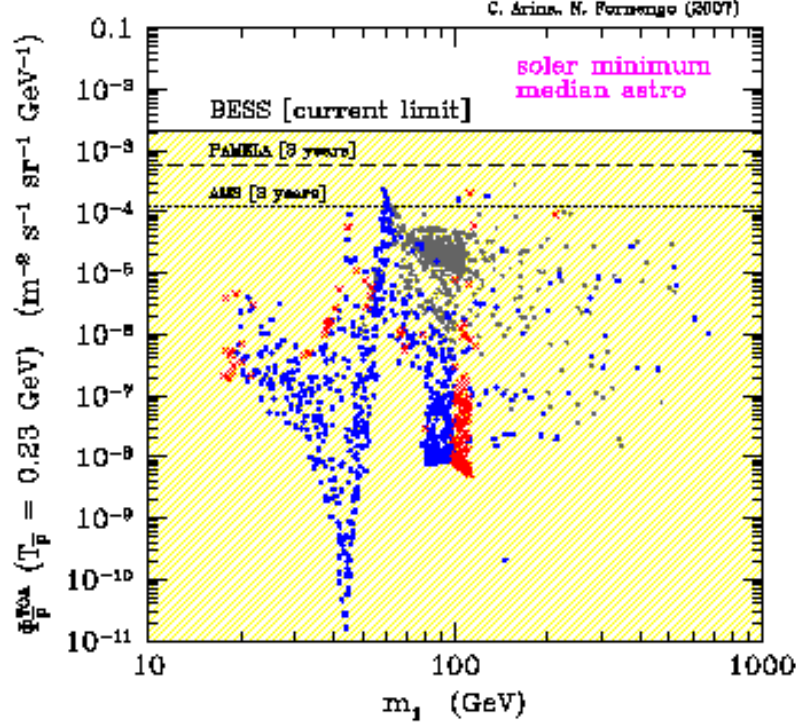


Figure 20: LR models – Antiproton flux at the antiproton kinetic energy $T_{\bar{p}} = 0.23$ GeV as a function of the sneutrino mass m_1 , for the galactic propagation parameters which provide the median value of antiproton flux and for a solar activity at its minimum. [Red] crosses refer to models with sneutrino relic abundance in the cosmologically relevant range; [blue] dots refer to cosmologically subdominant sneutrinos; light gray points denote configurations which are excluded by direct detection searches. The [yellow] shaded area denotes the amount of exotic antiprotons which can be accommodated in the BESS data [79, 80]. The dashed and dotted lines show the PAMELA [83] and AMS [84] sensitivities to exotic antiprotons for 3 years missions, respectively.

detectable also in the other channels, again in two different experiments. Moreover, one of the detector, AMS, has the capabilities to detect a signal in both channels. The possibility to cross-correlate different signals and to complement their information would be an extraordinary opportunity for dark matter searches. This is further complemented by direct detection, as discussed above.

We now move to discuss the signal which consists in the production of a diffuse gamma-rays flux. Sneutrino annihilations may produce, through the decay chain of their annihilation products, also gamma-rays, which mostly come from the decay of neutral pions and other mesons produced in the annihilation process. The gamma ray flux arriving at the Earth from a given angular position ψ in the sky is the integral along the line of sight of

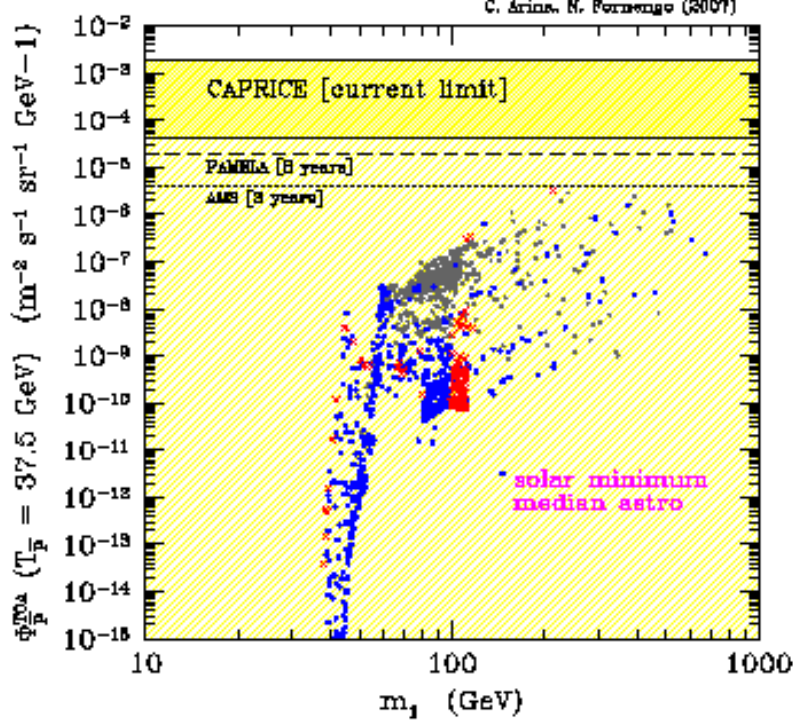


Figure 21: LR models – Antiproton flux at the antiproton kinetic energy $T_{\bar{p}} = 37.5$ GeV as a function of the sneutrino mass m_1 . Notations are as in Fig. 20, except for the upper [yellow] shaded band, which delimits the possible excess over the background in the CAPRICE data [85]. The lower [yellow] area refers to fluxes compatible with CAPRICE.

all the differential contributions of sneutrino annihilation:

$$\Phi_{\gamma}^{\text{DM}}(E_{\gamma}, \psi) = \frac{1}{4\pi} \frac{\langle \sigma_{\text{ann}} v \rangle_0}{2m_{\chi}^2} g_{\gamma}(E_{\gamma}) I(\psi) \quad (3.12)$$

where $g_{\gamma}(E_{\gamma})$ is the gamma-ray spectrum, defined analogously as we defined above the antiproton spectrum $g_{\bar{p}}(T_{\bar{p}})$ and $I(\psi)$ denotes the line-of-sight integral of the squared of the dark matter density in the direction ψ :

$$I(\psi) = \int_{\text{l.o.s.}} \rho_{\tilde{\nu}_1}^2[r(\lambda, \psi)] d\lambda \quad (3.13)$$

For the production of gamma-rays arising from the hadronization of quarks and the subsequent decay of hadrons, we use the detailed fit of PHYTIA simulations of Ref. [96, 97].

Fig. 24 shows our predictions for the gamma-ray flux at $E_{\gamma} = 1.5$ GeV coming from the center of the Galaxy, in an angular bin which corresponds to the EGRET [90, 91] field of view. The choice of the energy bin refers to the case where EGRET detects an excess

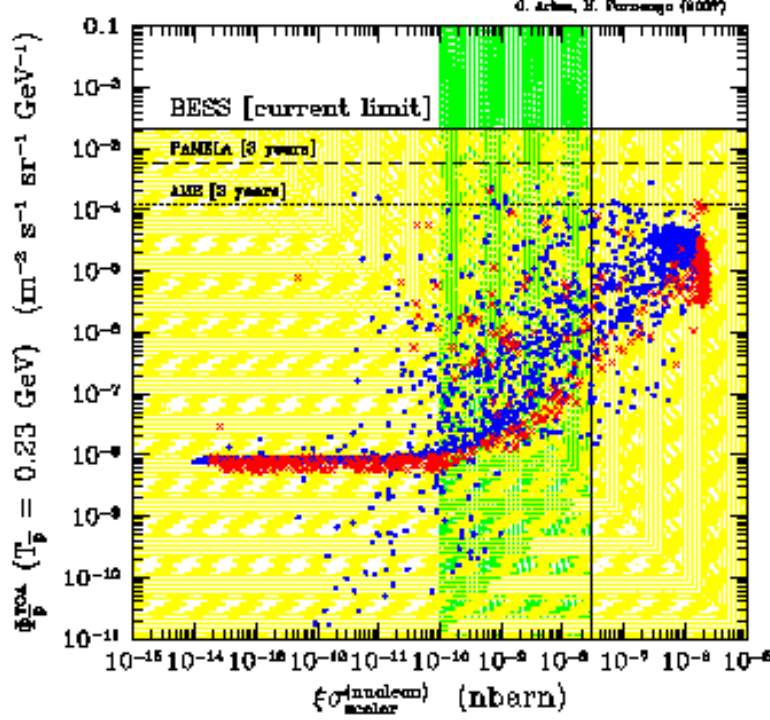


Figure 22: LR models – Antiproton flux at the antiproton kinetic energy $T_{\bar{p}} = 0.23$ GeV vs. the sneutrino–nucleon scattering cross section $\xi \sigma_{\text{nucleon}}^{(\text{scalar})}$. [Red] crosses refer to models with sneutrino relic abundance in the cosmologically relevant range; [blue] dots refer to cosmologically subdominant sneutrinos. The horizontal solid line denotes the upper limit from BESS [79, 80] and the [yellow] shaded area shows the amount of exotic antiprotons which can be accommodated in the BESS data. The dashed and dotted horizontal lines show the PAMELA [83] and AMS [84] sensitivities to exotic antiprotons for 3 years missions, respectively. The vertical solid line denotes a conservative upper limit from direct detection searches and the [green] vertical shaded area refers to the current sensitivity in direct detection searches.

of gamma-rays over the background from the galactic center. The [yellow] shaded area in fact refers to this excess: exotic gamma-ray fluxes inside this band are compatible with the EGRET measurement and those close to the solid horizontal line, which delimits the area, are able to explain the excess.

The gamma-ray signal is strongly sensitive to the behavior of the dark matter density profile toward the inner regions of the Galaxy. In Fig. 24 we have used a strongly peaked profile: the radial behavior is $r^{-1.5}$, like the Moore et al. profile [88, 89] or those obtained from milder distributions by effects due to the growth of a black hole [98, 99, 100] or of baryon dissipation [101, 102]. For a NFW profile with a r^{-1} behavior, our theoretical

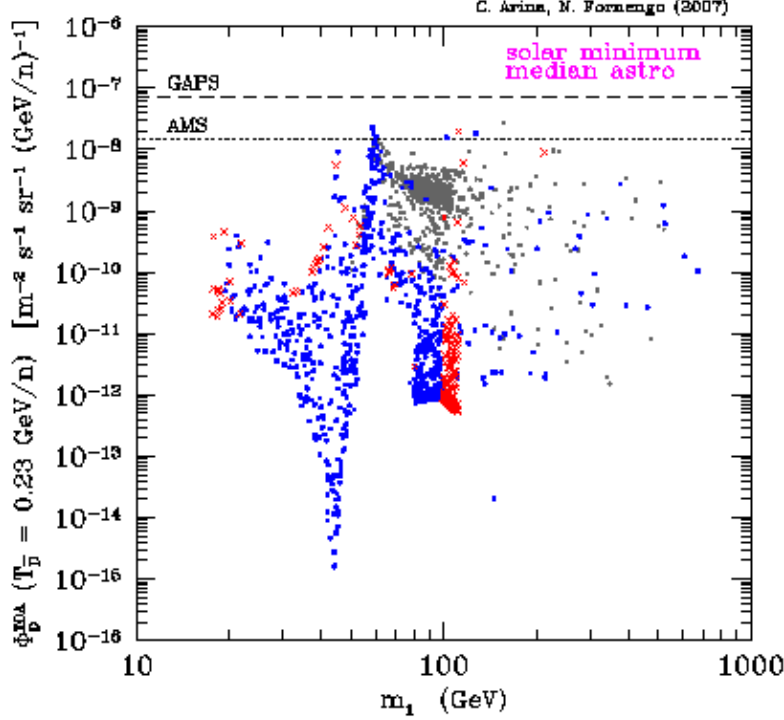


Figure 23: LR models – Antideuteron flux at the antideuteron kinetic energy (per nucleon) $T_{\bar{d}} = 0.23 \text{ GeV/n}$, as a function of the sneutrino mass m_1 . Notations are as in Fig. 20. The dashed and dotted lines show the GAPS [86, 87] and AMS [84] sensitivities.

estimates would decrease by a factor of 60 and an additional factor of 10 for cored profiles [96].

Fig. 24 shows that, for an $r^{-1.5}$ profile, sneutrino dark matter is at the level of explaining the EGRET excess, for masses in the range 60–250 GeV. Most of these configurations refer to subdominant sneutrinos. Clearly for an NFW profile the predicted fluxes are too low to fill the EGRET excess.

Fig. 24 also shows our estimate for the capabilities of GLAST, for a 1-year data-taking. We have taken into account GLAST effective area as shown in Ref. [92], and we have derived our predictions for the same angular energy bin of EGRET. We see that GLAST will be sensitive to configurations of masses between 30 GeV and 600 GeV, and will be close to access also very light sneutrinos with further live-time of data. Again we have to warn that in the case of less steep profiles, the sensitivity of GLAST will be restricted to a smaller mass range (60–300 GeV), but nevertheless a good deal of configurations will be probed. We comment also that the angular resolution of GLAST will be much better than the EGRET one and therefore the capabilities of GLAST would be even more promising

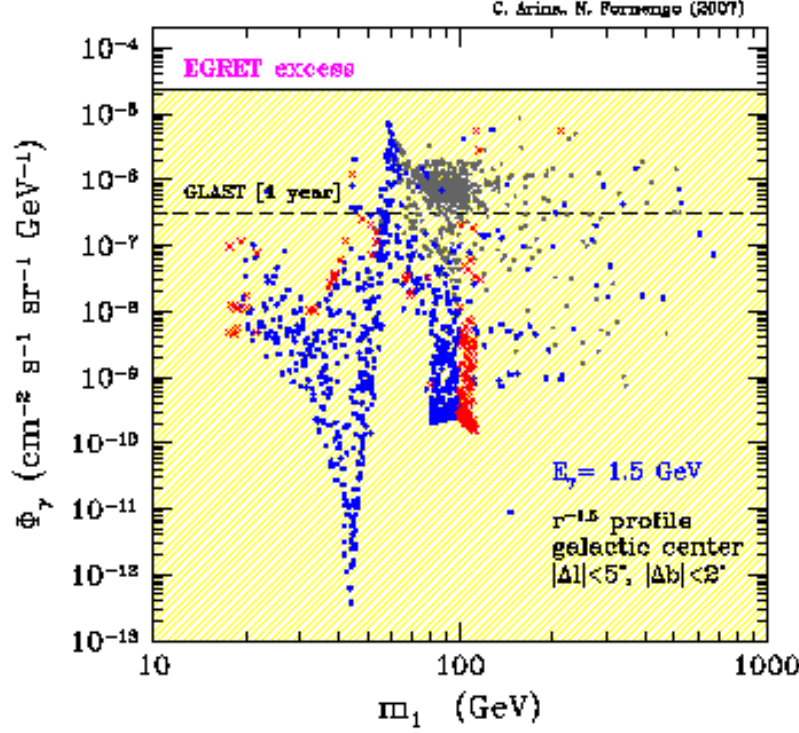


Figure 24: LR models – Gamma-ray flux from the galactic center at the photon energy $E_\gamma = 1.5$ GeV, as a function of the sneutrino mass m_1 , for a galactic profile of Moore’s type [88, 89] and for the angular resolution of EGRET [90, 91]. [Red] crosses refer to models with sneutrino relic abundance in the cosmologically relevant range; [blue] dots refer to cosmologically subdominant sneutrinos; light gray points denote configurations which are excluded by direct detection searches. The [yellow] shaded area denotes the amount of exotic gamma-rays compatible with the EGRET excess [90, 91]. The dashed line shows the GLAST [92] sensitivity for a 1 year data-taking and for the same EGRET angular bin.

than those shown in Fig. 24.

Finally, we mention that indirect detection of dark matter could also be performed at neutrino telescopes, since dark matter may accumulate in the central regions of the Earth and the Sun by gravitational capture and there annihilate. The only annihilation products which can escape are neutrinos, and these can be searched for as upgoing muons in a neutrino telescope. In Fig. 25 we show the predictions for upgoing muons from the Earth [103] and compare them with the current experimental limits from SuperKamionande, MACRO and AMANDA. We see that neutrino telescopes are sensitive to a large fraction of sneutrino configurations, although many of the configuration which are excluded by this technique are also excluded by direct detection. This is manifest in Fig. 26, which shows

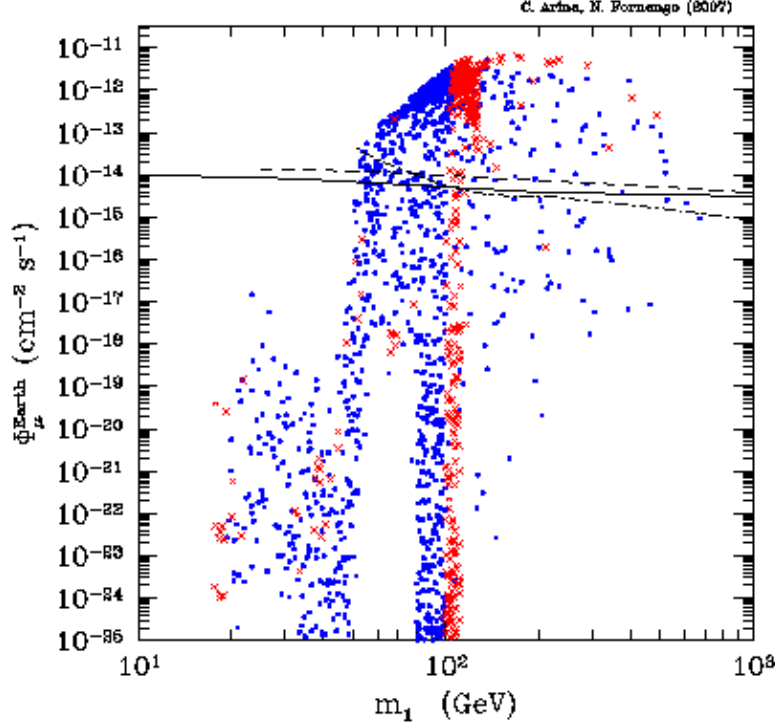


Figure 25: LR models – Upgoing muon flux from sneutrino pair annihilation in the center of the Earth $\Phi_{\mu}^{\text{Earth}}$, as a function of the sneutrino mass m_1 . [Red] crosses refer to models with sneutrino relic abundance in the cosmologically relevant range; [blue] dots refer to cosmologically subdominant sneutrinos. The solid, dashed and dot-dashed lines denote the upper limits from the SuperKamiokande [93], MACRO [94] and AMANDA [95] detectors, respectively.

the correlation of the upgoing muon flux from the Earth with the direct detection cross section $\xi\sigma_{\text{nucleon}}^{(\text{scalar})}$.

4. Models with a lepton–number violating term

Models with lepton–number violating terms can allow for Majorana neutrino masses. The most direct way to include a Majorana mass term is to introduce a gauge–invariant dimension–5 operator of the type [7, 13, 35, 28]:

$$\mathcal{L} = \frac{g_{IJ}}{M_{\Lambda}} (\epsilon_{ij} L_i^I H_j) (\epsilon_{kl} L_k^J H_l) + \text{h.c.} \quad (4.1)$$

In this case, a Majorana mass term for the neutrino is generated when the neutral component of the Higgs field acquires a vacuum expectation value and the neutrino mass which arises is of the order of $m_M \sim gv^2/M_{\Lambda}$. This can be made compatible with neutrino mass

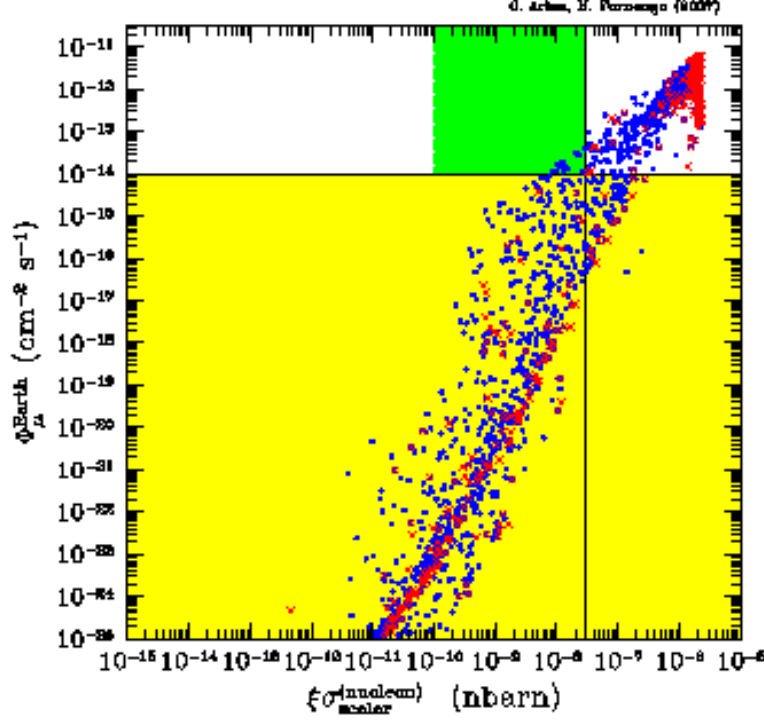


Figure 26: LR models – Upgoing muon flux from sneutrino pair annihilation in the center of the Earth $\Phi_{\mu}^{\text{Earth}}$ vs. the sneutrino–nucleon scattering cross section $\xi \sigma_{\text{nucleon}}^{(\text{scalar})}$. [Red] crosses refer to models with sneutrino relic abundance in the cosmologically relevant range; [blue] dots refer to cosmologically subdominant sneutrinos. The horizontal solid line denotes the current upper limit from neutrino telescopes. The vertical solid line denotes a conservative upper limit from direct detection searches and the [green] vertical shaded area refers to the current sensitivity in direct detection searches.

bounds for M_{Λ} close to the GUT scale. The dimension–5 operator is clearly not fundamental as an extension, and makes the supersymmetric lagrangian non–renormalizable. Nevertheless, this operator may arise as an effective term from new physics at the high energy scale M_{Λ} .

If we apply this extension at the MSSM lagrangian, we are allowed for a L –number violating term also in the sneutrino lagrangian, which modifies the mass–term potential as:

$$V_{\text{mass}} = \left[m_L^2 + \frac{1}{2} m_Z^2 \cos(2\beta) \right] \tilde{\nu}_L^* \tilde{\nu}_L + \frac{1}{2} m_B^2 (\tilde{\nu}_L \tilde{\nu}_L + \tilde{\nu}_L^* \tilde{\nu}_L^*) \quad (4.2)$$

where m_B is a mass parameter that makes the mass lagrangian no longer diagonal in the

$(\tilde{\nu}_L \tilde{\nu}_L^*)$ basis. In this basis the squared-mass matrix reads:

$$\mathcal{M}_{\tilde{\nu}}^2 = \begin{pmatrix} m_L^2 + \frac{1}{2}m_Z^2 \cos(2\beta) & m_B^2 \\ m_B^2 & m_L^2 + \frac{1}{2}m_Z^2 \cos(2\beta) \end{pmatrix} \quad (4.3)$$

and it may be conveniently diagonalized by a rotation into a basis defined by the CP-even $\tilde{\nu}_+$ and CP-odd $\tilde{\nu}_-$ sneutrino eigenstates [7]:

$$\begin{cases} \tilde{\nu}_+ = \frac{1}{\sqrt{2}} (\tilde{\nu} + \tilde{\nu}^*) \\ \tilde{\nu}_- = \frac{-i}{\sqrt{2}} (\tilde{\nu} - \tilde{\nu}^*) \end{cases} \quad (4.4)$$

The states $\tilde{\nu}_+$ and $\tilde{\nu}_-$ are also mass eigenstates. The squared-mass eigenvalues are easily computed:

$$m_{1,2}^2 = m_L^2 + \frac{1}{2}m_Z^2 \cos(2\beta) \pm m_B^2 \quad (4.5)$$

which implies $\Delta m^2 \equiv m_2^2 - m_1^2 = 2m_B^2$. The mixing angle is fixed at the value $\theta = \pi/4$. We name this models “ \mathcal{L} models”. They have the same field content as the minimal MSSM, but include the additional \mathcal{L} terms. The parameters relevant for the sneutrino sector are m_L and m_B .

The Z coupling to sneutrinos is non-diagonal in the $(\tilde{\nu}_+, \tilde{\nu}_-)$ basis, which are now non-degenerate in mass. The first consequence is that the invisible Z -width decay occurs via the process $Z \rightarrow \nu_1 \nu_2$. By keeping $m_L \gtrsim 100$ GeV (which assures that the charged lepton mass bounds are satisfied) and using suitable values of the off-diagonal m_B parameter, we may obtain lightest sneutrinos lighter than in the minimal MSSM models. From Eq. (4.5) is clear that when m_B is large (close to its allowed upper limit, which is due to preventing a tachionic sneutrino) m_1 can be small. At the same time m_2 is large and the sum of the two never gets smaller than m_Z (for our parameter intervals). In this case, the Z invisible width does not get contributions and light sneutrinos are possible.

In \mathcal{L} models, however, we have an additional bound, which is related to neutrino physics. The \mathcal{L} terms may induce radiative contributions to the neutrino masses [8, 13, 35, 28]. At 1-loop, these corrections arise from diagrams involving sneutrinos and neutralinos. We include this constraint by calculating the 1-loop radiative contribution to the neutrino mass $\Delta m_{\text{neutrino}}^{\text{1loop}}$ as detailed in Ref. [35], and then imposing that $|\Delta m_{\text{neutrino}}^{\text{1loop}}|$ does not exceed the experimental upper bound on the neutrino mass. This constraint coming from the 1-loop contribution $\Delta m_{\text{neutrino}}^{\text{1loop}}$ introduces a direct connection of the sneutrino sector to neutrino physics. The 1-loop correction $|\Delta m_{\text{neutrino}}^{\text{1loop}}|$ is basically proportional to the mass difference between the two mass eigenstates $\Delta m_{\text{sneutrino}} = m_2 - m_1$ (which in turn depends on the parameter m_B , as well as m_N). Sneutrino dark matter phenomenology will be therefore bounded by neutrino physics in a non trivial way. This fact will occur also for the class of models of Section 5, where a \mathcal{L} term will also be present.

In Fig. 27 we show the correlation between $|\Delta m_{\text{neutrino}}^{\text{1loop}}|$ and the sneutrino mass difference, for a scan of the sneutrino mass parameters varied in the interval: $80 \text{ GeV} \leq m_L \leq 1000 \text{ GeV}$ and $10^{-4} \text{ GeV} \leq m_B \leq 10^2 \text{ GeV}$. In this figure, the lightest neutralino has been assumed to be a pure bino of 1 TeV mass. As for the neutrino mass bounds, we show in

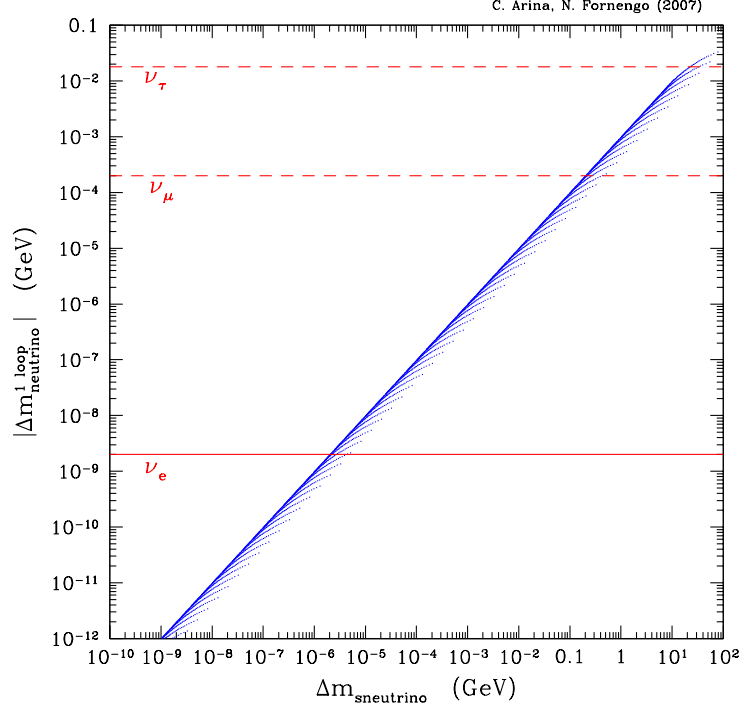


Figure 27: \mathcal{L} models – Absolute value of the 1-loop contribution to the neutrino mass as a function of the mass difference of the two sneutrinos. The sneutrino mass parameters are varied as: $80 \text{ GeV} \leq m_L \leq 1000 \text{ GeV}$ and $10^{-4} \text{ GeV} \leq m_B \leq 10^2 \text{ GeV}$. The lightest neutralino is a pure bino of 1 TeV mass. The horizontal lines denote the upper limits on the neutrino mass, as labelled.

the plot the limits of kinematical origin: 2 eV for electron-type neutrinos [39], 0.2 MeV for muon-type neutrinos [39] and 18 MeV for tau neutrinos [39]. Solar and atmospheric neutrino results [23, 24, 25, 26, 27] as well as cosmological bounds on massive light neutrinos [27, 104, 105] are not compatible with the kinematical bounds on muon and tau neutrinos listed above, unless more than 3 families are present and/or additional sterile neutrinos are introduced with special mixing patterns with active neutrinos. A mass bound of 2 eV is instead a more reliable upper bound on the neutrino mass [27, 104, 105], and our main conclusion will be based on this case.

Fig. 27 shows that a mass bound of 2 eV on the neutrino mass implies a strong degeneracy between the two sneutrino mass eigenstates. In this case, sneutrino phenomenology does not deviate significantly from the minimal MSSM discussed in Section 2. Only when a larger mass bound for neutrinos is allowed, the split between the two mass eigenstates becomes sizeable, reaching the level of 100 MeV for the muon neutrino kinematical mass bound, and even 30 GeV for the tau neutrino kinematical bound. These large corrections

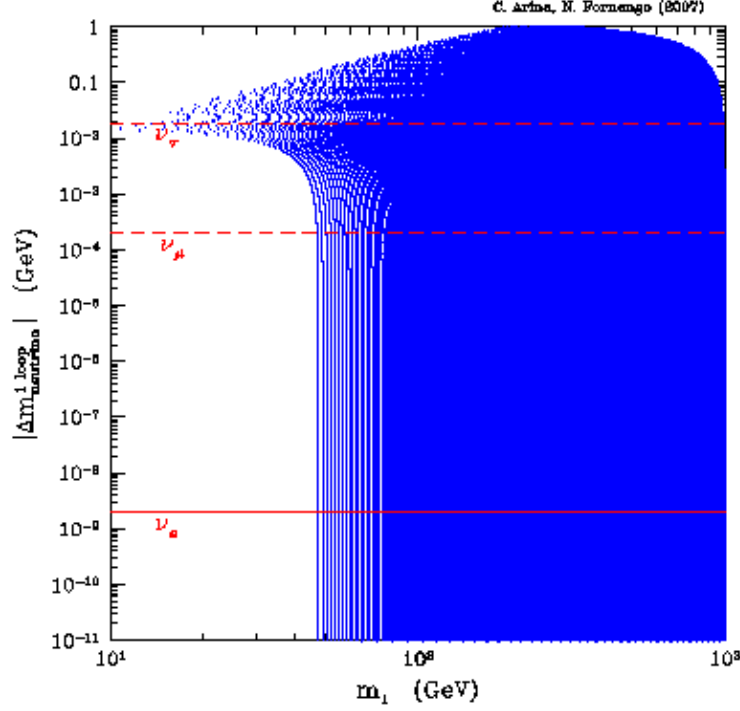


Figure 28: \mathcal{L} models – Absolute value of the 1-loop contribution to the neutrino mass as a function of the mass of lightest sneutrino. The parameters as as in Fig. 27. The horizontal lines denote the upper limits on the neutrino mass, as labelled.

$\Delta m_{\text{neutrino}}^{\text{1loop}}$, and the ensuing large sneutrino mass splittings, occur when one of the sneutrino mass eigenstate is light, opening up the possibility of light sneutrinos, which were precluded in the minimal MSSM. This is shown in Fig. 28, where the 1-loop correction $|\Delta m_{\text{neutrino}}^{\text{1loop}}|$ is plotted versus m_1 . This shows that, under this hypothesis, sneutrinos as light as 10 GeV are possible.

The off-diagonal Z coupling affects also the relic abundance calculations [12]. In this case, the lightest sneutrino is actually co-annihilating with the heavier eigenstate, when a Z -boson is exchanged (while this is not the case, for instance, for higgs exchange: in that case the coupling is diagonal). Therefore, when the mass splitting is large the Z -mediated (co)annihilation cross section gets reduced and the relic abundance may increase. The relic abundance for the \mathcal{L} models is shown in Fig. 29, for a mass bound on the neutrino mass of 18 MeV. This would correspond to the case of a tau sneutrino dark matter, since we are applying the tau neutrino kinematical mass bound. We see that the relic abundance increases, and light sneutrinos down to 10 GeV are acceptable. If we reduce the mass bound on the neutrinos down to 2 eV, this figure reduces to the case of minimal MSSM

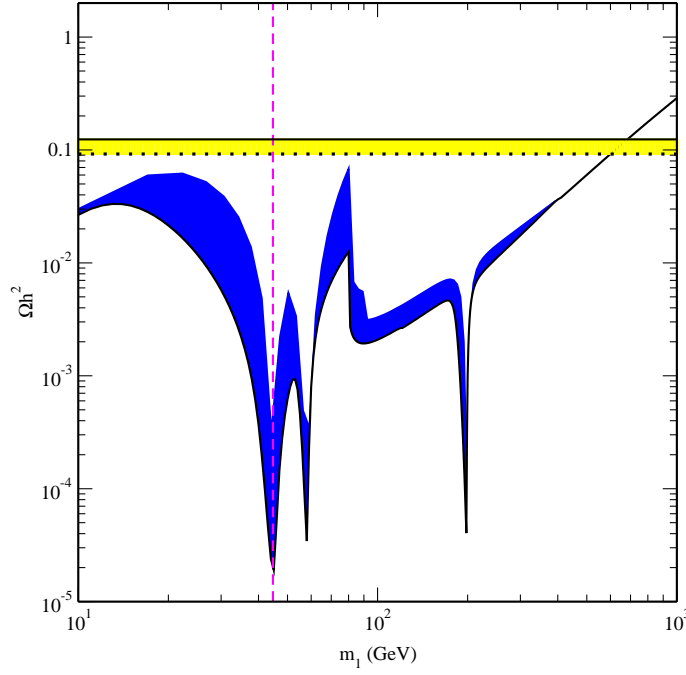


Figure 29: \mathcal{L} models – Sneutrino relic abundance Ωh^2 as a function of the sneutrino mass m_1 . The [blue] band denotes the relic abundance for allowable models due to a variation of the sneutrino parameters in the intervals: $80 \text{ GeV} \leq m_L \leq 1000 \text{ GeV}$ and $10^{-4} \text{ GeV} \leq m_B \leq 10^2 \text{ GeV}$. The other relevant supersymmetric parameters are: lightest neutralino 30% heavier than the sneutrino, higgs masses of 120 GeV for the lightest CP-even higgs h and 400 GeV for the heaviest CP-even H and the CP-odd A . The horizontal solid and dotted lines delimit the WMAP interval for cold dark matter.

discussed in Section 2.

The off-diagonal Z coupling has impact also on direct detection [12]. In this case, the sneutrino–nucleus scattering for Z exchange is no longer elastic, since we have to produce the heavier eigenstate. When the mass difference between the two sneutrinos is large enough, elastic scattering in the detector is suppressed. The lightest sneutrino can scatter on the nucleus only when:

$$\Delta m < \frac{\beta^2 m_1 m_{\mathcal{N}}}{2(m_1 + m_{\mathcal{N}})} \quad (4.6)$$

This is a nice realization of inelastic dark matter, which was discussed extensively in connection with direct detection in Refs. [9, 10, 11].

We therefore have to include this effect in the calculation of the direct detection cross section. This inelasticity effect produces a suppression in the direct detection rates, which depends on the energy of the recoil, the type of nucleus and on the energy threshold of the detector. We define a suppression factor for direct detection as:

$$\mathcal{S} = \frac{\mathcal{R}(E_1, E_2; \Delta m)}{\mathcal{R}(E_1, E_2; 0)} \quad (4.7)$$

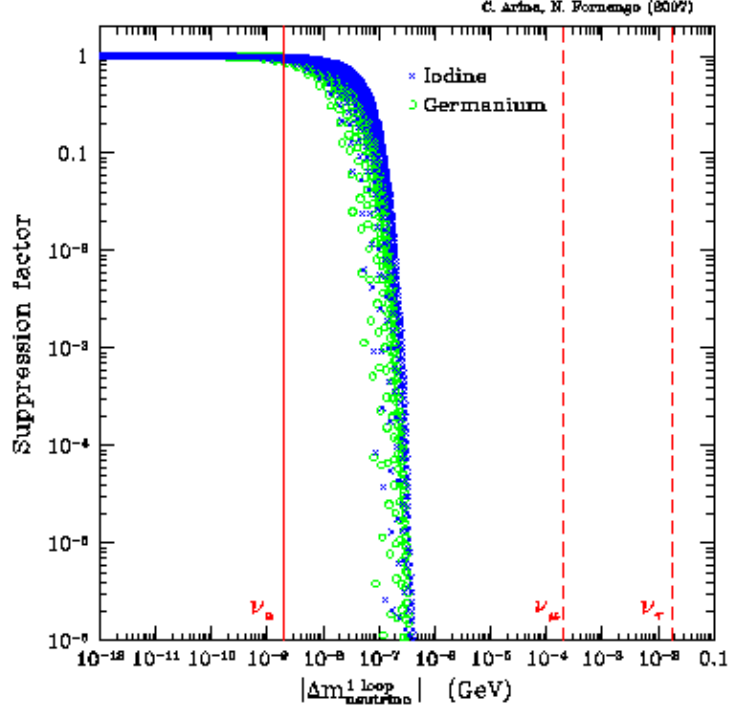


Figure 30: \mathcal{L} models – Suppression factor of the direct detection rate due to the off-diagonal Z -coupling, plotted vs. the absolute value of the 1-loop contribution to the neutrino mass. The sneutrino mass parameters are varied as: $100 \text{ GeV} \leq m_L \leq 1000 \text{ GeV}$ and $10^{-4} \text{ GeV} \leq m_B \leq 10^2 \text{ GeV}$. [Blue] crosses refer to the Iodine nucleus, open [green] circles to the Germanium nucleus. The vertical lines denote the upper limits on the neutrino mass, as labelled.

where $\mathcal{R}(E_1, E_2; \Delta m)$ denotes the direct detection rate integrated in the energy range (E_1, E_2) and calculated for a sneutrino mass difference Δm , while $\mathcal{R}(E_1, E_2; 0)$ is the same quantity calculated for $\Delta m = 0$, *i.e.* in the standard case. The quenched energies $E_1^{\text{ee}}, E_2^{\text{ee}}$ have been chosen to be: $E_1^{\text{ee}} = 2 \text{ KeV}$ and $E_2^{\text{ee}} = 10 \text{ KeV}$ for the Iodine (representative for the DAMA/NAI experiment) and $E_1^{\text{ee}} = 10 \text{ KeV}$ and $E_2^{\text{ee}} = 100 \text{ KeV}$ for the Germanium (representative for the CDMS experiment). The chosen values of E^{ee} correspond to the threshold energy of DAMA/NaI and CDMS. We apply this reduction factor in the following way: instead of modifying the experimental result (which we cannot do separately for each configuration of the model parameter space), we compare the experimental results obtained for the standard case with a redefined scattering cross section:

$$\left[\xi \sigma_{\text{nucleon}}^{(\text{scalar})} \right]_{\text{eff}} = \mathcal{S}(\xi \sigma_{\text{nucleon}}^{(\text{scalar})})^Z + (\xi \sigma_{\text{nucleon}}^{(\text{scalar})})^{h,H} \quad (4.8)$$

where we have applied the reduction factor only to the Z -mediated cross section. These

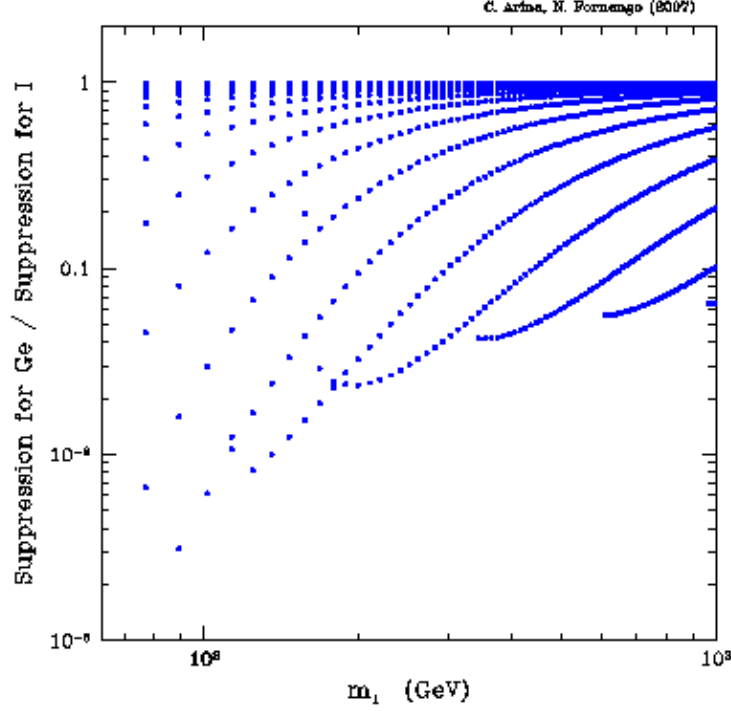


Figure 31: \mathcal{L} models – Relative suppression in the direct detection rate on Germanium and Iodine, as a function of the sneutrino mass m_1 . The sneutrino mass parameters are varied as: $100 \text{ GeV} \leq m_L \leq 1000 \text{ GeV}$ and $10^{-4} \text{ GeV} \leq m_B \leq 10^2 \text{ GeV}$.

suppression factors (which apply to the Z -exchange case only) are shown in Fig. 30 for the case of a Iodine and a Germanium nucleus. The relative reduction between scattering on the Iodine and Germanium nuclei is shown in Fig. 31, where it is manifest that for sneutrinos lighter than about 200 GeV the detection rates in CDMS can be much more suppressed than in the DAMA/NAI experiment. This is a consequence of the different responses of the two detectors to the dark matter velocity distribution function and mass, as a consequence of the different quenches and threshold energies. This is a practical realization of the inelastic dark matter scenario able to explain why current CDMS sensitivity could be insensitive to some cross sections which explain the DAMA/NAI effect [9, 10, 11]. We see that this is indeed a possibility for sneutrinos in LR models.

The effective direct detection cross section of Eq. (4.8) is shown in Fig. 32. The combination of the reduction effect due to the inelasticity of the Z -exchange contribution and the increase of the relic abundance, which affect $\xi \sigma_{\text{nucleon}}^{(\text{scalar})}$ through the rescaling factor ξ , produces a small effect for heavy sneutrinos. On the contrary, light sneutrinos possess a wide range of variation of the direct detection cross section, most of which are not excluded

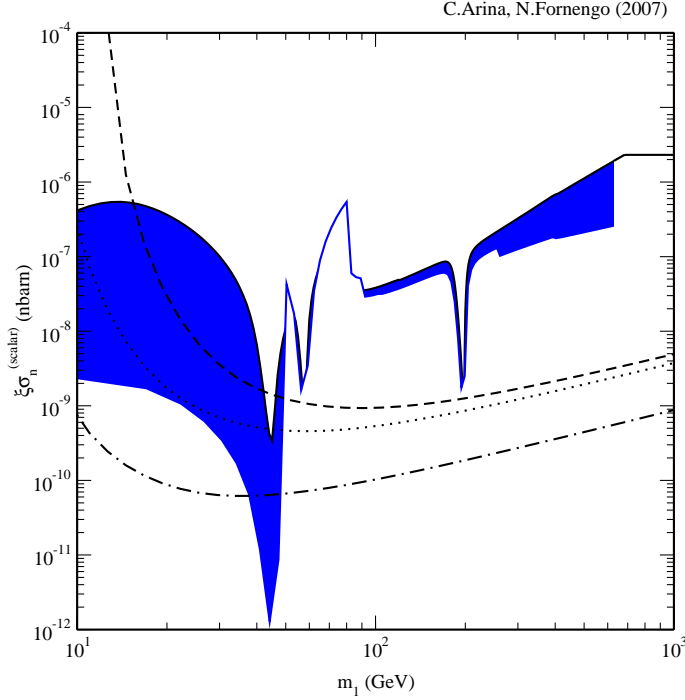


Figure 32: \mathcal{L} models – Sneutrino–nucleon scattering cross section $\xi\sigma_{\text{nucleon}}^{(\text{scalar})}$ as a function of the sneutrino mass m_1 , for the same set of parameters of Fig. 29. The suppression factor in the direct detection rate, due to the off-diagonal Z -coupling, is included in the theoretical predictions. The dashed, dotted and dot-dashed curves denote the CDMS upper bounds [46, 47], as in Fig. 3.

by experimental constraints. This is due to the large mass splitting of the two sneutrino states which effectively suppresses direct detection through Z exchange. By adopting the highest (dashed) line as a conservative limit from CDMS, we see that whenever $m_1 < m_Z/2$ sneutrinos in \mathcal{L} models are viable dark matter candidates. This nevertheless occurs if we allow the 1-loop corrections to the neutrino mass to be as large as the tau-neutrino kinematical mass limit: when a more reliable bound of 2 eV is assumed, we basically recover the minimal MSSM case (which also implies a lower bound on the sneutrino mass of about 80 GeV).

In conclusion, once a neutrino mass bound of 2 eV is assumed, the \mathcal{L} models do not exhibit a phenomenology much richer than the minimal MSSM. Direct detection almost excludes this possibility, except for the occurrence of mass-matching condition between the sneutrino mass and the Z or higgs masses (like in the case of minimal MSSM), and also in this case the compatibility with direct detection is marginal.

For these reason we do not elaborate any further on the \mathcal{L} models, and we do not discuss neither the full supersymmetric parameter-space scan neither indirect detection signals for this case.

5. Models with right-handed sneutrinos and lepton-number violating interactions: the case for a see-saw neutrino mass

A supersymmetric model which can accommodate a Majorana mass-term for neutrinos and explain the observed neutrino mass pattern, and which relies on a renormalizable lagrangian, may be built by adding to the minimal MSSM right-handed fields \tilde{N}^I and allowing for \mathcal{L} terms. The most general form of the superpotential which accomplishes this conditions is [7, 8]:

$$W = \epsilon_{ij}(\mu \hat{H}_i^1 \hat{H}_j^2 - Y_l^{IJ} \hat{H}_i^1 \hat{L}_j^I \hat{R}^J + Y_\nu^{IJ} \hat{H}_i^2 \hat{L}_j^I \hat{N}^J) + \frac{1}{2} M^{IJ} \hat{N}^I \hat{N}^J \quad (5.1)$$

where M^{IJ} , Y_l^{IJ} and Y_ν^{IJ} are matrices, which we again choose real and diagonal. For the \mathcal{L} parameters we therefore assume: $M^{IJ} = M \delta^{IJ}$, in order to reduce the number of free parameters. The Dirac mass of the neutrinos is obtained as: $m_D^I = v_2 Y_\nu^{II}$, while M^I represent a Majorana mass-term for neutrinos.

The general form of the soft supersymmetry-breaking potential may be written as [35]:

$$V_{\text{soft}} = (M_L^2)^{IJ} \tilde{L}_i^{I*} \tilde{L}_j^J + (M_N^2)^{IJ} \tilde{N}^{I*} \tilde{N}^J - [(m_B^2)^{IJ} \tilde{N}^I \tilde{N}^J + \epsilon_{ij}(\Lambda_l^{IJ} H_i^1 \tilde{L}_j^I \tilde{R}^J + \Lambda_\nu^{IJ} H_i^2 \tilde{L}_j^I \tilde{N}^J) + \text{h.c.}] \quad (5.2)$$

where we again use the same assumptions of diagonality in flavour space for the matrices $(M_L^2)^{IJ}$, $(M_N^2)^{IJ}$, $(m_B^2)^{IJ}$, Λ_l^{IJ} and Λ_ν^{IJ} as we already did before. The Dirac-mass parameter is not chosen as a free parameter: it is instead derived by the condition that the neutrino mass is determined by the see-saw mechanism. In this case: $m_\nu^I = m_D^I/M^2$. In our analyses we will fix, for definiteness, the neutrino mass to be 2 eV, in order to saturate the bound which comes from the radiative contribution to the neutrino mass discussed in the previous Section. The naming convention for this class of models is “MAJ models”.

Sneutrinos now are a superpositions of two complex fields: the left-handed field ν_L and the right-handed field \tilde{N} . Since we introduced \mathcal{L} terms, it is convenient, as we did in the previous Section, to work in a basis of CP eigenstates. By defining them accordingly to Eq. (4.4), the mass matrix for the state vector $\Phi_{\text{MAJ}}^\dagger = (\tilde{\nu}_+^* \tilde{N}_+^* \tilde{\nu}_-^* \tilde{N}_-^*)$ has the form:

$$\mathcal{M}_{\text{MAJ}}^2 = \begin{pmatrix} m_L^2 + D^2 + m_D^2 & F^2 + m_D M & 0 & 0 \\ F^2 + m_D M & m_N^2 + M^2 + m_D^2 + m_B^2 & 0 & 0 \\ 0 & 0 & m_L^2 + D^2 + m_D^2 & F^2 - m_D M \\ 0 & 0 & F^2 - m_D M & m_N^2 + M^2 + m_D^2 - m_B^2 \end{pmatrix} \quad (5.3)$$

where $D^2 = 0.5 m_Z^2 \cos(2\beta)$ and F^2 has already been defined in Eq. (3.4). The free parameters of the models for sneutrino sector are therefore: m_L , m_N , M , m_B and F^2 .

Sneutrino mass eigenstates are obtained by diagonalizing Eq. (5.4). We define them as follows:

$$\tilde{\nu}_i = Z_{i1} \tilde{\nu}_+ + Z_{i2} \tilde{N}_+ + Z_{i3} \tilde{\nu}_- + Z_{i4} \tilde{N}_- \quad i = 1, 2, 3, 4 \quad (5.4)$$

The lightest state, which is our dark matter candidate, may now exhibit a mixing with the right-handed field \tilde{N} and the non-diagonal nature of the Z -coupling with respect of the CP eigenstates. These models therefore share the properties of both LR models and \mathcal{L} models, but bring in a more rich set of parameters. In general, the terms $F^2 \pm m_D M$ induce left-right mixing on the sneutrino eigenstates, while the m_B^2 term is responsible for CP splitting. The new Majorana-mass parameter M may lead to left-right mixing for its presence in the off-diagonal elements of the mass matrix $\mathcal{M}_{\text{MAJ}}^2$, and, if it is large, can drive the mass of the two heavier mass eigenstates, since it enters also in the diagonal elements. More specifically, if $F^2 = 0$ M can lead only to a left-right mixing, while if $F \neq 0$ it can contribute also to the CP splitting. A sizeable splitting however occurs when $m_D M \sim F^2$ are of the order of the diagonal elements.

The actual phenomenology of the lightest sneutrino is therefore due to the relative values of the various parameters. While m_L , which is in common with the charged slepton sector, has to be necessarily larger than about 80–100 GeV to fulfill the charged sleptons mass bounds, the other parameters are free in nature and not directly related to the electroweak symmetry-breaking and its scale (at least at the tree level). The right-handed parameter m_N and the CP-splitting parameter m_B may be taken to be of the same order of magnitude as m_L , but since they are in general independent from m_L we assume them to vary freely, as we did in the previous Sections. The same occurs for the parameter F^2 . The parameter M is related to the Majorana mass of neutrinos: a natural scale for this parameter is therefore a high-energy scale, larger than 10^9 GeV, in order to obtain a see-saw neutrino mass below the eV scale with a Dirac-mass term of the order of the GeV scale. However, a value of $M = 1$ TeV which produces a eV neutrino mass with $m_D \sim 1$ MeV is an equally viable possibility, since m_D is a Dirac-type mass which originates from a neutrino Yukawa interaction of unknown strength. We therefore distinguish two cases in our analysis: a low-scale Majorana mass, which we fix at the value of 1 TeV (this class of models are named for convenience MAJ[A]); a large-scale Majorana mass, which we fix at 10^9 GeV (models MAJ[B]). We will see that a different phenomenology arises. For a further discussion of these parameters and their ranges, see also Ref. [35].

The experimental constraints we adopt for the MAJ models (in addition to the one discussed in Appendix 7) are the invisible Z -width for all the relevant mass eigenstates at hand and the neutrino mass bound on the 1-loop corrections to the neutrino mass $|\Delta m_{\text{neutrino}}^{\text{1loop}}| \leq 2$ eV. With our choice of the parameters, we do not have terms which mix different families and therefore we do not generate contributions to the flavour-violating decays of charged leptons, as in general may be the case [35]. We therefore do not have additional bounds from limits on processes like $\mu \rightarrow e + \gamma$ decays.

5.1 Models with a TeV-scale Majorana mass-term

Let us first discuss the case of TeV-scale Majorana mass term M . In this case, sizeable mass splittings are possible and the mass bound from the radiative contribution to the neutrino mass is relevant. Fig. 33 shows $|\Delta m_{\text{neutrino}}^{\text{1loop}}|$ versus the mass splitting of the two lightest sneutrino eigenstate, for $M = 1$ TeV and a scan of the sneutrino relevant parameters in the ranges: 10^2 GeV $\leq m_N \leq 10^3$ GeV, 1 GeV $\leq m_B \leq 10^3$ GeV and

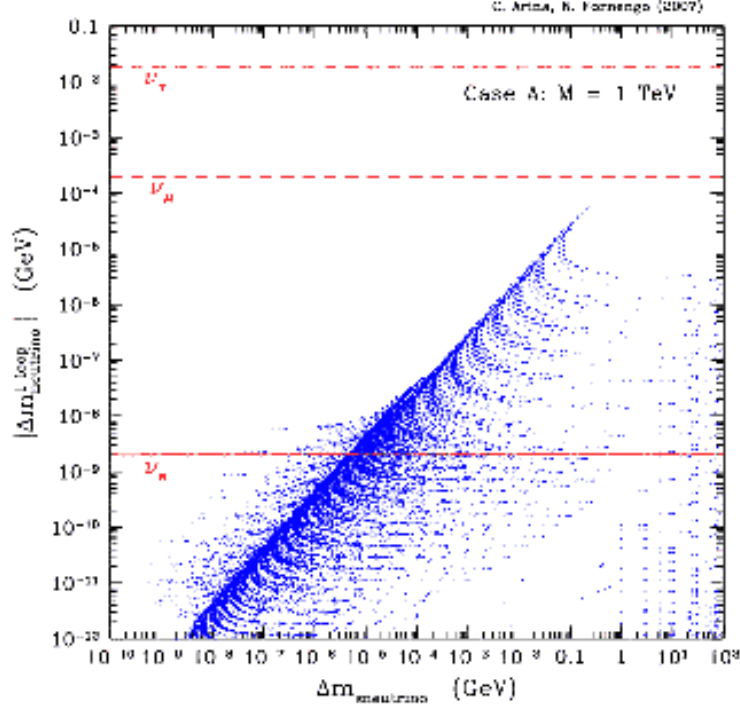


Figure 33: MAJ[A] models – Absolute value of the 1-loop contribution to the neutrino mass as a function of the mass difference of the two lightest sneutrino CP eigenstates, for the case of a Majorana-mass parameter $M = 1$ TeV. The other sneutrino mass parameters are varied as: $10^2 \text{ GeV} \leq m_N \leq 10^3 \text{ GeV}$, $1 \text{ GeV} \leq m_B \leq 10^3 \text{ GeV}$ and $1 \text{ GeV}^2 \leq F^2 \leq 10^4 \text{ GeV}^4$. The horizontal lines denote the upper limits on the neutrino mass, as labelled.

$1 \text{ GeV}^2 \leq F^2 \leq 10^4 \text{ GeV}^4$. We see that, contrary to the case of the pure \mathcal{L} models discussed in the previous Section, large sneutrino mass splittings are possible even with a neutrino mass bound of 2 eV. This is related to the fact that the large mass splittings are here related to a large mixing with the right-handed field \tilde{N} : this therefore suppresses the sneutrino couplings and as a consequence also the 1-loop contribution to the neutrino mass. This is manifest in Fig. 34 where we show, for the same variation of parameters, the distribution of the sterile component of the lightest sneutrino state versus the mass splitting. Typically, when the sneutrino is mostly left-handed the mass splitting is also small, and the sterile component increases with the increase of the mass separation.

The large sneutrino mass splitting which is now allowed also for a neutrino mass bound of 2 eV is relevant for the direct detection suppression effect: this is at variance with the \mathcal{L} models, where this bound implied a strong restriction of the sneutrino phenomenology, bringing it to the minimal MSSM case. In addition to the mass splitting, a sizeable sterile

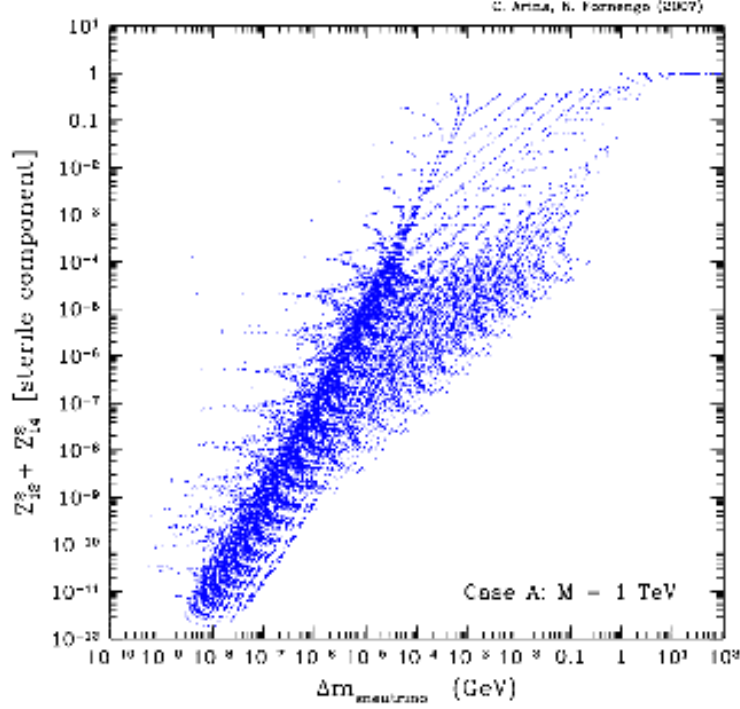


Figure 34: MAJ[A] models – Component of the lightest sneutrino into sterile fields as a function of the mass splitting of the two lightest sneutrinos, for the case of a Majorana-mass parameter $M = 1$ TeV. The other sneutrino mass parameters are varied as in Fig. 33.

component now also appears. The suppression factor is shown in Fig. 35, which can be compared to the corresponding case of \mathcal{L} models of Fig. 30.

The relic abundance of the MAJ[A] models is shown in Fig. 36. It is remarkable that in the whole mass range from 5 GeV to 1 TeV sneutrinos can explain the required amount of dark matter in the Universe. For the same mass range, sneutrinos may as well be a subdominant component.

Direct detection is shown in Fig. 37. We see that three different populations arise: configurations on the upper right are clearly excluded by direct detection searches. Most of them refer to subdominant sneutrinos. Configurations on the lower right part of the plot are allowed but well below current direct detection sensitivity. Configurations on the center and left part of the plot all fall inside the current sensitivity region, and in this specific plot show that could explain the annual modulation effect observed by the DAMA/NaI experiment. We notice that a large fraction of the configurations which fall inside the DAMA/NaI region are also cosmologically dominant. The correlation of the direct detection cross section $\xi\sigma_{\text{nucleon}}^{(\text{scalar})}$ and the relic abundance are plotted in Fig. 38, which shows how almost all

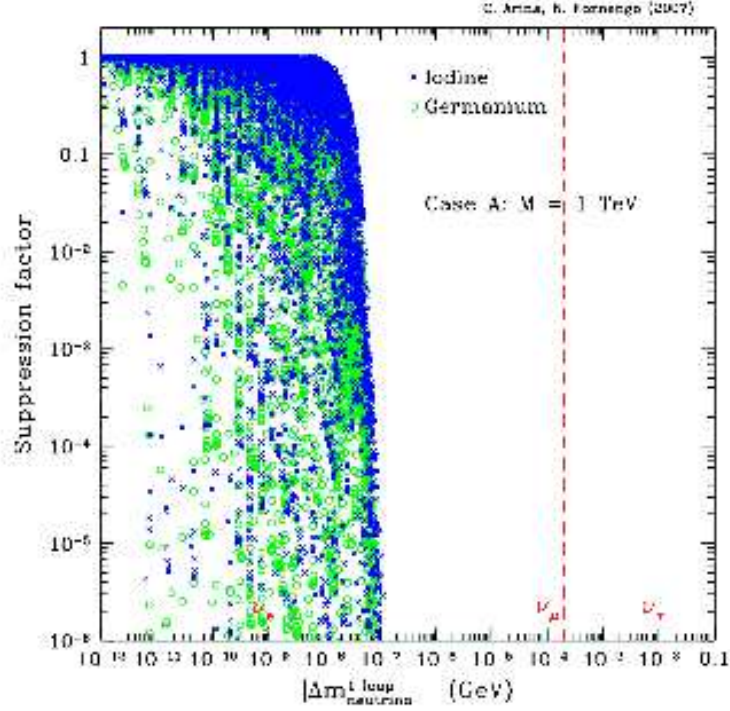


Figure 35: MAJ[A] models – Suppression factor of the direct detection rate due to the off-diagonal Z -coupling plotted vs. the absolute value of the 1-loop contribution to the neutrino mass, for the case of a Majorana-mass parameter $M = 1$ TeV. The other sneutrino mass parameters are varied as in Fig. 33. [Blue] crosses refer to the Iodine nucleus, open [green] circles to the Germanium nucleus. The vertical lines denote the upper limits on the neutrino mass, as labelled.

the cosmologically relevant configurations are under investigation or under reach of direct detection studies. This can be confronted with the case of pure LR models shown in Fig. 16, where a large fraction of the cosmologically relevant configurations were either already excluded by direct detection or with very low values of $\xi\sigma_{\text{nucleon}}^{(\text{scalar})}$. We remind that now $\xi\sigma_{\text{nucleon}}^{(\text{scalar})}$ contains the suppression factor as discussed in Eq. (4.8).

Contrary to the case of LR models, indirect detection is not currently sensitive to the MAJ[A] models. Fig. 39 shows the correlation between the upgoing muon flux from the Earth as a function of $\xi\sigma_{\text{nucleon}}^{(\text{scalar})}$. We notice that all the configurations are below the current limits from neutrino telescopes. However, there is a large fraction of configurations which could be accessible by an increase of sensitivity, although the increase should be sizeable.

Figs. 40 shows the distribution of the sterile components with respect to the sneutrino mass. We see that, when sneutrinos are light, they are typically right-handed, and therefore they do not couple to the Z boson (although they still have couplings with higgses). For

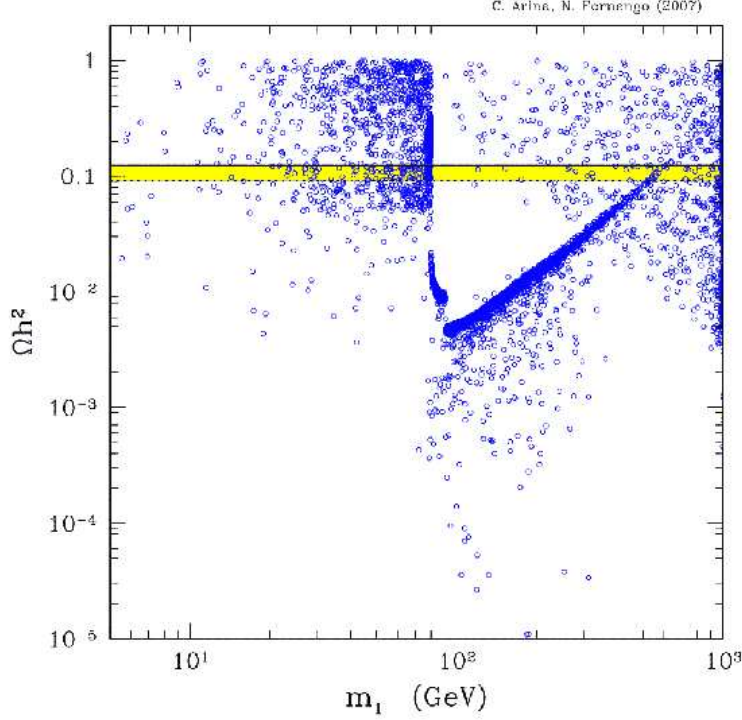


Figure 36: MAJ[A] models – Sneutrino relic abundance Ωh^2 as a function of the sneutrino mass m_1 , for the case of a Majorana-mass parameter $M = 1$ TeV and for a full scan of the supersymmetric parameter space. The sneutrino parameters (other than M) are varied as follows: $10^2 \text{ GeV} \leq m_N \leq 10^3 \text{ GeV}$, $1 \text{ GeV} \leq m_B \leq 10^3 \text{ GeV}$ and $1 \text{ GeV}^2 \leq F^2 \leq 10^4 \text{ GeV}^4$. All the models shown in the plot are acceptable from the point of view of all experimental constraints. The horizontal solid and dotted lines delimit the WMAP interval for cold dark matter.

masses above 80 GeV they may exhibit both right- or left-handed behaviour.

The distribution of the cosmologically allowed configurations in the sneutrino parameter space is shown in Figs. 41 and 42. Light states typically have small values of both m_N and F^2 , and as it was already shown in Fig. 37 they are almost all acceptable and currently explored by direct detection experiments. The distribution of configurations in these sectors of the parameter space are somewhat different from the analogous results for the LR models, shown in Fig. 17 and 18: in that case, larger values of F^2 were required also for light sneutrinos, a difference which is traced into the new structure of the sneutrino mass matrix and neutrino couplings which arise here from the introduction of \mathcal{L} terms in the lagrangian.

The antiproton flux at $T_{\bar{p}} = 0.23 \text{ GeV}$ is shown in Fig. 43. We notice that a fraction of the configurations with low mass are currently excluded by the BESS data. This is at

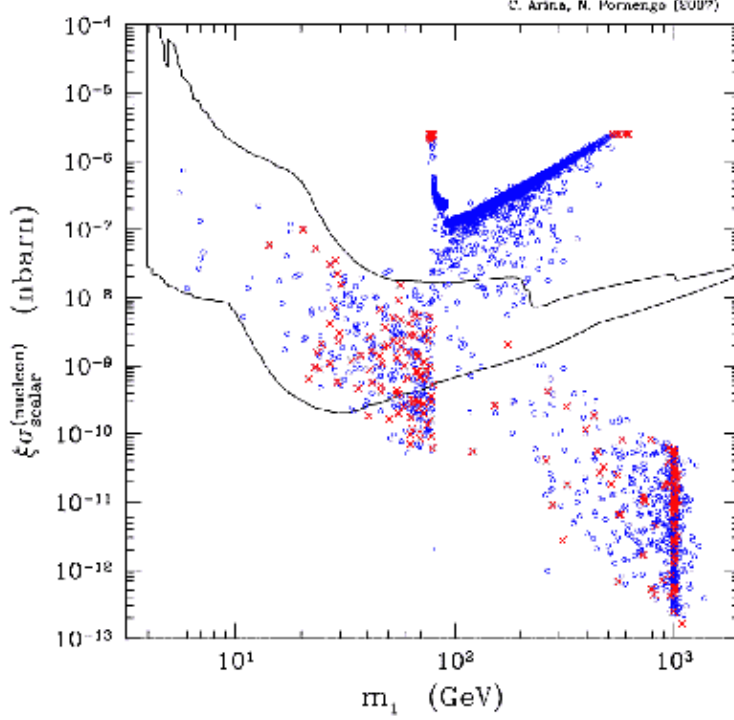


Figure 37: MAJ[A] models – Sneutrino–nucleon scattering cross section $\xi\sigma_{\text{nucleon}}^{(\text{scalar})}$ as a function of the sneutrino mass m_1 , for the case of a Majorana–mass parameter $M = 1$ TeV and for a full scan of the supersymmetric parameter space. Parameters are varied as in Fig. 36. [Red] crosses refer to models with sneutrino relic abundance in the cosmologically relevant range; [blue] open circles refer to cosmologically subdominant sneutrinos. The solid curve shows the DAMA/NaI region, compatible with the annual modulation effect observed by the experiment [41, 42, 43, 44, 45].

variance with the case of LR models, where instead the antiproton flux for light sneutrinos were all well below the BESS sensitivity. Another remarkable difference from the LR models is that now the configurations which are excluded by direct detection refer to very low antiproton fluxes, practically undetectable. These two features show that for the MAJ[A] models antiproton searches and direct detection studies exhibit a high degree of complementarity, both in the ability to exclude model configurations and the prospects of detection. This is clearly summarized in Fig. 44, where the high level of complementarity is manifest. It is also remarkable that a fraction of configurations which are currently under study by direct detection experiments (either just inside the CDMS sensitivity range or, even more interestingly, inside the DAMA/NaI annual modulation region) have a chance of detection by the future PAMELA and AMS flights, or by some slightly more sensitive and future experiments.

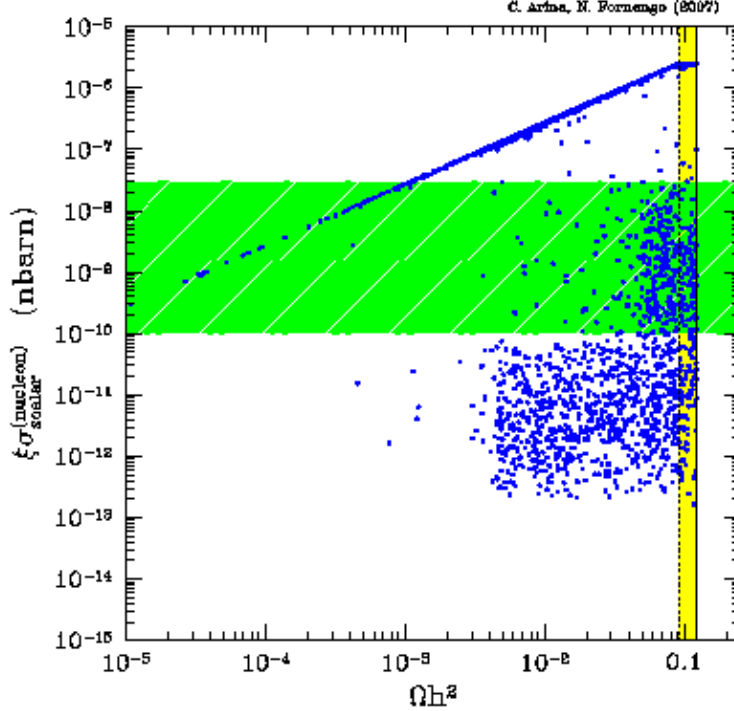


Figure 38: MAJ[A] models – Sneutrino–nucleon scattering cross section $\xi\sigma_{\text{nucleon}}^{(\text{scalar})}$ vs. the sneutrino relic abundance Ωh^2 , for the case of a Majorana–mass parameter $M = 1$ TeV and for a full scan of the supersymmetric parameter space. Parameters are varied as in Fig. 36. The horizontal [green] band denotes the current sensitivity of direct detection experiments; the vertical [yellow] band delimits the WMAP interval for cold dark matter.

The antideuteron searches are as well appealing, as Fig. 45 shows: the configurations for light sneutrinos above the GAPS sensitivity line are almost all excluded already by the BESS data on antiprotons, but those under the GAPS and AMS sensitivity line are under reach. Figs. 43 and 45 also show that for MAJ[A] models, antimatter searches are not sensitive to heavy sneutrinos.

Also the gamma–ray signal is interesting, since EGRET and GLAST are sensitive to sneutrino dark matter also for dark matter profiles of the NFW type [106, 107]. This is at variance with the LR models, where a steeper profile was needed in order to obtain sizeable fluxes. Fig. 46 shows the gamma–ray flux at $E_\gamma = 1.5$ GeV from the center of the Galaxy, for a EGRET–like angular resolution. Like for the antimatter signals, only sneutrinos with masses below 80 GeV produce sizeable signals. There are configuration which are at the level of explaining the EGRET excess. GLAST will be sensitive to a large fraction of the sneutrino configurations.

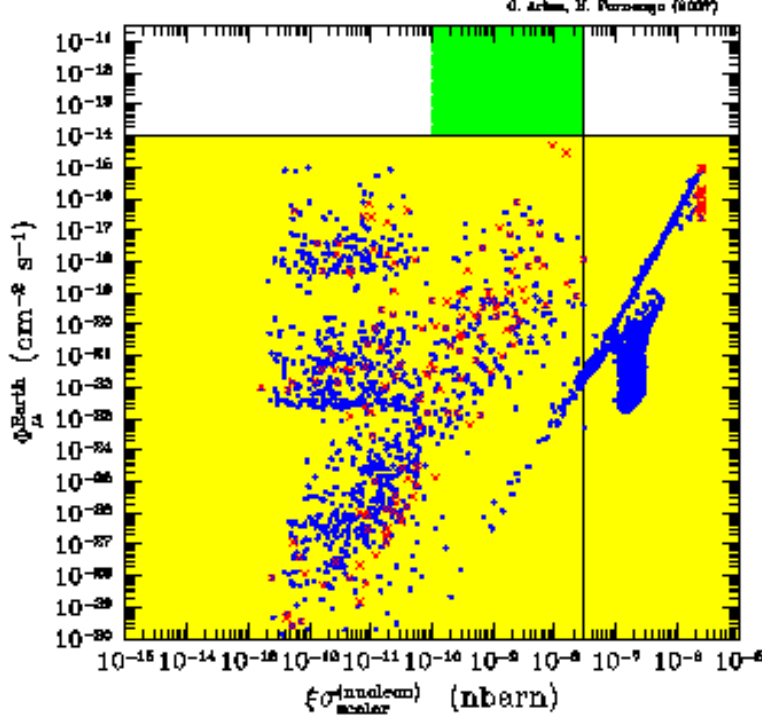


Figure 39: MAJ[A] models – Upgoing muon flux from sneutrino pair annihilation in the center of the Earth $\Phi_{\mu}^{\text{Earth}}$ vs. the sneutrino–nucleon scattering cross section $\xi\sigma_{\text{nucleon}}^{(\text{scalar})}$, for the case of a Majorana–mass parameter $M = 1$ TeV and a full scan of the supersymmetric parameter space. Parameters are varied as in Fig. 36. [Red] crosses refer to models with sneutrino relic abundance in the cosmologically relevant range; [blue] dots refer to cosmologically subdominant sneutrinos. The horizontal solid line denotes the current upper limit from neutrino telescopes. The vertical solid line denotes a conservative upper limit from direct detection searches and the [green] vertical shaded area refers to the current sensitivity in direct detection searches.

5.2 Models with a large–scale Majorana mass–parameter

As a second example of this class of models we consider the case of a large–scale Majorana mass–parameter, which we fix at $M = 10^9$ GeV. We call these models MAJ[B]. In this case, the large value of M drives the two highest sneutrino mass eigenstates to be very heavy and decoupled from the rest. The model for the light sneutrino sector is somehow less rich phenomenologically as compared to the case of a TeV–scale Majorana mass–parameter. The 1–loop neutrino mass contribution $|\Delta m_{\text{neutrino}}^{\text{loop}}|$ is shown in Fig. 47 as a function of the sneutrino mass difference. Contrary to the case of \mathcal{L} models, larger sneutrino mass splittings are allowed, up to almost 10 MeV. This is an interesting range for the inelasticity properties in direct detection dark matter [9, 10, 11]. Directly from the MAJ[A] case,

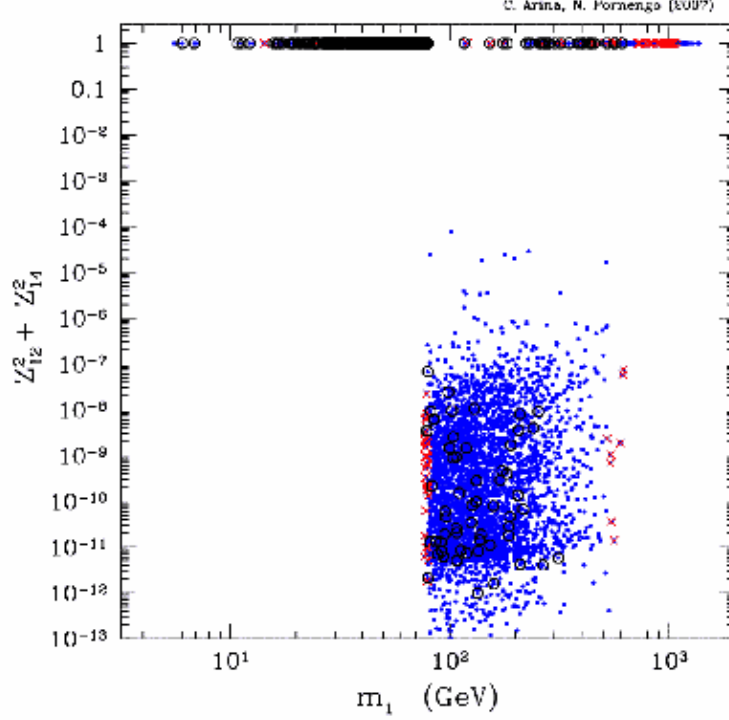


Figure 40: MAJ[A] models – Distribution of cosmologically acceptable models in the m_1 vs. sterile-component plane, for the case of a Majorana-mass parameter $M = 1$ TeV and a full scan of the supersymmetric parameter space. Parameters are varied as in Fig. 36. [Red] crosses refer to models with sneutrino relic abundance in the cosmologically relevant range; [blue] dots refer to cosmologically subdominant sneutrinos; open dots mark the configurations which have a direct-detection cross section in the current sensitivity range.

instead, larger mass splittings are not possible now. This is related to the fact that light sneutrinos are not obtained in this class of models. This is shown in Fig. 48 where the relic abundance is plotted versus m_1 . We see that now cosmologically relevant sneutrinos are present only for very restricted mass ranges, one around 80–90 GeV and the second at 500–600 GeV. For masses above 600 GeV sneutrinos are cosmologically excluded. In the whole interval 90–500 GeV, sneutrinos are subdominant.

Direct detection comes back to be a strong constraint. Fig. 49 shows that direct detection bounds exclude most of the configurations, and in particular all the cosmologically relevant ones. Nevertheless, sneutrinos in the mass range 90–300 GeV are allowed, although subdominant.

Indirect detection for MAJ[B] models is not very appealing: the antiproton flux at $T_{\bar{p}} = 0.23$ GeV is shown in Fig. 50: configurations which pass the direct detection bound

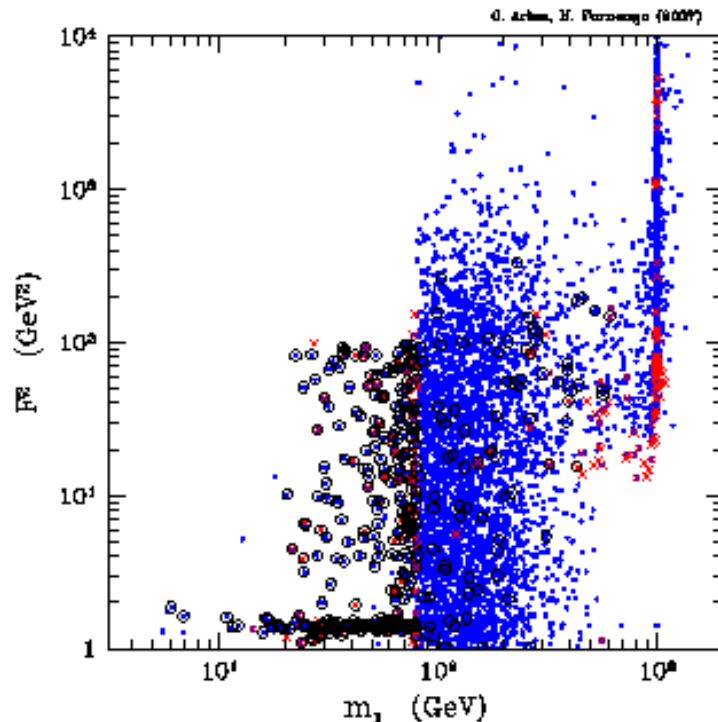


Figure 41: MAJ[A] models – Distribution of cosmologically acceptable models in the $m_1 - F^2$ plane, for the case of a Majorana-mass parameter $M = 1$ TeV and a full scan of the supersymmetric parameter space. Parameters are varied as in Fig. 36. [Red] crosses refer to models with sneutrino relic abundance in the cosmologically relevant range; [blue] dots refer to cosmologically subdominant sneutrinos; open dots mark the configurations which have a direct-detection cross section in the current sensitivity range.

all refer to very low antiproton fluxes, practically undetectable. A similar situation occurs for antideuterons and gamma-rays.

6. Conclusions

In this paper we have analyzed the possibility to have sneutrinos as dark matter candidates. We have discussed various supersymmetric models, and specifically extensions of the Minimal Supersymmetric Standard Model which could lead to explanations of the neutrino mass problem.

We have first re-analyzed the minimal version of the MSSM. Sneutrinos are here typically subdominant dark matter components, with low values of the relic abundance in all the mass range from 50-70 (their lower mass bound in the MSSM) up to 700 GeV. They may represent the dominant dark matter component for masses in the 600-700 GeV range.

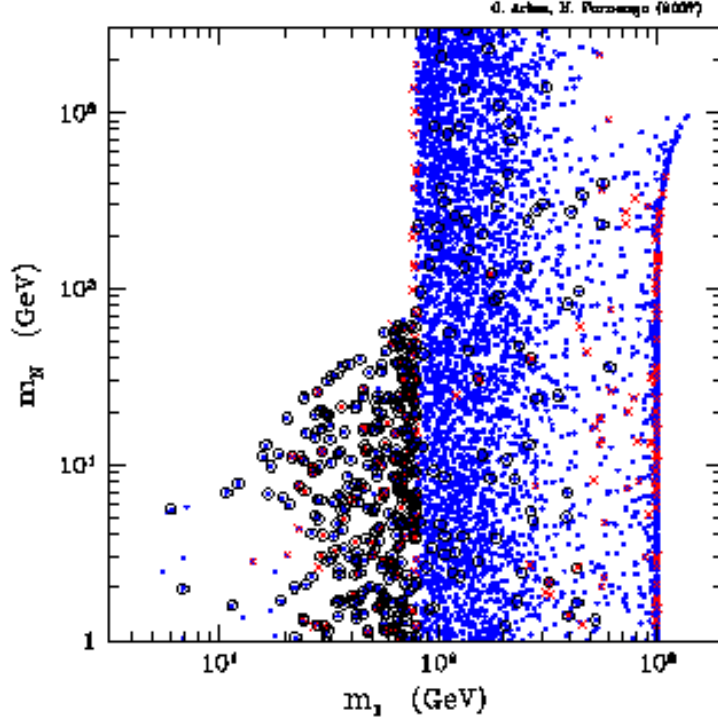


Figure 42: MAJ[A] models – Distribution of cosmologically acceptable models in the $m_1 - m_N$ plane, for the case of a Majorana-mass parameter $M = 1$ TeV and a full scan of the supersymmetric parameter space. Parameters are varied as in Fig. 36. [Red] crosses refer to models with sneutrino relic abundance in the cosmologically relevant range; [blue] dots refer to cosmologically subdominant sneutrinos; open dots mark the configurations which have a direct-detection cross section in the current sensitivity range.

This possibility is actually excluded by direct detection searches, which allow sneutrinos to be a subdominant dark matter component only very marginally, and for mass-matching conditions that pose the sneutrino annihilation cross-section on one of the higgs poles or the Z pole.

The inclusion of right-handed superfields to the supersymmetric lagrangian allows for a much richer phenomenology. The mixing with right-handed fields suppresses the Z -coupling and leads to some increase of the relic abundance and to some decrease of the direct detection rate. The reduced Z coupling is also instrumental in allowing light sneutrinos, by circumventing the invisible Z -width bound. From a full scan of the supersymmetric parameter space, we find that cosmologically dominant relic sneutrinos are present in the mass range from 15 GeV up to 1 TeV (where we stop our scan). When the full supersymmetric parameter space is considered, we find that 15 GeV is actually the mass lower bound,

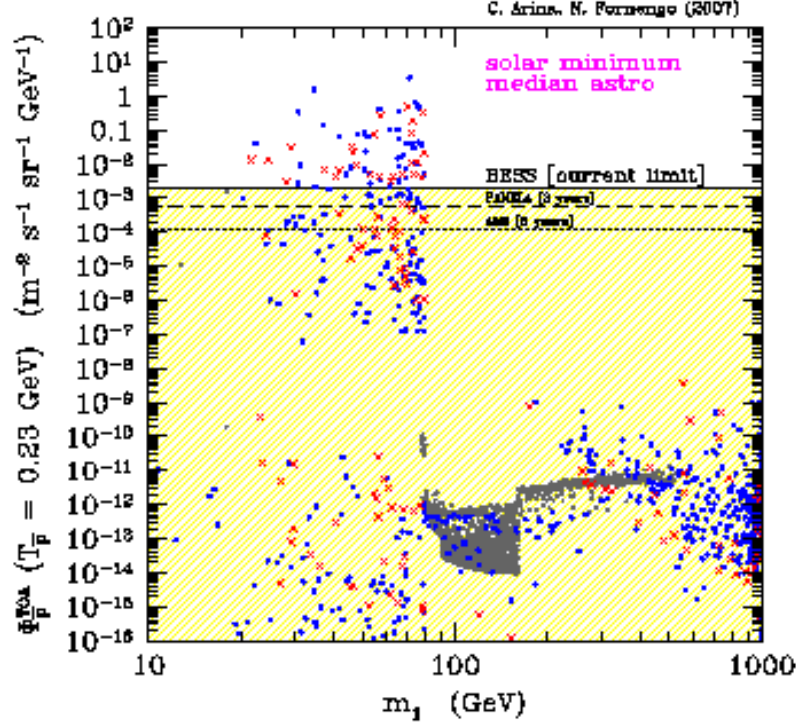


Figure 43: MAJ[A] models – Antiproton flux at the antiproton kinetic energy $T_{\bar{p}} = 0.23$ GeV as a function of the sneutrino mass m_1 , for the galactic propagation parameters which provide the median value of antiproton flux and for a solar activity at its minimum. The plot refers to the case of a Majorana-mass parameter $M = 1$ TeV and a full scan of the supersymmetric parameter space. Parameters are varied as in Fig. 36. [Red] crosses refer to models with sneutrino relic abundance in the cosmologically relevant range; [blue] dots refer to cosmologically subdominant sneutrinos; light gray points denote configurations which are excluded by direct detection searches. The [yellow] shaded area denotes the amount of exotic antiprotons which can be accommodated in the BESS data [79, 80]. The dashed and dotted lines show the PAMELA [83] and AMS [84] sensitivities to exotic antiprotons for 3 years missions, respectively.

induced by the cosmological limit on the relic abundance. Direct detection is acceptable for all the allowed mass range. We also find that cosmologically dominant sneutrinos are accepted by direct detection, and a large fraction of the supersymmetric configurations predict direct detection rates at the level of the current experimental sensitivities (including the possibility to explain the DAMA/NaI annual modulation effect). Indirect detection rates offer good possibilities: antiproton fluxes are under reach of the PAMELA and AMS detectors in the 50–200 GeV mass range. The configurations accessible to indirect searches are typically cosmologically subdominant. The same occurs also for the antideuteron signal, which is accessible by GAPS and AMS to the same configurations to which PAMELA

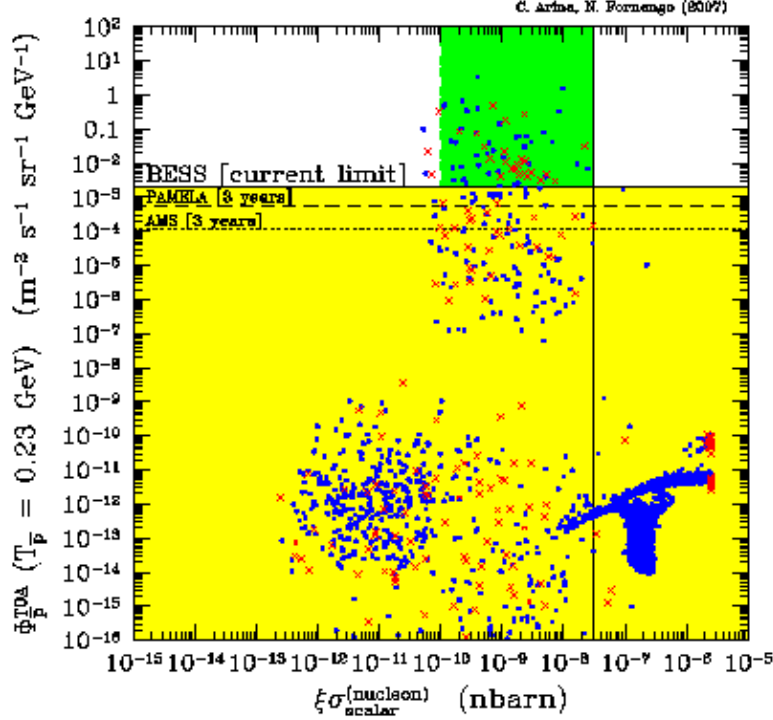


Figure 44: MAJ[A] models – Antiproton flux at the antiproton kinetic energy $T_{\bar{p}} = 0.23$ GeV vs. the sneutrino–nucleon scattering cross section $\xi \sigma_{\text{nucleon}}^{(\text{scalar})}$, for the case of a Majorana–mass parameter $M = 1$ TeV and a full scan of the supersymmetric parameter space. Parameters are varied as in Fig. 36. [Red] crosses refer to models with sneutrino relic abundance in the cosmologically relevant range; [blue] dots refer to cosmologically subdominant sneutrinos. The horizontal solid line denotes the upper limit from BESS [79, 80] and the [yellow] shaded area shows the amount of exotic antiprotons which can be accommodated in the BESS data. The dashed and dotted horizontal lines show the PAMELA [83] and AMS [84] sensitivities to exotic antiprotons for 3 years missions, respectively. The vertical solid line denotes a conservative upper limit from direct detection searches and the [green] vertical shaded area refers to the current sensitivity in direct detection searches.

and AMS are sensitive for antiprotons. This offers a great opportunity for dark matter searches: a signal detectable in one antimatter channel by two different detectors, will be detectable also in the other channels, again by two different detectors. Gamma-rays from the center of the galaxy do not provide very large signals: we predict fluxes not too far from the EGRET excess in the 50–200 GeV mass range, but this requires a very steep dark matter density profile toward the galactic center (of the $r^{-1.5}$ type). GLAST will be sensitive to configurations in this same mass range, again for a very steep profile.

Models with a lepton–number violating term, introduced as non–renormalizable 5–dimensional operator, do not lead to a phenomenology very different from the standard

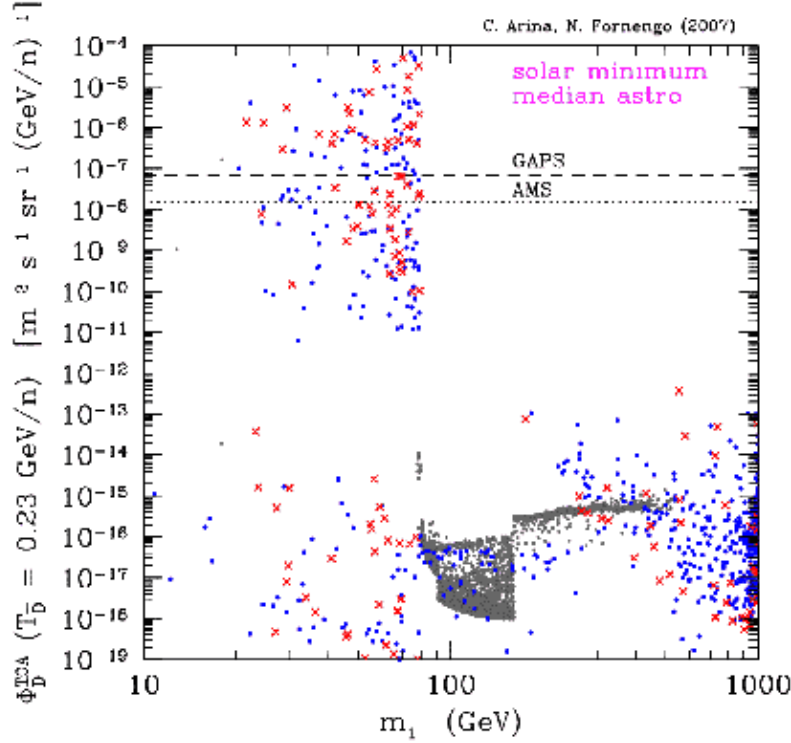


Figure 45: MAJ[A] models – Antideuteron flux at the antideuteron kinetic energy (per nucleon) $T_{\bar{p}} = 0.23 \text{ GeV/n}$, as a function of the sneutrino mass m_1 , for the case of a Majorana-mass parameter $M = 1 \text{ TeV}$ and a full scan of the supersymmetric parameter space. Parameters are varied as in Fig. 36. Notations are as in Fig. 20. The dashed and dotted lines show the GAPS [86, 87] and AMS [84] sensitivities.

MSSM, once a mass bound of 2 eV on the 1-loop correction to the neutrino mass (which is induced by the \mathbb{L} terms) is considered. Only for a neutrino mass bound of 18 MeV, which corresponds to the kinematical mass bound for the tau neutrino, some increase of the relic abundance is possible. However, the direct detection limit strongly bounds these models, making them almost marginal.

A renormalizable lagrangian with both right-handed fields and \mathbb{L} terms, which offers the possibility to include neutrino masses via a see-saw mechanism, again offers very rich sneutrino phenomenology. In the case of a TeV-scale Majorana mass-parameter, sneutrinos may be the dominant dark matter component for masses in the range 5 GeV up to 1 TeV (upper bound in our scan). The direct detection is nicely evaded in all the mass range, and most of the configurations fall inside the current experimental sensitivity range (including the possibility to explain the DAMA/NaI annual modulation effect). Antiproton fluxes are a stringent bound for light sneutrinos, complementary to the bound imposed by direct

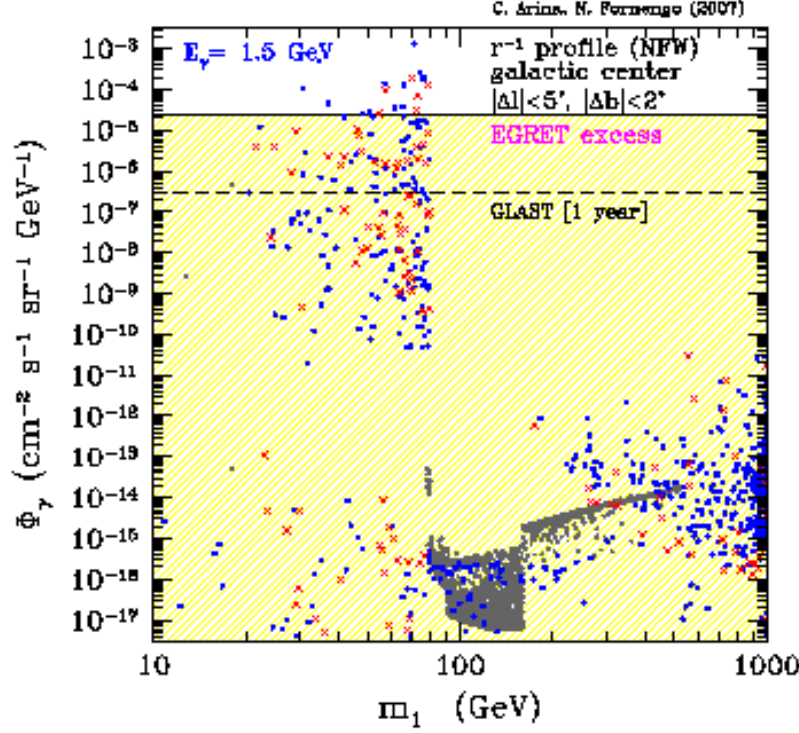


Figure 46: MAJ[A] models – Gamma-ray flux from the galactic center at the photon energy $E_\gamma = 1.5 \text{ GeV}$, as a function of the sneutrino mass m_1 , for a galactic profile of Moore’s type [88, 89] and for the angular resolution of EGRET [90, 91]. The plot refers to the case of a Majorana-mass parameter $M = 1 \text{ TeV}$ and a full scan of the supersymmetric parameter space. Parameters are varied as in Fig. 36. [Red] crosses refer to models with sneutrino relic abundance in the cosmologically relevant range; [blue] dots refer to cosmologically subdominant sneutrinos; light gray points denote configurations which are excluded by direct detection searches. The [yellow] shaded area denotes the amount of exotic gamma-rays compatible with the EGRET excess [90, 91]. The dashed line shows the GLAST [92] sensitivity for a 1 year data-taking and for the same EGRET angular bin.

detection which instead is more severe for heavier particles. Many configurations for masses below 80–90 GeV will be explored by PAMELA and AMS, while for masses above 90 GeV antiproton searches loose sensitivity. Also for antideuterons, AMS and GAPS will have sensitivity to probe a fraction of the configurations for masses below 80–90 GeV. For these light sneutrinos, also gamma-rays provide a significant probe, also for NFW profiles. GLAST will have sensitivity to a fraction of those configurations with mass below 80–90 GeV. Finally, models with a large Majorana mass-parameter are strongly bounded by direct detection: configurations with masses in the range 90–300 GeV are not excluded by direct detection, but they all refer to cosmologically subdominant sneutrinos. Indirect detection rates are typically very suppressed.

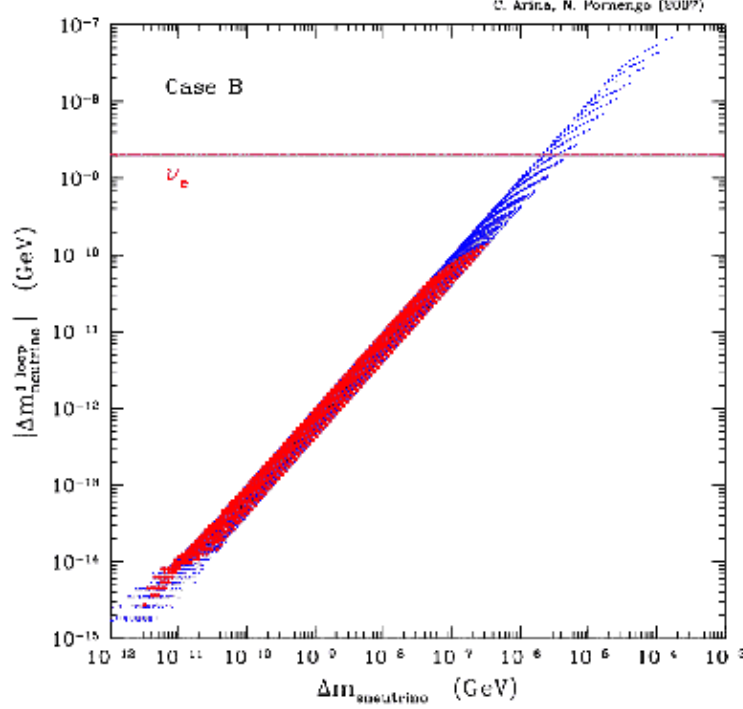


Figure 47: MAJ[B] models – Absolute value of the 1-loop contribution to the neutrino mass as a function of the mass difference of the two lightest sneutrino CP eigenstates, for the case of a Majorana-mass parameter $M = 10^9$ GeV. The other sneutrino mass parameters are varied as: $m_N = 0$, $10^3 \text{ GeV} \leq m_B \leq 10^8 \text{ GeV}$ and $1 \text{ GeV}^2 \leq F^2 \leq 10^4 \text{ GeV}^4$. The horizontal lines denote the upper limits on the electron neutrino mass.

We therefore conclude that sneutrinos offer a rich phenomenology as dark matter candidates, and they are a viable alternative to relic neutralinos in a wide class of supersymmetric models. Their phenomenology is also linked and constrained by neutrino physics through the problem of the origin of neutrino masses.

Acknowledgments

We acknowledge Research Grants funded jointly by the Italian Ministero dell’Istruzione, dell’Università e della Ricerca (MIUR), by the University of Torino and by the Istituto Nazionale di Fisica Nucleare (INFN) within the *Astroparticle Physics Project*.

7. Appendix: The supersymmetric model

The supersymmetric model we adopt in this paper is an effective MSSM scheme at the

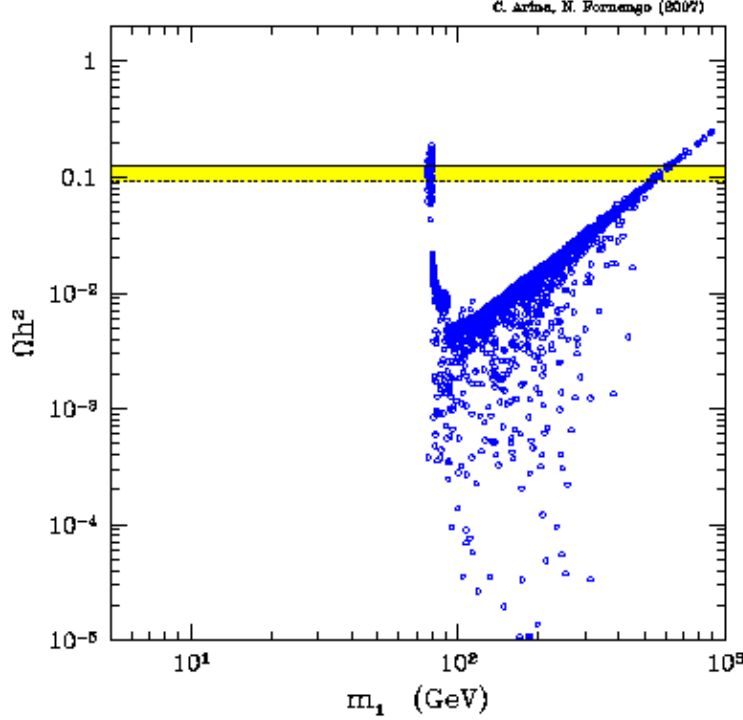


Figure 48: MAJ[B] models – Sneutrino relic abundance Ωh^2 as a function of the sneutrino mass m_1 , for the case of a Majorana-mass parameter $M = 10^9$ GeV and for a full scan of the supersymmetric parameter space. The sneutrino parameters (other than M) are varied as follows: $m_N = 0$, $10^3 \text{ GeV} \leq m_B \leq 10^8 \text{ GeV}$ and $1 \text{ GeV}^2 \leq F^2 \leq 10^4 \text{ GeV}^4$. All the models shown in the plot are acceptable from the point of view of all experimental constraints. The horizontal solid and dotted lines delimit the WMAP interval for cold dark matter.

electroweak scale. The free independent parameters of the model, which are not directly related to the sneutrino sector, are the following: the SU(2) gaugino-mass parameter M_2 ; the ratio between the U(1) and SU(2) gaugino-mass parameters $R \equiv M_1/M_2$ (in the GUT-induced case $R = 5/3 \tan^2 \theta_W \simeq 0.5$, where θ_W is the Weinberg angle); the Higgs-mixing parameter μ ; $\tan \beta = v_2/v_1$; the mass of the pseudoscalar higgs m_A ; a common soft-mass for all the squarks m_Q (both right- and left-handed); a common dimensionless trilinear parameter for the third family A ($A_{\tilde{b}} = A_{\tilde{t}} \equiv A m_{\tilde{q}}$ and $A_{\tilde{\tau}} \equiv A m_{\tilde{l}}$; the trilinear parameters for the other families being set equal to zero). The masses of the CP-even and charged higgses are calculated from m_A (and the other relevant supersymmetric parameters) by employing 2-loop corrections.

The full scans of the parameter space are performed over the following ranges of the MSSM parameters: $1 \leq \tan \beta \leq 50$, $100 \text{ GeV} \leq |\mu| \leq 3000 \text{ GeV}$, $100 \text{ GeV} \leq M_2 \leq$

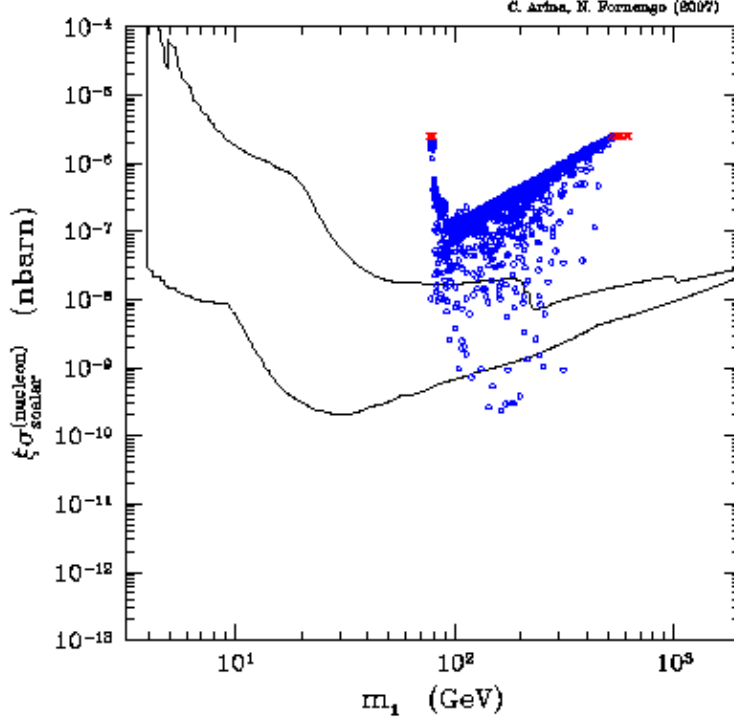


Figure 49: MAJ[B] models – Sneutrino–nucleon scattering cross section $\xi\sigma_{\text{nucleon}}^{(\text{scalar})}$ as a function of the sneutrino mass m_1 , for the case of a Majorana–mass parameter $M = 10^9$ GeV and for a full scan of the supersymmetric parameter space. Parameters are varied as in Fig. 48. [Red] crosses refer to models with sneutrino relic abundance in the cosmologically relevant range; [blue] open circles refer to cosmologically subdominant sneutrinos. The solid curve shows the DAMA/NaI region, compatible with the annual modulation effect observed by the experiment [41, 42, 43, 44, 45].

3000 GeV, $100 \text{ GeV} \leq m_Q \leq 3000 \text{ GeV}$, $90 \text{ GeV} \leq m_A \leq 1000 \text{ GeV}$, $-3 \leq A \leq 3$. As for the R parameter, we use either its mSUGRA value $R = 0.5$ or we scan over the interval $0.005 \leq R \leq 0.5$, depending on the case at study. In order to have the sneutrino as a dark matter candidate, we accept only parameter configurations for which the lightest sneutrino is also the lightest among all the supersymmetric particles.

We impose the following experimental constraints: accelerators data on supersymmetric particles and Higgs–boson searches (CERN e^+e^- collider LEP2 [67, 68, 54, 69] and Collider Detectors D0 and CDF at Fermilab [55, 108]); measurements of the $b \rightarrow s + \gamma$ decay process [109]: we adopt the interval $2.89 \leq B(b \rightarrow s + \gamma) \cdot 10^{-4} \leq 4.21$, which is larger by 25% with respect to the experimental determination [109] in order to take into account theoretical uncertainties in the SUSY contributions [110] to the branching ratio of the process (for the Standard Model calculation, we employ the recent NNLO results from

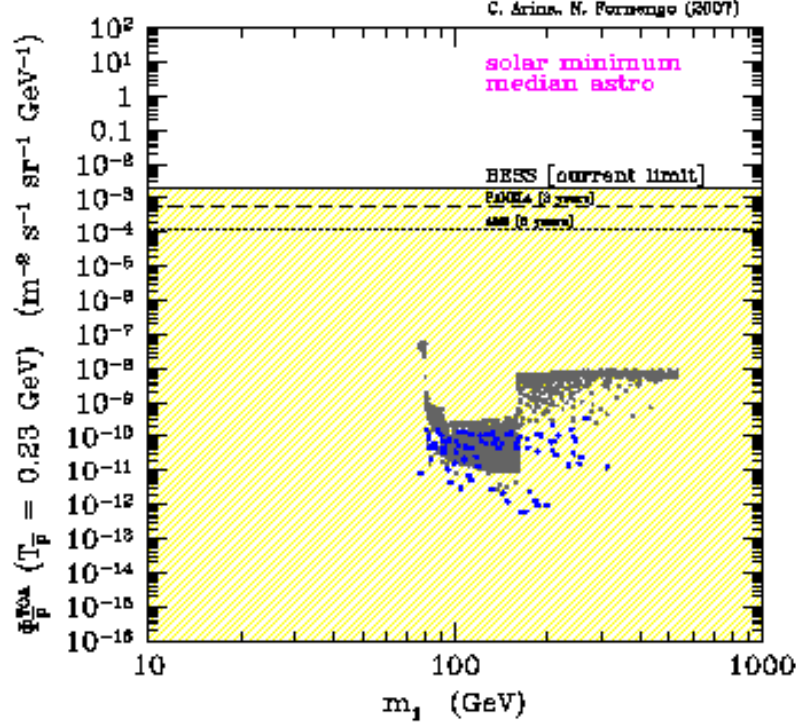


Figure 50: MAJ[B] models – Antiproton flux at the antiproton kinetic energy $T_{\bar{p}} = 0.23$ GeV as a function of the sneutrino mass m_1 , for the galactic propagation parameters which provide the median value of antiproton flux and for a solar activity at its minimum. The plot refers to the case of a Majorana-mass parameter $M = 10^9$ GeV and a full scan of the supersymmetric parameter space. Parameters are varied as in Fig. 48. [Red] crosses refer to models with sneutrino relic abundance in the cosmologically relevant range; [blue] dots refer to cosmologically subdominant sneutrinos; light gray points denote configurations which are excluded by direct detection searches. The [yellow] shaded area denotes the amount of exotic antiprotons which can be accommodated in the BESS data [79, 80]. The dashed and dotted lines show the PAMELA [83] and AMS [84] sensitivities to exotic antiprotons for 3 years missions, respectively.

Ref. [111]); the upper bound on the branching ratio $BR(B_s^0 \rightarrow \mu^- + \mu^+)$ [112]: we take $BR(B_s^0 \rightarrow \mu^- + \mu^+) < 1.2 \cdot 10^{-7}$; measurements of the muon anomalous magnetic moment $a_\mu \equiv (g_\mu - 2)/2$: for the deviation Δa_μ of the experimental world average from the theoretical evaluation within the Standard Model we use here the range $-98 \leq \Delta a_\mu \cdot 10^{11} \leq 565$, derived from the latest experimental [113] and theoretical [114] data. The invisible Z -width constraints is also imposed on neutralinos lighter than $m_Z/2$ which occur in the gaugino non-universal models.

References

- [1] L. E. Ibanez, *The scalar neutrinos as the lightest supersymmetric particles and cosmology*, *Phys. Lett.* **B137** (1984) 160.
- [2] J. R. Ellis, J. S. Hagelin, D. V. Nanopoulos, K. A. Olive, and M. Srednicki, *Supersymmetric relics from the big bang*, *Nucl. Phys.* **B238** (1984) 453–476.
- [3] J. S. Hagelin, G. L. Kane, and S. Raby, *Perhaps scalar neutrinos are the lightest supersymmetric partners*, *Nucl. Phys.* **B241** (1984) 638.
- [4] M. W. Goodman and E. Witten, *Detectability of certain dark-matter candidates*, *Phys. Rev.* **D31** (1985) 3059.
- [5] K. Freese, *Can scalar neutrinos or massive dirac neutrinos be the missing mass?*, *Phys. Lett.* **B167** (1986) 295.
- [6] T. Falk, K. A. Olive, and M. Srednicki, *Heavy sneutrinos as dark matter*, *Phys. Lett.* **B339** (1994) 248–251, [[hep-ph/9409270](#)].
- [7] N. Arkani-Hamed, L. J. Hall, H. Murayama, D. R. Smith, and N. Weiner, *Small neutrino masses from supersymmetry breaking*, *Phys. Rev.* **D64** (2001) 115011, [[hep-ph/0006312](#)].
- [8] Y. Grossman and H. E. Haber, *Sneutrino mixing phenomena*, *Phys. Rev. Lett.* **78** (1997) 3438–3441, [[hep-ph/9702421](#)].
- [9] D. R. Smith and N. Weiner, *Inelastic dark matter*, *Phys. Rev.* **D64** (2001) 043502, [[hep-ph/0101138](#)].
- [10] D. R. Smith and N. Weiner, *Inelastic dark matter at DAMA, CDMS and future experiments*, *Nucl. Phys. Proc. Suppl.* **124** (2003) 197–200, [[astro-ph/0208403](#)].
- [11] D. Tucker-Smith and N. Weiner, *The status of inelastic dark matter*, *Phys. Rev.* **D72** (2005) 063509, [[hep-ph/0402065](#)].
- [12] L. J. Hall, T. Moroi, and H. Murayama, *Sneutrino cold dark matter with lepton-number violation*, *Phys. Lett.* **B424** (1998) 305–312, [[hep-ph/9712515](#)].
- [13] M. Hirsch, H. V. Klapdor-Kleingrothaus, and S. G. Kovalenko, *B-L violating masses in softly broken supersymmetry*, *Phys. Lett.* **B398** (1997) 311–314, [[hep-ph/9701253](#)].
- [14] H. V. Klapdor-Kleingrothaus, S. Kolb, and V. A. Kuzmin, *Light lepton number violating sneutrinos and the baryon number of the universe*, *Phys. Rev.* **D62** (2000) 035014, [[hep-ph/9909546](#)].
- [15] S. Kolb, M. Hirsch, H. V. Klapdor-Kleingrothaus, and O. Panella, *Collider signatures of sneutrino cold dark matter*, *Phys. Lett.* **B478** (2000) 262–268, [[hep-ph/9910542](#)].
- [16] T. Han and R. Hempfling, *Messenger sneutrinos as cold dark matter*, *Phys. Lett.* **B415** (1997) 161–169, [[hep-ph/9708264](#)].
- [17] T. Han, D. Marfatia, and R.-J. Zhang, *A gauge-mediated supersymmetry breaking model with an extra singlet higgs field*, *Phys. Rev.* **D61** (2000) 013007, [[hep-ph/9906508](#)].
- [18] D. Hooper, J. March-Russell, and S. M. West, *Asymmetric sneutrino dark matter and the $\Omega(b)/\Omega(DM)$ puzzle*, *Phys. Lett.* **B605** (2005) 228–236, [[hep-ph/0410114](#)].
- [19] T. Asaka, K. Ishiwata, and T. Moroi, *Right-handed sneutrino as cold dark matter*, *Phys. Rev.* **D73** (2006) 051301, [[hep-ph/0512118](#)].

- [20] H.-S. Lee, K. T. Matchev, and S. Nasri, *Revival of the thermal sneutrino dark matter*, *Phys. Rev. D* **76** (2007) 041302, [[hep-ph/0702223](#)].
- [21] S. Gopalakrishna, A. de Gouvea, and W. Porod, *Right-handed sneutrinos as nonthermal dark matter*, *JCAP* **0605** (2006) 005, [[hep-ph/0602027](#)].
- [22] S. Dimopoulos, G. F. Giudice, and A. Pomarol, *Dark matter in theories of gauge-mediated supersymmetry breaking*, *Phys. Lett. B* **389** (1996) 37–42, [[hep-ph/9607225](#)].
- [23] M. C. Gonzalez-Garcia, M. Maltoni, C. Pena-Garay, and J. W. F. Valle, *Global three-neutrino oscillation analysis of neutrino data*, *Phys. Rev. D* **63** (2001) 033005, [[hep-ph/0009350](#)].
- [24] M. C. Gonzalez-Garcia and Y. Nir, *Developments in neutrino physics*, *Rev. Mod. Phys.* **75** (2003) 345–402, [[hep-ph/0202058](#)].
- [25] M. Maltoni, T. Schwetz, M. A. Tortola, and J. W. F. Valle, *Status of global fits to neutrino oscillations*, *New J. Phys.* **6** (2004) 122, [[hep-ph/0405172](#)].
- [26] G. L. Fogli, E. Lisi, A. Marrone, and A. Palazzo, *Global analysis of three-flavor neutrino masses and mixings*, *Prog. Part. Nucl. Phys.* **57** (2006) 742–795, [[hep-ph/0506083](#)].
- [27] G. L. Fogli *et al.*, *Observables sensitive to absolute neutrino masses: Constraints and correlations from world neutrino data*, *Phys. Rev. D* **70** (2004) 113003, [[hep-ph/0408045](#)].
- [28] M. Hirsch, H. V. Klapdor-Kleingrothaus, and S. G. Kovalenko, *Sneutrino oscillations and neutrinoless double beta decay*, *Phys. Lett. B* **403** (1997) 291–296.
- [29] P. Minkowski, $\mu \rightarrow e\gamma$ at a rate of one out of 1-billion muon decays?, *Phys. Lett. B* **67** (1977) 421.
- [30] M. Gell-Mann, P. Ramond, and R. Slansky, *Supergravity*, p. 135. North Holland, Amsterdam, 1979.
- [31] T. Yanagida, *Proceedings of the Workshop on Unified Theory and Baryon Number in the Universe*, p. 95. KEK, Tsukuba, Japan, 1979.
- [32] R. N. Mohapatra and G. Senjanovic, *Neutrino mass and spontaneous parity nonconservation*, *Phys. Rev. Lett.* **44** (1980) 912.
- [33] R. N. Mohapatra and G. Senjanovic, *Neutrino masses and mixings in gauge models with spontaneous parity violation*, *Phys. Rev. D* **23** (1981) 165.
- [34] J. Schechter and J. W. F. Valle, *Neutrino masses in $SU(2) \times U(1)$ theories*, *Phys. Rev. D* **22** (1980) 2227.
- [35] A. Dedes, H. E. Haber, and J. Rosiek, *Seesaw mechanism in the sneutrino sector and its consequences*, [arXiv:0707.3718](#).
- [36] H. E. Haber and G. L. Kane, *The search for supersymmetry: probing physics beyond the standard model*, *Phys. Rept.* **117** (1985) 75.
- [37] J. F. Gunion and H. E. Haber, *Higgs bosons in supersymmetric models. 1*, *Nucl. Phys. B* **272** (1986) 1.
- [38] C. Arina, *Sneutrino phenomenology in Supersymmetric Models: relevance as Cold Dark Matter in the light of its cosmological and detection properties*. PhD thesis, Università di Torino, 2007.

- [39] **Particle Data Group** Collaboration, W. M. Yao *et al.*, *Review of particle physics*, *J. Phys.* **G33** (2006) 1–1232. and 2007 partial update (<http://pdg.lbl.gov>).
- [40] **ALEPH** Collaboration, A. Heister *et al.*, *Absolute lower limits on the masses of selectrons and sneutrinos in the MSSM*, *Phys. Lett.* **B544** (2002) 73–88, [[hep-ex/0207056](#)].
- [41] R. Bernabei *et al.*, *Dark matter search*, *Riv. Nuovo Cim.* **26N1** (2003) 1–73, [[astro-ph/0307403](#)].
- [42] R. Bernabei *et al.*, *Dark matter particles in the galactic halo: Results and implications from DAMA/NaI*, *Int. J. Mod. Phys.* **D13** (2004) 2127–2160, [[astro-ph/0501412](#)].
- [43] R. Bernabei *et al.*, *Investigating pseudoscalar and scalar dark matter*, *Int. J. Mod. Phys.* **A21** (2006) 1445–1470, [[astro-ph/0511262](#)].
- [44] R. Bernabei *et al.*, *Investigating halo substructures with annual modulation signature*, *Eur. Phys. J.* **C47** (2006) 263–271, [[astro-ph/0604303](#)].
- [45] R. Bernabei *et al.*, *On electromagnetic contributions in WIMP quests*, *Int. J. Mod. Phys.* **A22** (2007) 3155–3168, [[arXiv:0706.1421](#) [[astro-ph](#)]].
- [46] **CDMS** Collaboration, M. S. Armel-Funkhouser *et al.*, *Exclusion limits on the WIMP nucleon cross-section from the first run of the Cryogenic Dark Matter Search in the Soudan underground lab*, *Phys. Rev.* **D72** (2005) 052009, [[astro-ph/0507190](#)].
- [47] **CDMS** Collaboration, D. S. Akerib *et al.*, *Limits on spin-independent WIMP nucleon interactions from the two-tower run of the Cryogenic Dark Matter Search*, *Phys. Rev. Lett.* **96** (2006) 011302, [[astro-ph/0509259](#)].
- [48] A. Bottino, F. Donato, N. Fornengo, and S. Scopel, *Do current WIMP direct measurements constrain light relic neutralinos?*, *Phys. Rev.* **D72** (2005) 083521, [[hep-ph/0508270](#)].
- [49] J. Edsjo and P. Gondolo, *Neutralino relic density including coannihilations*, *Phys. Rev.* **D56** (1997) 1879–1894, [[hep-ph/9704361](#)].
- [50] J. R. Ellis, T. Falk, G. Gani, K. A. Olive, and M. Srednicki, *The CMSSM parameter space at large $\tan \beta$* , *Phys. Lett.* **B510** (2001) 236–246, [[hep-ph/0102098](#)].
- [51] L. Roszkowski, R. Ruiz de Austri, and T. Nihei, *New cosmological and experimental constraints on the CMSSM*, *JHEP* **08** (2001) 024, [[hep-ph/0106334](#)].
- [52] G. Belanger, F. Boudjema, A. Cottrant, A. Pukhov, and A. Semenov, *WMAP constraints on SUGRA models with non-universal gaugino masses and prospects for direct detection*, *Nucl. Phys.* **B706** (2005) 411–454, [[hep-ph/0407218](#)].
- [53] **WMAP** Collaboration, D. N. Spergel *et al.*, *Wilkinson Microwave Anisotropy Probe (WMAP) three year results: Implications for cosmology*, *Astrophys. J. Suppl.* **170** (2007) 377, [[astro-ph/0603449](#)].
- [54] **ALEPH, DELPHI, L3 and OPAL** Collaboration, *Search for the standard model higgs boson at LEP*, [hep-ex/0107029](#). LEP Higgs Working Group for Higgs boson searches.
- [55] **CDF** Collaboration, A. A. Affolder *et al.*, *Search for neutral supersymmetric higgs bosons in $p\bar{p}$ collisions at $\sqrt{s} = 1.8$ TeV*, *Phys. Rev. Lett.* **86** (2001) 4472–4478, [[hep-ex/0010052](#)].
- [56] A. Bottino, F. Donato, N. Fornengo, and S. Scopel, *Size of the neutralino nucleon cross-section in the light of a new determination of the pion nucleon sigma term*, *Astropart. Phys.* **18** (2002) 205–211, [[hep-ph/0111229](#)].

- [57] J. R. Ellis, K. A. Olive, Y. Santoso, and V. C. Spanos, *Update on the direct detection of supersymmetric dark matter*, *Phys. Rev.* **D71** (2005) 095007 and references therein, [[hep-ph/0502001](#)].
- [58] A. K. Drukier, K. Freese, and D. N. Spergel, *Detecting Cold Dark Matter candidates*, *Phys. Rev.* **D33** (1986) 3495–3508.
- [59] K. Freese, J. A. Frieman, and A. Gould, *Signal modulation in Cold Dark Matter detection*, *Phys. Rev.* **D37** (1988) 3388.
- [60] P. Belli, R. Cerulli, N. Fornengo, and S. Scopel, *Effect of the galactic halo modeling on the DAMA/NaI annual modulation result: An extended analysis of the data for WIMPs with a purely spin-independent coupling*, *Phys. Rev.* **D66** (2002) 043503, [[hep-ph/0203242](#)].
- [61] R. Bernabei *et al.*, *Particle dark matter: From dama/nai to dama/libra*, *Phys. Atom. Nucl.* **69** (2006) 2056–2067.
- [62] **XENON Collaboration**, J. Angle *et al.*, *First results from the XENON10 dark matter experiment at the Gran Sasso National Laboratory*, [arXiv:0706.0039](#).
- [63] P. Belli, *Review of direct searches for WIMPs (non-cryogenic detectors)*, Sendai, Japan, September 11-15, 2007. Talk given at the Tenth International Conference on Topics in Astroparticle and Underground Physics (Taup 2007).
- [64] G. Gerbier and D. Bauer, *Review of direct searches for WIMPs (cryogenic detectors)*, Sendai, Japan, September 11-15, 2007. Talk given at the Tenth International Conference on Topics in Astroparticle and Underground Physics (Taup 2007).
- [65] M. Beck *et al.*, *Searching for dark matter with the enriched detectors of the heidelberg - moscow double beta decay experiment*, *Phys. Lett.* **B336** (1994) 141–146.
- [66] A. Bottino, N. Fornengo, and S. Scopel, *Light relic neutralinos*, *Phys. Rev.* **D67** (2003) 063519, [[hep-ph/0212379](#)].
- [67] A. Colaleo, “*Search for MSSM topologies at LEP and lower limit on LSP mass.*” Prepared for 9th International Conference on Supersymmetry and Unification of Fundamental Interactions (SUSY01), Dubna, Russia, 11-17 Jun 2001.
- [68] **DELPHI 2001-085 CONF 513 Collaboration**, J. Abdallah *et al.*, *Searches for supersymmetric particles in $e+e-$ collisions up to 208 GeV and interpretation of the results within the MSSM*, 2001.
- [69] **LEP2 Joint SUSY Working Group Collaboration**. <http://lepsusy.web.cern.ch/lepsusy/>.
- [70] A. Bottino, F. Donato, N. Fornengo, and S. Scopel, *Lower bound on the neutralino mass from new data on CMB and implications for relic neutralinos*, *Phys. Rev.* **D68** (2003) 043506, [[hep-ph/0304080](#)].
- [71] G. Belanger, F. Boudjema, A. Pukhov, and S. Rosier-Lees, *A lower limit on the neutralino mass in the MSSM with non- universal gaugino masses. $((t)) ((u))$* , [hep-ph/0212227](#).
- [72] D. Hooper and T. Plehn, *Supersymmetric dark matter - how light can the LSP be?*, *Phys. Lett.* **B562** (2003) 18–27, [[hep-ph/0212226](#)].
- [73] A. Bottino, F. Donato, N. Fornengo, and S. Scopel, *Further investigation of a relic neutralino as a possible origin of an annual-modulation effect in wimp direct search*, *Phys. Rev.* **D62** (2000) 056006, [[hep-ph/0001309](#)].

- [74] A. Bottino, F. Donato, N. Fornengo, and S. Scopel, *Light neutralinos and wimp direct searches*, *Phys. Rev.* **D69** (2004) 037302, [[hep-ph/0307303](#)].
- [75] D. G. Cerdeno, C. Hugonie, D. E. Lopez-Fogliani, C. Munoz, and A. M. Teixeira, *Theoretical predictions for the direct detection of neutralino dark matter in the NMSSM*, *JHEP* **12** (2004) 048, [[hep-ph/0408102](#)].
- [76] F. Donato, N. Fornengo, and P. Salati, *Antideuterons as a signature of supersymmetric dark matter*, *Phys. Rev.* **D62** (2000) 043003, [[hep-ph/9904481](#)].
- [77] F. Donato, N. Fornengo, D. Maurin, P. Salati, and R. Taillet, *Antiprotons in cosmic rays from neutralino annihilation*, *Phys. Rev.* **D69** (2004) 063501, [[astro-ph/0306207](#)].
- [78] T. Sjostrand *et al.*, *High-energy-physics event generation with pythia 6.1*, *Comput. Phys. Commun.* **135** (2001) 238–259, [[hep-ph/0010017](#)].
- [79] **BESS** Collaboration, S. Orito *et al.*, *Precision measurement of cosmic-ray antiproton spectrum*, *Phys. Rev. Lett.* **84** (2000) 1078–1081, [[astro-ph/9906426](#)].
- [80] **BESS** Collaboration, T. Maeno *et al.*, *Successive measurements of cosmic-ray antiproton spectrum in a positive phase of the solar cycle*, *Astropart. Phys.* **16** (2001) 121–128, [[astro-ph/0010381](#)].
- [81] F. Donato *et al.*, *Antiprotons from spallation of cosmic rays on interstellar matter*, *Astrophys. J.* **536** (2001) 172–184, [[astro-ph/0103150](#)].
- [82] D. Maurin, F. Donato, R. Taillet, and P. Salati, *Cosmic rays below $Z=30$ in a diffusion model: new constraints on propagation parameters*, *Astrophys. J.* **555** (2001) 585–596, [[astro-ph/0101231](#)].
- [83] **PAMELA** Collaboration, M. Boezio *et al.*, *The space experiment PAMELA*, 2004.
- [84] **AMS** Collaboration, M. Aguilar *et al.*, *The Alpha Magnetic Spectrometer (AMS) on the International Space Station. I: Results from the test flight on the space shuttle*, *Phys. Rept.* **366** (2002) 331–405.
- [85] **WiZard/CAPRICE** Collaboration, M. Boezio *et al.*, *The cosmic-ray anti-proton flux between 3-GeV and 49-GeV*, *Astrophys. J.* **561** (2001) 787–799, [[astro-ph/0103513](#)].
- [86] K. Mori *et al.*, *A novel antimatter detector based on X-ray deexcitation of exotic atoms*, *Astrophys. J.* **566** (2002) 604–616, [[astro-ph/0109463](#)].
- [87] J. Koglin, Fermilab, May 10-12, 2007. Talk given at the The Hunt for Dark Matter.
- [88] B. Moore *et al.*, *Dark matter substructure within galactic halos*, *Astrophys. J.* **524** (1999) L19–L22.
- [89] B. Moore, T. Quinn, F. Governato, J. Stadel, and G. Lake, *Cold collapse and the core catastrophe*, *Mon. Not. Roy. Astron. Soc.* **310** (1999) 1147–1152, [[astro-ph/9903164](#)].
- [90] S. Hunter *et al.*, *EGRET observations of the diffuse gamma-ray emission from the galactic plane*, *Astrophys. J.* **481** (1997) 205.
- [91] H. A. Mayer-Hasselwander *et al.*, *High-energy gamma ray emission from the galactic center*, *Astron. Astrophys.* **335** (1998) 161–172.
- [92] **GLAST** Collaboration, A. Morselli, A. Lionetto, A. Cesarini, F. Fucito, and P. Ullio, *Search for dark matter with GLAST*, *Nucl. Phys. Proc. Suppl.* **113** (2002) 213–220, [[astro-ph/0211327](#)].

- [93] **Super-Kamiokande** Collaboration, A. Habig, *An indirect search for WIMPs with Super-Kamiokande*, [hep-ex/0106024](#).
- [94] **MACRO** Collaboration, M. Ambrosio *et al.*, *Limits on dark matter WIMPs using upward-going muons in the MACRO detector*, *Phys. Rev.* **D60** (1999) 082002, [[hep-ex/9812020](#)].
- [95] **IceCube** Collaboration, A. Achterberg *et al.*, *The IceCube collaboration: Contributions to the 29th international cosmic ray conference (ICRC 2005), Pune, India, Aug. 2005*, [astro-ph/0509330](#).
- [96] A. Bottino, F. Donato, N. Fornengo, and S. Scopel, *Indirect signals from light neutralinos in supersymmetric models without gaugino mass unification*, *Phys. Rev.* **D70** (2004) 015005, [[hep-ph/0401186](#)].
- [97] N. Fornengo, L. Pieri, and S. Scopel, *Neutralino annihilation into gamma-rays in the milky way and in external galaxies*, *Phys. Rev.* **D70** (2004) 103529, [[hep-ph/0407342](#)].
- [98] P. Gondolo and J. Silk, *Dark matter annihilation at the galactic center*, *Phys. Rev. Lett.* **83** (1999) 1719–1722, [[astro-ph/9906391](#)].
- [99] D. Merritt, M. Milosavljevic, L. Verde, and R. Jimenez, *Dark matter spikes and annihilation radiation from the galactic center*, *Phys. Rev. Lett.* **88** (2002) 191301, [[astro-ph/0201376](#)].
- [100] D. Merritt, *Evolution of the dark matter distribution at the galactic center*, *Phys. Rev. Lett.* **92** (2004) 201304, [[astro-ph/0311594](#)].
- [101] F. Prada, A. Klypin, J. Flix, M. Martinez, and E. Simonneau, *Astrophysical inputs on the susy dark matter annihilation detectability*, [astro-ph/0401512](#).
- [102] O. Y. Gnedin, A. V. Kravtsov, A. A. Klypin, and D. Nagai, *Response of dark matter halos to condensation of baryons: cosmological simulations and improved adiabatic contraction model*, *Astrophys. J.* **616** (2004) 16–26, [[astro-ph/0406247](#)].
- [103] M. Cirelli *et al.*, *Spectra of neutrinos from dark matter annihilations*, *Nucl. Phys.* **B727** (2005) 99–138, [[hep-ph/0506298](#)].
- [104] **SDSS** Collaboration, U. Seljak *et al.*, *Cosmological parameter analysis including sdss ly-alpha forest and galaxy bias: Constraints on the primordial spectrum of fluctuations, neutrino mass, and dark energy*, *Phys. Rev.* **D71** (2005) 103515, [[astro-ph/0407372](#)].
- [105] J. Lesgourgues and S. Pastor, *Massive neutrinos and cosmology*, *Phys. Rept.* **429** (2006) 307–379, [[astro-ph/0603494](#)].
- [106] J. F. Navarro, C. S. Frenk, and S. D. M. White, *The structure of Cold Dark Matter halos*, *Astrophys. J.* **462** (1996) 563–575, [[astro-ph/9508025](#)].
- [107] J. F. Navarro, C. S. Frenk, and S. D. M. White, *A universal density profile from hierarchical clustering*, *Astrophys. J.* **490** (1997) 493–508, [[astro-ph/9611107](#)].
- [108] **D0** Collaboration, V. M. Abazov *et al.*, *Search for pair production of scalar bottom quarks in p anti- p collisions at $s^{(1/2)} = 1.96$ TeV*, *Phys. Rev. Lett.* **97** (2006) 171806, [[hep-ex/0608013](#)].
- [109] **Heavy Flavor Averaging Group (HFAG)** Collaboration, E. Barberio *et al.*, *Averages of b -hadron properties at the end of 2005*, [hep-ex/0603003](#).

- [110] M. Ciuchini, G. Degrandi, P. Gambino, and G. F. Giudice, *Next-to-leading QCD corrections to $B \rightarrow X_s \gamma$ in supersymmetry*, *Nucl. Phys.* **B534** (1998) 3–20, [[hep-ph/9806308](#)].
- [111] M. Misiak *et al.*, *The first estimate of $BR(B \rightarrow X_s \gamma)$ at $\mathcal{O}(\alpha(s)^2)$* , *Phys. Rev. Lett.* **98** (2007) 022002, [[hep-ph/0609232](#)].
- [112] **D0** Collaboration, V. M. Abazov *et al.*, *Search for $B_s \rightarrow \mu^+ \mu^-$ at $D0$* , [arXiv:0707.3997](#).
- [113] **Muon G-2** Collaboration, G. W. Bennett *et al.*, *Final report of the muon $E821$ anomalous magnetic moment measurement at BNL*, *Phys. Rev.* **D73** (2006) 072003, [[hep-ex/0602035](#)].
- [114] J. Bijnens and J. Prades, *The hadronic light-by-light contribution to the muon anomalous magnetic moment: Where do we stand?*, *Mod. Phys. Lett.* **A22** (2007) 767–782, [[hep-ph/0702170](#)].